

ScholarWorks@GSU

Kinetic Mechanism and Inhibitory Study of Protein Arginine Methyltransferase 1

Authors	Feng, You
Citation	Feng, You. (2012). "Kinetic Mechanism and Inhibitory Study of Protein Arginine Methyltransferase 1". Georgia State University. https://doi.org/3006031
DOI	https://doi.org/10.57709/3006031
Download date	2026-05-20 04:03:24
Link to Item	https://hdl.handle.net/20.500.14694/2819

KINETIC MECHANISM AND INHIBITORY STUDY OF PROTEIN ARGININE
METHYLTRANSFERASE 1

by

YOU FENG

Under the Direction of Professor Yujun George Zheng

ABSTRACT

Protein arginine methyltransferase 1 (PRMT1) is a key posttranslational modification enzyme that catalyzes the methylation of specific arginine residues in histone and nonhistone protein substrates, regulating diverse cellular processes such as transcriptional initiation, RNA splicing, DNA repair, and signal transduction. Recently the essential roles of PRMT1 in cancer and cardiovascular complications have intrigued much attention. Developing effective PRMT inhibitors therefore is of significant therapeutic value. The research on PRMT inhibitor development however is greatly hindered by poor understanding of the biochemical basis of protein arginine methylation and lack of effective assays for PRMT1 inhibitor screening.

Herein, we report our effort in the kinetic mechanism study as well as the fluorescent probe and inhibitor development for PRMT1. New fluorescent reporters were designed and applied to perform single-step analysis of substrate binding and methylation of PRMT1. Using these reporters, we performed transient-state fluorescence measurements to dissect the rate constants along the PRMT1 catalytic coordinate. The data give evidence that the chemistry of

methyl transfer is the major rate-limiting step, and that binding of the cofactor SAM or SAH affects the association and dissociation of H4 with PRMT1. Importantly, we identified a critical kinetic step suggesting a precatalytic conformational transition induced by substrate binding. On the other hand, we discovered a type of naphthyl-sulfo (NS) compounds that block PRMT1-mediated arginine methylation at micromolar potency through a unique mechanism: they directly target the substrates but not PRMT enzymes for the observed inhibition. We also found that suramin, an anti-parasite and anti-cancer drug bearing similar functional groups, effectively inhibited PRMT1 mediated methylation. These findings about novel PRMT inhibitors and their unique inhibition mechanism provide a new way for chemical regulation of protein arginine methylation. Additionally, to dissect the interplaying relationship between different histone modification marks, we investigated how individual lysine acetylations and their different combinations at the H4 tail affect Arg-3 methylation *in cis*. Our data reveal that the effect of lysine acetylation on arginine methylation depends on the site of acetylation and the type of methylation. While certain acetylations present a repressive impact on PRMT-1 mediated methylation (type I methylation), lysine acetylation generally is correlated with enhanced methylation by PRMT5 (type II dimethylation). In particular, Lys-5 acetylation decreases activity of PRMT1 but increases that of PRMT5. Furthermore, hyperacetylation increases the content of ordered secondary structures of H4 tail. These findings provide new insights into the regulatory mechanism of Arg-3 methylation by H4 acetylation, and unravel that complex intercommunications exist between different posttranslational marks *in cis*.

INDEX WORDS: Protein arginine methyltransferases, Fluorescence reporters, Substrate-targeting inhibitors, Transient-state kinetics, Histone tail modifications

KINETIC MECHANISM AND INHIBITORY STUDY OF PROTEIN ARGININE
METHYLTRANSFERASE 1

by

YOU FENG

A Dissertation Submitted in Partial Fulfillment of the Requirements for the Degree of

Doctor of Philosophy

in the College of Arts and Sciences

Georgia State University

2012

Copyright by
You Feng
2012

KINETIC MECHANISM AND INHIBITORY STUDY OF PROTEIN ARGININE
METHYLTRANSFERASE 1

by

YOU FENG

Committee Chair: Dr. Yujun George Zheng

Committee: Dr. Jenny Yang

Dr. David Wilson

Dr. Aimin Liu

Electronic Version Approved:

Office of Graduate Studies

College of Arts and Sciences

Georgia State University

August 2012

DEDICATION

I dedicate this dissertation to my families, who gave me great spiritual and financial support selflessly for my pursuit of knowledge for the past five years.

ACKNOWLEDGEMENTS

Firstly, I would like to give my deepest appreciation to my advisor, Dr. Yujun (George) Zheng (Georgia State University in USA, 2006-2012) for giving me the opportunity to join his research group. Dr. Zheng gave me encouragement, guidance and support from the earliest stages of this dissertation and taught me the skills in academic study. I am indebted to my laboratory members for their assistance and discussion of my research projects. Specially, I am obliged to Dr. Nan Xie, Sabrina Asher, Miyeong Jin and Linh Hong for their great contributions to prepare peptide compounds, to Dr. Juxian Wang for her assistance to calibrate the peptide concentrations and test some of their activities, to Jiang Wu, Chao Yang, Dr. Tielong Gao, Dr. Leilei Yan, Emilia N Elangwe, Yutao Yang, Sarmistha Halder Sinha, and other lab members for their generous hand and fruitful discussion in protein expression and purification and for their valuable ideas and suggestions to my projects and lab research. I also thank Dr. Binghe Wang and Dr. Minyong Li for the virtual screening work, Dr. Siming Wang and Yanyi Chen for MS analysis, Dr. Xiaodong Chen for the PRMT1 plasmid, and Dr. Philip Cole for the p300 protein.

Secondly, I would like to thank my committee members, Dr. Jenny Yang, Dr. David Wilson and Dr. Aimin Liu, for their great suggestions and valuable discussions. They always guide me to the right path using their knowledge and experience. In addition, I thank Dr. Al Baumstark, Dr. David Wilson and Dr. Aimin Liu for recommending me for the American Heart Association predoctoral award.

Finally, I would like to thank Georgia Cancer Coalition Distinguished Cancer Scholar Award, American Heart Association predoctoral fellowship, Georgia State University Center for Diagnostics and Therapeutics program fellowship, and NIH grant R01GM086717-01A2 for supporting the research work.

TABLE OF CONTENTS

ACKNOWLEDGMENTS	v
LIST OF TABLES	xii
LIST OF FIGURES	xiii
LIST OF SCHEMENCES	xvi
LIST OF ABBREVIATIONS	xvii
LIST OF BUFFERS.....	xix
CHAPTER 1. INTRODUCTION	1
<i>1.1. The structure and function of chromatin</i>	1
<i>1.2. Histone posttranslational modifications</i>	2
<i>1.3. Histone arginine methylation</i>	4
<i>1.4. Protein arginine methyltransferases</i>	5
<i>1.5. Protein arginine methyltransferase 1 (PRMT1)</i>	7
<i>1.6. The study points in this work</i>	12
1.6.1. The development of fluorescent peptide probes for PRMT1.....	12
1.6.2. The inhibition study of PRMT1.....	14
1.6.3. The transient-state kinetics and catalytic mechanism of PRMT1.....	15
1.6.4. The interaction between lysine acetylation and arginine 3 methylation on H4 tail.....	16
CHAPTER 2. INHIBITORY STUDY OF PROTEIN ARGININE METHYLTRANSFERASE 1 USING A FLUORESCENT APPROACH	19
<i>2.1. Introduction</i>	19
<i>2.2. Results and discussion</i>	21
2.2.1. Expression and purification of PRMT1	21

2.2.2. Design and synthesis of fluorescent PRMT1 reporters	21
2.2.3. Fluorescence response of the PRMT1 reporters	22
2.2.4. Inhibitory study of AMI-1 using the fluorescent strategy.....	27
2.3. <i>Conclusion</i>	31
2.4. <i>Experimental</i>	31
2.4.1. Synthesis of the fluorescent reporters	31
2.4.2. Enzymatic methylation assay.....	32
2.4.3. Fluorescence assay	33
CHAPTER 3. DISCOVERY AND MECHANISTIC STUDY OF A CLASS OF PROTEIN ARGININE METHYLATION INHIBITORS	35
3.1. <i>Introduction</i>	35
3.2. <i>Results and discussion</i>	37
3.2.1. Screening for new PRMT1 inhibitors	37
3.2.2. The kinetic pattern of PRMT1 inhibition by NS-1	41
3.2.3. Selectivity of NS-1	44
3.2.4. NS-1 directly targets the substrates, but not PRMT1	45
3.2.5. NS-1 inhibits the activity of histone acetyltransferase (HAT) p300.....	52
3.2.6. Suramin inhibits arginine methylation	55
3.3. <i>Conclusion</i>	55
3.4. <i>Experimental</i>	56
3.4.1. Materials	56
3.4.2. Synthesis of peptide substrates	57
3.4.3. Protein expression and purification	57

3.4.4. Virtual screening	58
3.4.5. Radioactive methylation assay	59
3.4.6. Inhibition of p300 catalysis	60
3.4.7. Fluorescent binding assay	60
3.4.8. UV-Vis spectroscopy of 3 upon titration with H4(1-20) or PRMT1	61
3.4.9. CD measurement	61
CHAPTER 4. A TRANSIENT KINETIC ANALYSIS OF PRMT1 CATALYSIS	62
4.1. Introduction	62
4.2. Results and Discussion	64
4.2.1. Oligomerization of PRMT1 stimulates its activity	64
4.2.2. H4 peptide synthesis and steady-state kinetic characterization	66
4.2.3. Measurement of the binding rate constants of the H4 peptides with PRMT1	71
4.2.4. Measurement of dissociation rate constants of peptides from PRMT1	75
4.2.5. Effect of SAH on enzyme binding and dissociation of H4FLme1	76
4.2.6. Progression of arginine methylation probed by stopped-flow fluorescence	80
4.3. Conclusion	83
4.4. Experimental	83
4.4.1. Design and synthesis of modified H4 peptides	83
4.4.2. Expression and purification of PRMT1	84
4.4.3. Chemical crosslinking and western blotting of PRMT1 oligomers	85
4.4.4. Radioactive methyltransferase assay	85
4.4.5. Equilibrium fluorescent titration	86
4.4.6. Stopped-flow fluorescence measurements	86

CHAPTER 5. HISTONE H4 ACETYLATION DIFFERENTIALLY MODULATES ARGININE METHYLATION BY AN IN CIS MECHANISM.....	89
<i>5.1. Introduction.....</i>	<i>89</i>
<i>5.2. Result and Discussion</i>	<i>93</i>
5.2.1. Design, synthesis, and characterization of modified H4 peptide library	93
5.2.2. Impact of H4 acetylation on PRMT1-catalyzed R3 methylation.....	95
5.2.3. Impact of H4 acetylation on PRMT5-mediated R3 methylation.....	100
5.2.4. Impact of H4 acetylation on PRMT1 and PRMT5 activity using H4 protein and nucleosome as substrates	102
5.2.5. The structural changes of H4 induced by acetylation	105
<i>5.3. Conclusion.....</i>	<i>110</i>
<i>5.4. Experimental</i>	<i>112</i>
5.4.1. Design and synthesis of acetylated H4 peptides	112
5.4.2. Calibration of peptide concentrations with NMR.....	112
5.4.3. Protein expression and purification	113
5.4.4. Radioactive methylation assays	113
5.4.5. Circular Dichroism (CD) measurement and analysis.....	115
5.4.6. Structure simulation for the unacetylated and tetraacetylated H4 peptides.....	115
CHAPTER 6. SUMMARY.....	117
APPENDIX.....	128
REFERENCES.....	141

LIST OF TABLES

Table 1.1. Different types of histone modifications.....	3
Table 2.1. Sequences of H4, H4-FL, R4, and R4-FL.....	22
Table 2.2. Steady state kinetic parameters of rPRMT1 in the methylation of H4, R4 and their fluorescent derivatives.....	27
Table 3.1. Inhibition of PRMT1 by selected compounds	40
Table 3.2. Comparison of the inhibition of PRMT-1, -3, -4, and -6 by Compound 3	44
Table 4.1. Sequences of H4 peptides.....	67
Table 4.2. Steady-state kinetic characterization of PRMT1 binding and catalysis	68
Table 4.3. Summary of rate constant data obtained from stopped-flow fluorescence measurements.....	82
Table 5.1. Sequences of synthetic H4 peptides	93
Table 5.2. Steady-state kinetic parameters of PRMT1 catalysis	98
Table 5.3. Kinetic parameters of PRMT5 catalysis	101

LIST OF FIGURES

Figure 1.1. The structure and modification sites of nucleosome in chromatin	2
Figure 1.2. Post-translational modifications on histone N-terminal tail domains	3
Figure 1.3. Scheme of protein arginine methylation.....	5
Figure 1.4. Protein arginine methyltransferase family members expressed in human	6
Figure 1.5. Structures of hPRMT1 and rPRMT1	9
Figure 1.6. Structure of ternary complex of PRMT1-AdoHcy-R3 peptide	10
Figure 1.7. Proposed kinetic mechanisms of PRMT1.....	12
Figure 2.1. SDS-PAGE of rPRMT1 after purification	21
Figure 2.2. Fluorescence intensity changes of H4-FL and R4-FL upon interaction with PRMT1.....	23
Figure 2.3. Inhibition effect of sinefungin on PRMT1 methylation	25
Figure 2.4. Fluorescence anisotropy titration.....	26
Figure 2.5. Competitive inhibition assays of AMI-1 against H4-FL (a) and R4-FL (b) using the mode of fluorescence anisotropy	29
Figure 2.6. Inhibition pattern analysis of AMI-1 to PRMT1 plotted as reciprocal plots.....	30
Figure 3.1. Structures of selected PRMT1 inhibitors	40
Figure 3.2. Competitive binding measurement with fluorescence anisotropy	43
Figure 3.3. Kinetic analysis of PRMT1 inhibition by 3	43
Figure 3.4. Association of 1 with H4(1-20) peptide detected by MALDI-MS	47
Figure 3.5. UV-Vis spectral change of 3 upon the addition of H4(1-20) or His6x-PRMT1 ..	48
Figure 3.6. Impact of 3 on the fluorescence spectra of H4(1-20)FL	49

Figure 3.7. Determination of the binding stoichiometry of 3—H4(1-20)FL complex by Job’s Method	50
Figure 3.8. CD study of H4(1-20) association with 3	51
Figure 3.9. Inhibition of p300 HAT activity by 3, 1, suramin and stilbamidine	54
Figure 3.10. Inhibition mechanism of NS compounds.....	56
Figure 4.1. Concentration dependence of PRMT1 oligomerization and catalytic activity ...	66
Figure 4.2. Fluorescence anisotropy titration of fluorescent peptides with PRMT1.....	70
Figure 4.3. Fluorescence anisotropy change of H4FL binding to PRMT1 followed by H4(1-20) competitive titration	71
Figure 4.4. Fluorescence change of H4FLme1 association followed by H4(1-20) competitive titration	72
Figure 4.5. Stopped-flow measurements of peptide association with PRMT1.....	73
Figure 4.6. Plot of k_{obs} versus protein concentration obtained from stopped-flow fluorescence measurements.....	74
Figure 4.7. Stopped-flow measurements of peptide dissociation from PRMT1.....	76
Figure 4.8. Effect of SAH on the binding and dissociation of H4 substrate	78
Figure 4.9. Stopped-flow measurement of H4FLme2 dissociation from PRMT1-SAM complex	79
Figure 4.10. Time course of PRMT1 catalysis probed by stopped-flow fluorescence	82
Figure 5.1. Methylation of H4R3 by PRMT1 and PRMT5.....	93
Figure 5.2. A typical NMR spectrum used for calibration of H4 peptide concentration.....	95
Figure 5.3. Effects of lysine acetylation on Arg-3 methylation by PRMT1.....	97
Figure 5.4. Effects of acetylation on R3 methylation catalyzed by PRMT5.....	101

Figure 5.5. Acetylation on H4 protein inhibits its methylation by PRMT1, while promotes its methylation by PRMT5.....	103
Figure 5.6. Gel shift assay of the assembled nucleosome.....	104
Figure 5.7. Assembled nucleosome cannot be methylated by PRMT1 or PRMT5 in vitro	104
Figure 5.8. Secondary structure analysis of unacetylated H4 peptide (A) and tetraacetylated H4 peptide (P).....	106
Figure 5.9. Simulated structural changes upon tetraacetylation of the N-terminal H4 tail	108
Figure 5.10. Clustering of the equilibrium population of the unacetylated (left column) and tetraacetylated (right column) H4 peptides.....	109
Figure 5.11. Summary of the effects of lysine acetylation on R3 methylation in H4.....	111
Figure 6.1. The active site of PRMT5.....	126

LIST OF SCHEMES

Scheme 4.1. PRMT1-catalyzed arginine methylation.....	63
Scheme 4.2. Two different kinetic models of substrate association with PRMT1 apoenzyme and holoenzyme.....	80
Scheme 4.3. Proposed minimal kinetic model of PRMT1 catalysis.....	83

LIST OF ABBREVIATIONS

Protein arginine methyltransferase (PRMT)

S-Adenosyl-*L*-methionine (SAM, AdoMet)

S-Adenosyl-*L*-homocysteine (SAH)

1, 4-Dithiothreitol (DTT)

2-(6-Chloro-1H-benzotriazole-1-yl)-1,1,3,3-tetramethylammonium hexafluorophosphate (HCTU)

2,3-diaminopropionic acid (Dpr)

4-(2-hydroxyethyl)-1-piperazineethanesulfonic acid (HEPES)

Acetyl-coenzyme A (AcCoA)

Androgen receptor (AR)

Bovine serum albumin (BSA)

CREB-binding protein (p300/CBP)

Dimethyl sulfoxide (DMSO)

Dimethyldioxocyclohexylidene (Dde)

Dimethylformamide (DMF)

Electrospray ionization (ESI)

Enzyme-linked immunosorbent assay (ELISA)

Ethylenediaminetetraacetic acid (EDTA)

Fluorenylmethyloxycarbonyl (Fmoc)

Fluorescein (FL)

High-throughput screening (HTS)

Histone methyltransferases (HMTs)

Histone acetyltransferases (HATs)

Isopropyl- β -D-thiogalactopyranoside (IPTG)

Matrix assisted laser desorption ionization mass spectrometry (MALDI-MS)

Phenylmethanesulphonyl fluoride (PMSF)

Prostate-specific antigen (PSA)

Reverse-phased (RP)

Sodium dodecyl sulfate polyacrylamide gel electrophoresis (SDS-PAGE)

Solid phase peptide synthesis (SPPS)

Structure-activity relationship (SAR)

Ultraviolet-visible (UV)

LIST OF BUFFERS

Cell Lysis buffer: 25 mM Na-HEPES, pH 7.0; 150 mM NaCl; 1 mM MgSO₄; 5 % Ethylene glycol; 5 % Glycerol; 1 mM PMSF

Column buffer: 25 mM HEPES, pH 8.0; 500 mM NaCl; 1 mM PMSF; 30 mM Imidazole; 10 % Glycerol

Washing buffer: 25 mM HEPES, pH 8.0; 300 mM NaCl; 1 mM PMSF; 70 mM Imidazole; 10 % Glycerol

Elution buffer: 25 mM HEPES, pH 7.0; 300 mM NaCl; 1 mM PMSF; 10 % Glycerol; 200 mM Imidazole

Dialysis buffer: 25 mM HEPES, pH 7.0; 250 mM NaCl; 1 mM EDTA; 10 % Glycerol; 10 mM DTT

12 % SDS-PAGE stacking gel (10 mL total volume): 30 % acrylamide; 1.7 mL dd H₂O 6.8 mL; 1.5 M Tris-HCL; pH 6.8 1.25 mL; 10 % SDS 0.1 mL; 10 % APS (ammonium persulfate) 0.1 mL; TEMED 0.01 mL

12 % SDS-PAGE resolving gel (20 mL total volume): 30 % acrylamide 8.0 mL; dd H₂O 1.7 mL; 1.5 M Tris-HCL pH 8.8 1.25 mL; 10 % SDS 0.2 mL 10 % APS (ammonium persulfate); 0.2 mL TEMED 0.008 mL

Tris-glycine electrophoresis running buffer: 25 mM Tris, 192 mM glycine, 0.1% SDS, pH8.3

Reaction buffer: 50 mM HEPES pH 8.0; 50 mM NaCl, 1 mM EDTA; 0.5 mM DTT

TBS buffer (Tris Buffered Saline): 50 mM Tris.HCl, pH 7.4 and 150 mM NaCl

Western blot transfer buffer: 25 mM Tris, 192 mM glycine, 10% methanol

Culture media

LB- Media: 10 g Tryptone; 5 g Yeast extract; 5 g NaCl; 1 mL of 1 N NaOH; Fill up to 1000 mL

NZY Media: 1 mL LB media: 12.5 μ L 1M MgSO₄; 12.5 μ L 1M MgCl₂; 20 μ L 20 % Glucose

CHAPTER 1

INTRODUCTION

1.1. The structure and function of chromatin

Exclusively found in eukaryotic cells, chromatin is composed of regularly and intensively packed DNA and protein. ~146 bp DNA is wrapped around the histone octamer consisting of two of each of H3, H4, H2A and H2B proteins to form a fundamental repeating genetic element called nucleosome (Figure 1.1). As the smallest unit of genetic information storage, nucleosomes are linked by H1 protein and DNA to form compressed chromatin fibers with a beads-on-string structure. These ~30 nanometer fibers are further coiled into chromosome, which plays regulatory role in multiple nuclear processes like transcription, replication, DNA repair, mitosis and apoptosis.(1) The chromatin structure can be changed by epigenetic modifications of DNA and histones during different phases of cell division.(2-5)

Chromatin is categorized into euchromatin and heterochromatin according to its conformation and staining state. Euchromatin is loosely packed and stains lightly, and is usually composed of actively transcribed genes. On the other hand, heterochromatin is tightly packed and stains intensely, and is mainly composed of inactive genes or satellite sequences, such as centromere and telomere. H3K9 di and tri-methylation are usually linked with heterochromatin structure [Zhang MQ *et al*, BMC Genomics, 2009].

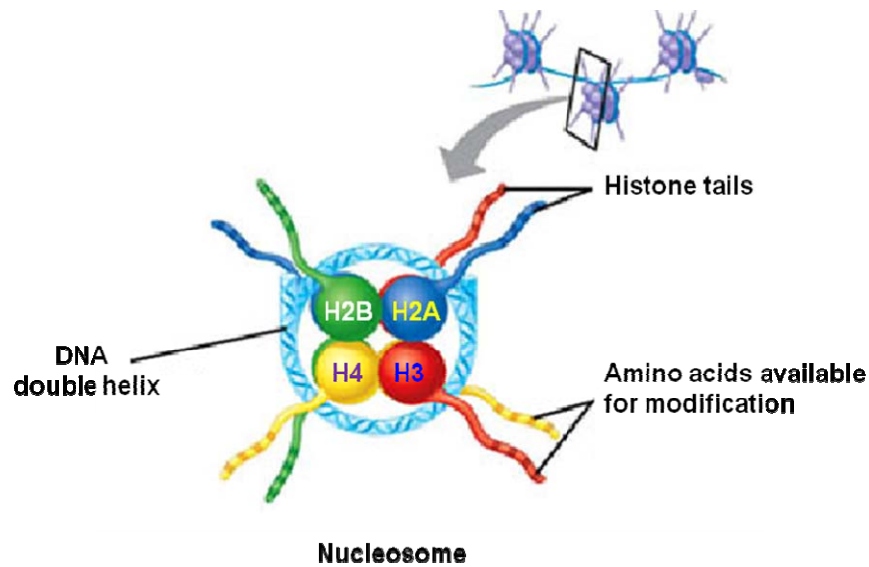


Figure 1.1. The structure and modification sites of nucleosome in chromatin (6)

1.2. Histone posttranslational modifications

Histones are the major protein components of chromatin, packaging DNA into nucleosome and helping regulate gene expression. Histones undergo extensive posttranslational modifications (PTMs) at its amino-terminal tail domain where lie multiple positively charged residues. Some of these modification sites have been detected by specific antibodies or tandem mass spectrometry,(7) including lysine acetylation/metylation, arginine methylation, serine phosphorylation, lysine ubiquitination, *etc* (Figure 1.2). These modifications represent enormous potential biological functions (Table 1.1).(8) For example, the residue Lys can be labeled with mono-, di-, or trimethyl group by various lysine methyltransferases; while the residue Arg can be marked with mono-, asymmetric di- or symmetric di-methyl group by different protein arginine methyltransferases (PRMTs).(9, 10) Many of these PTMs profoundly affect the on-and-off status of gene transcription by recruiting other modulator proteins or factors to initiate the downstream transcriptional activation or repression. Notably, the specificity of methylation may lead to

distinct biological functions, *e.g.*, H3 K4 or K27 methylation (mono-, di-, or tri-) activates transcription, but H3 K9 methylation (di- or tri-) represses transcription.(11) The molecular mechanism by which histone PTMs modulate genetic and epigenetic processes is not fully understood. In particular, how a PTM mark affects the presence and level of other histone modification marks needs to be addressed and is essential for better understanding the molecular basis of histone code hypothesis.

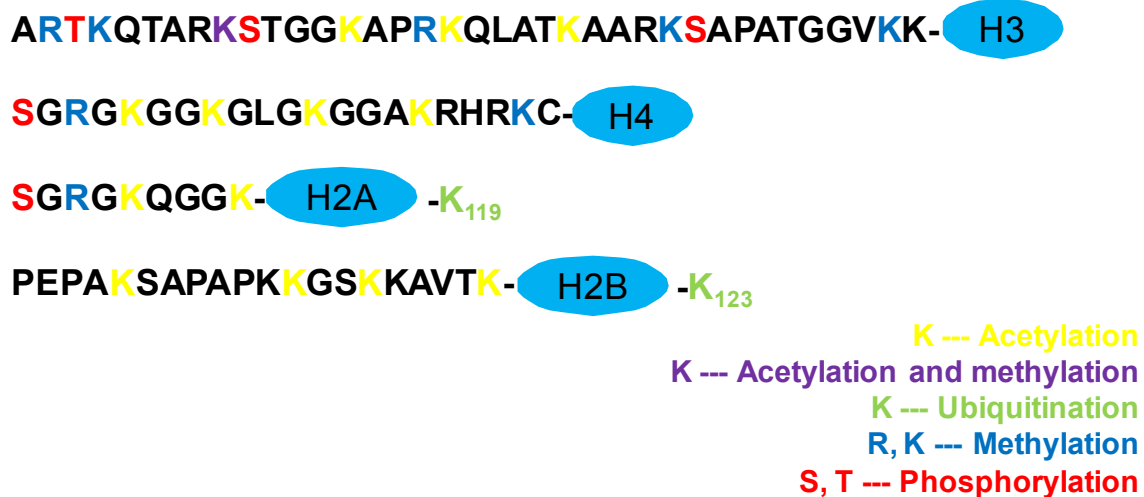


Figure 1.2. Post-translational modifications on histone N-terminal tail domains

Table 1.1. Different types of histone modifications

Modification	Residue	Function	Related disease	Typical enzyme
Acetylation	Lys	Transcription, Repair	Cancer	p300, pCAF, Tip60(12)
Methylation	Lys, Arg	Transcription, Repair, Splicing	Cancer, Cardiovascular disease	PRMT1, PRMT5 (13)

Phosphorylation	Ser, Thr	Transcription, Repair	Cancer	MSK1(14)
Ubiquitylation	Lys	Transcription, Repair	Cancer	E1(15)
Sumoylation	Lys	Transcription, Nuclear transport		SAE1/SAE2(16)

1.3. Histone arginine methylation

Posttranslational modifications (PTMs) are important strategies used by eukaryotic organisms to modulate their phenotypes. One of the well studied PTMs, arginine methylation, is catalyzed by protein arginine methyltransferases (PRMTs) with SAM as the methyl donor. The functions of PRMTs have been broadly studied in different biological processes and diseased states, but the molecular basis for arginine methylation is not well defined.

Taking Histone H4 arginine 3 (H4R3) methylation as an example, asymmetric dimethylation of H4R3 mediated by PRMT1 leads to gene activation, while symmetric dimethylation of H4R3 mediated by PRMT5 is related to gene repression. The two enzymes introducing these modifications exhibit identifiably similar sequences, but the molecular bases for their distinct catalytic mechanisms are unclear. A recent report suggested that a conserved phenylalanine in the active site of PRMT5 is critical for directing the symmetric di-methylation. (17) It has also been shown that asymmetric dimethylation at H3R17 by CARM1 enhances transcription activation, that symmetric dimethylation at H3R8 by PRMT5 induces transcription repression, and that asymmetric dimethylation at H3R2 by PRMT6 leads to gene repression and is mutually exclusive with H3K4 methylation.

1.4. Protein arginine methyltransferases

Protein arginine methyltransferases (PRMTs) belong to an important family of posttranslational modification enzymes that transfer the methyl group from AdoMet (S-adenosyl methionine, SAM) to specific arginine residues in histone or nonhistone protein substrates. Thus far, eleven PRMT members have been identified and are categorized into two major types, type I and type II, according to the substrate and product specificity. (18-20) Type I enzymes (PRMT-1, -2, -3, -4, -6, and -8) catalyze the transfer of the methyl group from AdoMet to one of the terminal nitrogen atoms of the guanidino group of specific arginine residues in a protein substrate, resulting in ω -N^G-monomethylarginine (MMA, L-NMMA) and ω -N^G,N^G-asymmetric dimethylarginine (ADMA) products. (19, 21-24) Type II enzymes (*e.g.*, PRMT 5, 7, and 9) catalyze the formation of MMA and ω -N^G, N^G-symmetric dimethylarginines (SDMA). (24-27) A more recent report demonstrated PRMT7 as a Type III enzyme forming only MMA. (28) The catalytic properties of PRMT-10, and -11 remain to be characterized.

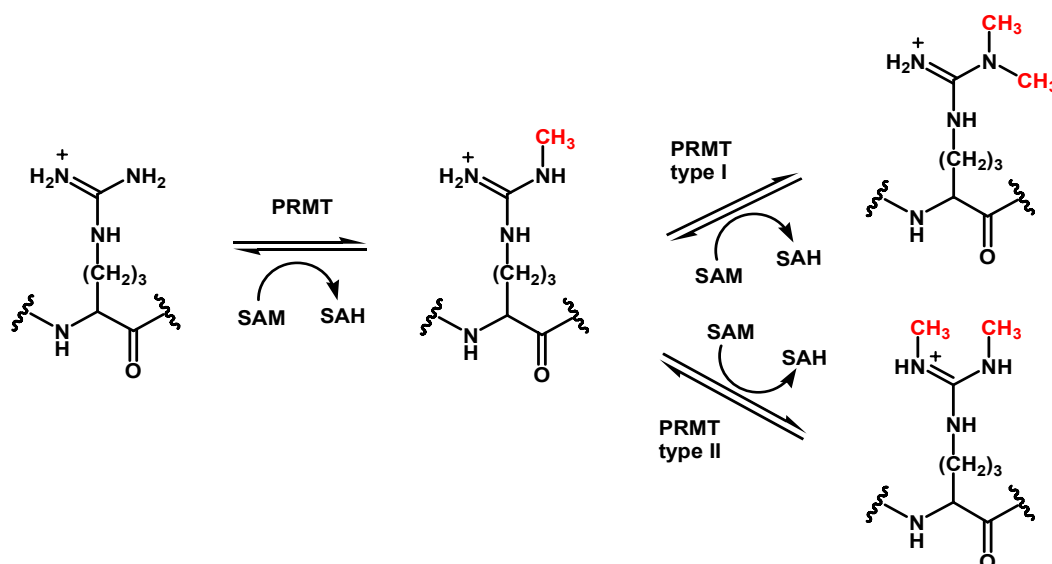


Figure 1.3. Scheme of protein arginine methylation

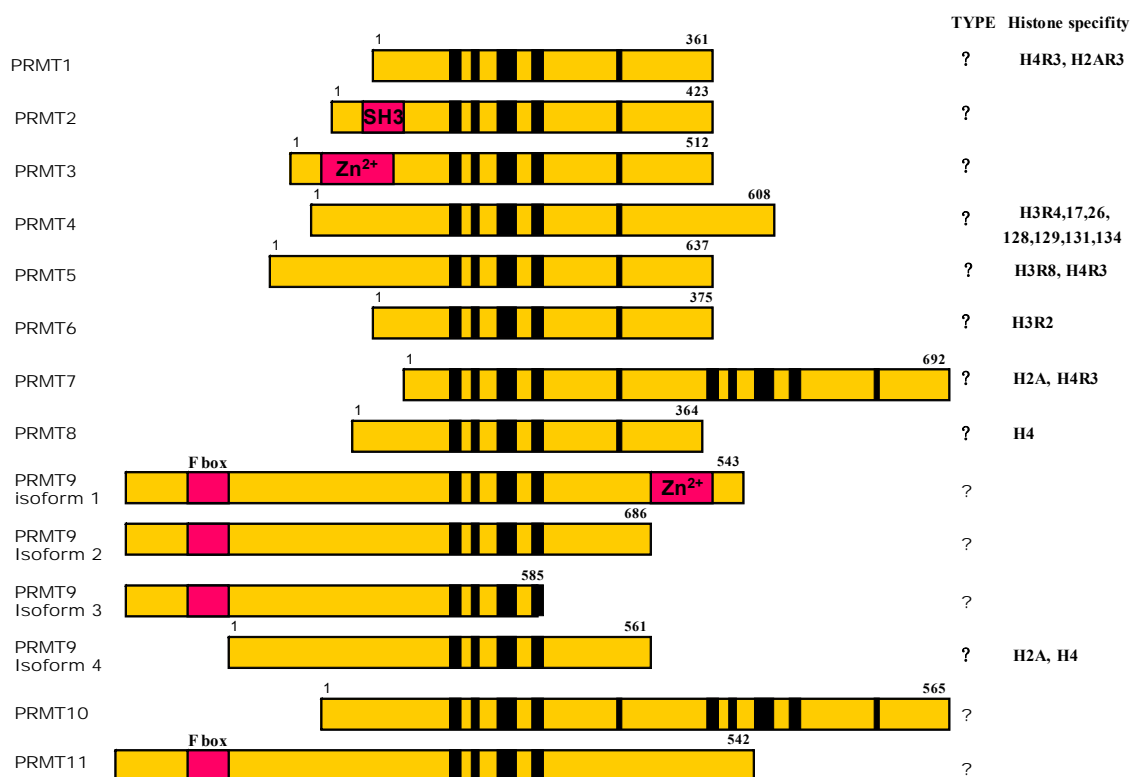


Figure 1.4. Protein arginine methyltransferase family members expressed in human.

Black: conserved catalytic domain. SH3: The SRC homology 3 domain. Zn^{2+} : Zinc finger binding domain. F box: encoding a protein motif of ~ 50 amino acids as a site of protein-protein interaction.

Protein arginine methylation is involved in a broad spectrum of biological processes, including transcriptional activation and repression, mRNA splicing, nuclear–cytoplasmic shuttling, DNA repair, and signal transduction.(29) The variety of PRMTs' cellular activities is partly due to their diverse substrate profiles, including RNA binding proteins (hnRNPa, fibrillarin, nucleolin, etc.), high molecular weight fibroblast growth factor 2 (HMW FGF-2),

interleukin enhancer binding factor 3 (ILF3), and histone H3 and H4. Each PRMT enzyme (PRMT1-9) has a specific set of substrates that partially overlap with the substrates of another family member. The specificity of PRMTs is demonstrated by the fact that only particular arginine residues out of all the arginines in a protein substrate are the target methylation sites.

The substrate specificity of PRMTs is determined by the structure of its active site and peptide binding grooves. PRMT enzymes are composed of a variable N-terminus and a conserved catalytic core; PRMT4 (CARM1) also contains a unique C-terminal region. So far the crystal structures of PRMT1, PRMT3 and PRMT4 (CARM1) are available, which are all type I PRMTs that catalyze the formation of monomethylated and asymmetrically dimethylated arginines.

1.5. Protein arginine methyltransferase 1 (PRMT1)

PRMT1 is the predominant type I protein arginine methyltransferase in mammals. Human PRMT1 gene is located on chromosome 19 (Location: 19q13.3). The protein contains 352 amino acids (AAH19268.2; GI:32425330). There is only one amino acid difference between human and rat PRMT1, that is, the Tyr161 in hPRMT1 is replaced with His in rPRMT1. Since His still bears similar aromatic property as Tyr, we can say that PRMT1 is highly conserved between human and rat species.

The methylation sites in PRMT1 substrates usually fall into RGG or RXR clusters contained within the Gly and Arg rich (GAR) domains. That means the methylation area is of multiple positive charges. Zhang and Cheng (**30**) reported the crystal structure of rPRMT1 bound with product SAH (S-adenosyl homocysteine) and substrate peptide R3 (GGRGGFGGRGGFGGRGGFG). PRMT1 monomer consists of an N-terminus, a SAM binding domain, a barrel-like domain, and a dimerization arm, with the active site pocket lying between

the two catalytic core domains (Figure 1.5A). The AdoMet binding domain adopts a rossmann fold structure that is conserved in other SAM-dependent methyltransferases. SAH is bound in a deep pocket formed by five parallel β strands. The interactions include the Van der Waals contacts between G78 and G80 backbone and SAH homocysteine and adenosine ribose, the bifurcated H-bonds between E100 and the ribose hydroxyl groups, and the H-bond between E129 and the amino group of adenine. Besides, R45 forms salt bridges between the carboxylate group of homocysteine and the active site residue E144, and His 45 interacts with one of the ribose hydroxyl groups through H-bond. The N-terminal helix α X helps to constrain the bound SAH. The barrel-like domain is special to PRMT family. Several conserved residues between the two core domains make up the active site, and form a hairpin between strand β 4 and helix α D. Two conserved glutamates - E144 and E153 on this “double-E loop” hydrogen bond the guanidine group, while the Y148 aromatic ring lies parallel to the hydrophobic methylene groups of the target arginine (Figure 1.5B). E153Q mutation completely abolished methylation activity, while E144Q mutation reduced the activity by 3000 fold, indicating that these two negatively charged glutamates are critical for catalysis. It is proposed that the two invariant glutamates fix the positive charge on the guanidine group on the δ and one of the ω nitrogens, so that the lone pair of electrons left on the other ω nitrogen can attack the active methylsulfonium group of SAM in close proximity. The attacking guanidine nitrogen is deprotonated by a His-Asp relay system. Therefore the active site pH environment can affect the stability of positively charged transition state and thus the catalytic efficiency. This puts electrostatic and steric requirements for the residues besides the target arginine.

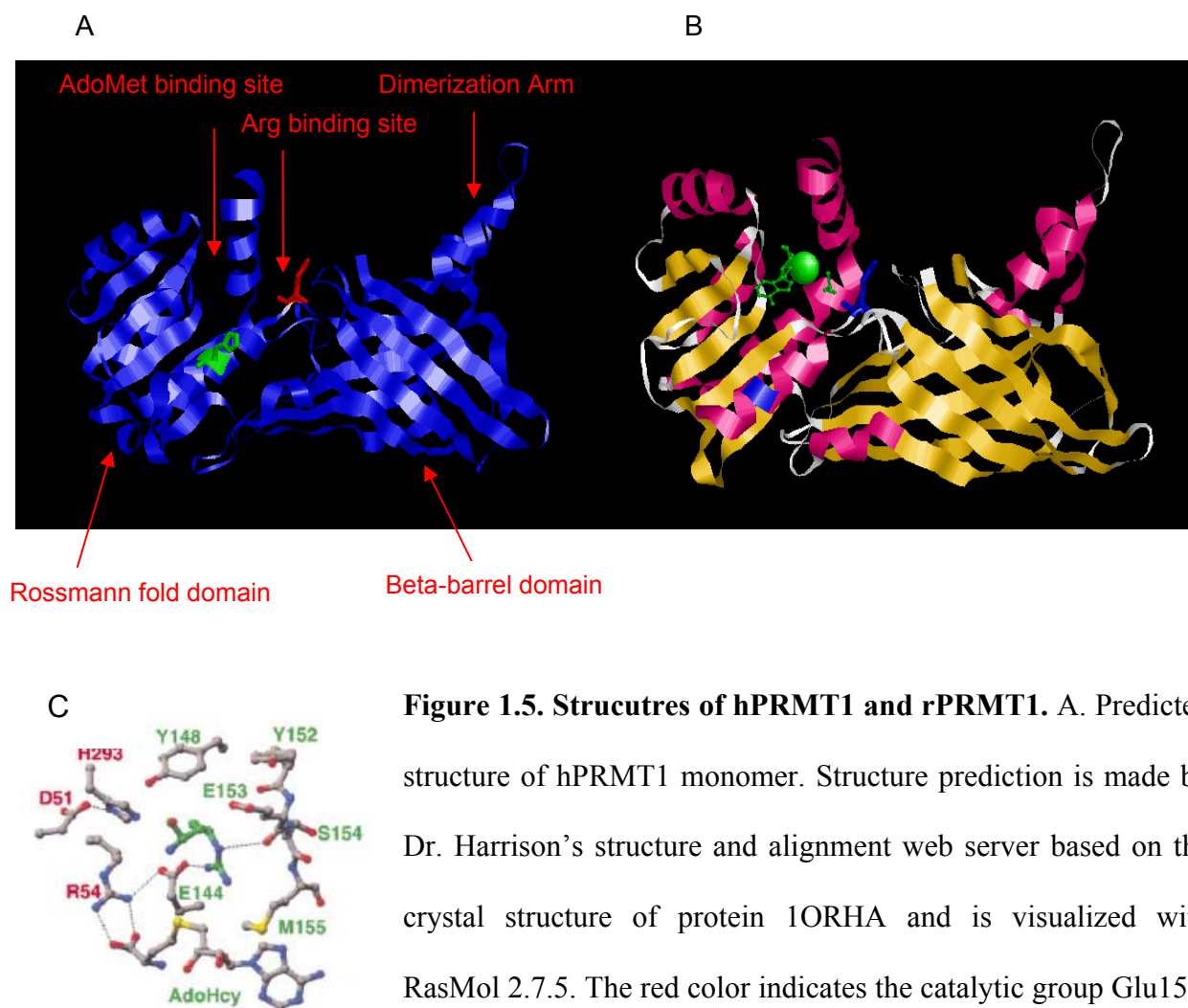


Figure 1.5. Structures of hPRMT1 and rPRMT1. A. Predicted structure of hPRMT1 monomer. Structure prediction is made by Dr. Harrison's structure and alignment web server based on the crystal structure of protein 1ORHA and is visualized with RasMol 2.7.5. The red color indicates the catalytic group Glu153.

The green color indicates the human to rat mutant (Tyr to His) residue, which should be Tyr161 here. B. Reported structure of rPRMT1(E153Q) (PDB/1ORH). Figure made with RasMol 2.7.5. The bound substrate Arginine and product SAH (Sulfur displaced in spacefill to show its close proximity with the terminal nitrogen of Arg) are shown in green; The E153Q mutant and H162 are shown in blue. C. Reported active site structure of rPRMT1 with bound Arginine. **(30)**

PRMT1 functions as dimer or oligomer, as the Δ ARM mutant completely lost catalytic activity, probably because it is unable to bind SAH properly. The dimer interface is formed

between the outer surface of Adomet binding domain and the dimerization arm. Acid residues (20 Asp and Glu) are predominant on the surface of PRMT1, forming several acid grooves which are supposed to generate an initial binding affinity for positively-charged arg substrates. Surface-scanning mutagenesis study indicated that some of these negatively charged residues were important for substrate specificity (E47, E129, and E236), substrate binding (E46 and D51), dimerization/oligomerization, or transcription coactivator function (31). In the crystal structure, the electron densities of bound peptide substrates were broken into three separate fragments (Figure 1.6). Other than the arginine bound in the active site, the amino acid residues of the peptide were not clearly identified due to low resolution of side chain densities. A mixture of peptide binding modes was proposed from the three disconnected densities. The fact multiple substrate binding grooves exist on the surface of PRMT1 may explain why PRMT1 methylates diverse protein substrates. The negatively charged C terminus is close to the active site and may play an important role for substrate binding or catalysis.

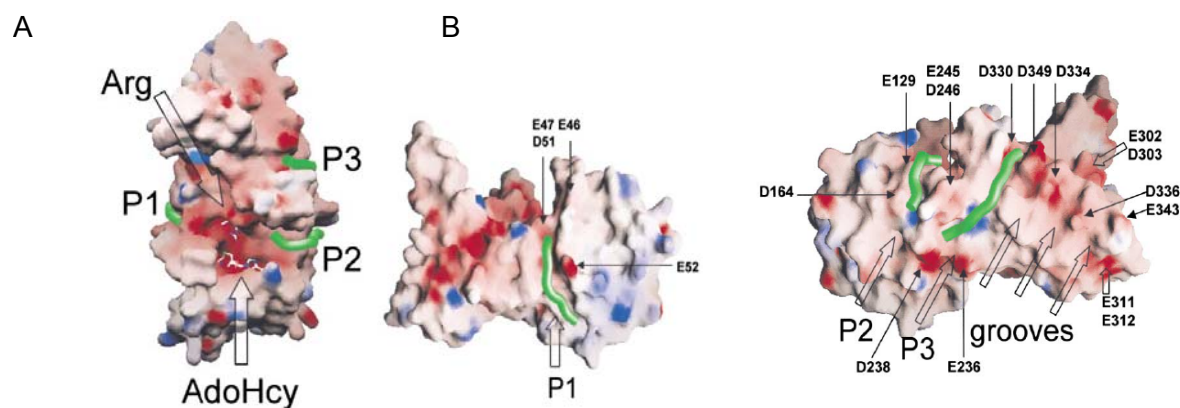


Figure 1.6. Structure of Ternary Complex of PRMT1-AdoHcy-R3 Peptide. (30) A.

Molecular surface of PRMT1 with bound AdoHcy and Arg. P1, P2, and P3 are three peptide

binding sites. B. Two side views of A showing the three peptide binding sites and other acidic grooves.

The crystal structures of PRMT3 and PRMT1 are very similar, with the only difference (beside N terminus) in β barrel domain - a single residue deletion and an eight-residue insertion; yet the structure of CARM1 shows significant difference in the β barrel, the helix-turn-helix of the dimerization arm, and the C-terminal extension which is not present in other PRMTs (32). The crystal structures of the apo and holo CARM1 catalytic core suggested that SAH binding induces a structural change forming a substrate binding channel for the access of arginine to the active site. The N-terminal helices αX and αY , and the first eight residues of the unique C-extension of CARM1 participate in supporting the groove. The central cavity of CARM1 dimer is much larger than that of PRMT1 or PRMT3 dimer, presumably to accommodate the C-extension. CARM1 with deleted C-extension failed to methylate H3 Arg17. Additionally, CARM1 possesses a less acidic surface (only five acidic residues). These may be the reasons why CARM1 methylates a different and smaller substrate profile including histone H3, p300/CBP and several RNA-binding proteins that lack the highly basic GAR domain or any consensus motif. But again as high resolution electron density for a bound peptide in the complex structure is unavailable, the features and specificity subsites within the substrate binding groove that can determine the selective recognition of residues flanking the target arginine haven't been revealed yet.

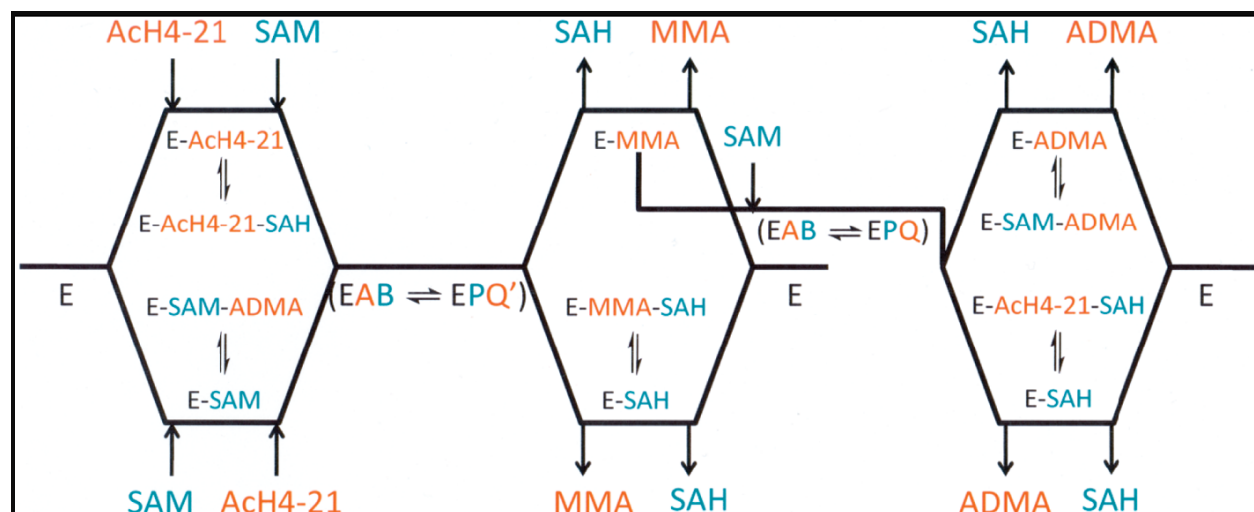


Figure 1.7. Proposed kinetic mechanisms of PRMT1(33)

Several studies of the kinetic mechanism of arginine methylation have been recently reported. Dr. Thompson's group suggested that PRMT1 utilizes a rapid equilibrium random mechanism (RER) for methyl transfer with the formation of dead-end EAP and EBQ complexes (33). However, Dr. Frankel's group showed that PRMT6 follows an ordered sequential mechanism in which SAM binds to the enzyme first and the methylated product is the first to dissociate (34). The different results in these two studies suggest that kinetics of arginine methylation can vary slightly among the individual isoforms.

1.6. The study points in this work

1.6.1. The development of fluorescent peptide probes for PRMT1

PRMTs play important roles in normal physiology and human diseases. Simple, rapid, non-radioactive, colorimetric/fluorescent assays are particularly needed for the enzymatic study of PRMTs and for the identification of potent PRMT inhibitors. The design of non-radioactive PRMT assays, however, is technically challenging because the substrates and products of PRMTs exhibited little spectroscopic difference.(35) Recently, several coupled

colorimetric and fluorescent methods are reported to study SAM-dependent methyltransferases, including PRMTs. In these methods, the enzymatic methylation reaction is carried out in conjugation with secondary enzymes that convert SAH to adenine and then hypoxanthine, a spectrometrically active compound,(35) or to homocysteine which is subsequently detected by thiol-reactive chromogenic/fluorogenic compounds.(36-38) The major advantage of the coupled methods is that they avoid using radioisotope-labeled materials and allow for the measurement of PRMT activity via absorption or fluorescent readouts. However, these methods involve multiple additional components which may potentially complicate the methylation results. Especially, when used for inhibitor screening, there is a high chance that the coupling components may be intervened thus leading to positive hits. Therefore, new alternative methods are highly demanded to serve as research tools to elucidate the functions of PRMTs in health and disease as well as to facilitate the discovery of PRMT inhibitors. Thus we tried to design and evaluate a fluorescent competitive binding assay of PRMT1 for both basic kinetic analysis and inhibition study. The fluorescent displacement strategy is particularly useful to probe PRMT-substrate interactions, and thus finding application in screening organic inhibitors that target the substrate-binding pocket of PRMTs. Importantly, by applying this method, we elucidated the inhibitory mode of AMI-1, a potent PRMT inhibitor, the mechanism of which was unknown.

To create the fluorescent reporters that can be used for non-radioactive PRMT binding assay, we synthesized fluorescein-labeled peptides based on two different substrates of PRMT1. First, PRMT1 and several other PRMT members are reported to robustly methylate a number of GAR motifs which frequently occur in RGG repeats of proteins such as fibrillarin and nucleolin.(23, 39) Herein, we synthesized a fluorescent GAR-rich peptide (R4-FL) which

contains a fluorescein labeling on a lysine residue. In addition, PRMT1 was previously shown to methylate histone H4 at the R3 residue.(26, 40, 41) In this case, we used a fluorescein-labeled H4 peptide, H4-FL,(42) based on the N-terminal 20-aa sequence of histone H4. The fluorescein group was linked at position 10 through a 2,3-diaminopropionic acid residue (Dpr). Fluorescein was selected as the reporter group because it has long absorption and emission wavelengths and its photophysical properties are relatively sensitive to local microenvironment. We rationalized that fluorescent signals (e.g., intensity, anisotropy) change accordingly when these small peptide ligands bind to and/or are methylated by PRMT1, and that when the interaction between PRMT1 and the ligand is disrupted, there is a recovery of fluorescent signal.

1.6.2. The inhibition study of PRMT1

Given the essential roles that PRMTs play in normal biology and in disease, quite a few efforts have been invested in developing small molecule PRMT inhibitors both as chemical genetic tools and as therapeutic agents.(43-45) The first type of chemical inhibitors for PRMTs are analogues of the AdoMet cofactor, including *S*-adenosylhomocysteine (SAH), methylthioadenosine, and sinefungin.(44) Due to structural similarities to AdoMet, these analogue inhibitors target all AdoMet-consuming methyltransferases, such as DNA methyltransferases, protein lysine methyltransferases, and O-methyltransferases. In the past few years, several groups reported their work in a row on developing small molecule inhibitors specific for PRMTs. Most of these studies on PRMT inhibitor discovery adopted targeted or random screening approaches. The screening strategy is so widely accepted largely because of technical advancement in computer-aided drug design and in medium- and high-throughput inhibitor screening. Thus far, the disclosed small molecule PRMT inhibitors include **1** (AMI-

1),(46) stilbamidine and allantodapsone,(47) the thioglycolic amide RM65,(48) pyrazole amide compounds,(49) and others.(50-54) It is important to point out that past inhibitor development efforts were mostly focused on inhibition of the enzyme, presumably, through binding to the active site. This is also the case with the vast majority of enzyme inhibition work reported related to other enzymes so far. Because a single PRMT catalyzes the methylation of arginine residues in multiple proteins, inhibition of a particular PRMT inevitably results in bulky inhibition of methylations of a large number of proteins, but not on a particular substrate sequence. Herein, we report a type of compounds that block PRMT1-mediated arginine methylation at micromolar potency through a unique mechanism. Most of the discovered compounds bear naphthalene and sulfonate groups and are structurally different from typical PRMT substrates, *e.g.*, histone H4 and glycine- and arginine-rich sequences. To elucidate the molecular basis of inhibition, we conducted a variety of kinetic and biophysical assays. The combined data reveal that this type of naphthyl-sulfo (NS) molecules directly targets the substrates but not PRMTs for the observed inhibition. We also found that suramin effectively inhibited PRMT1 activity. These findings about novel PRMT inhibitors and their unique inhibition mechanism provide a new way for chemical regulation of protein arginine methylation.

1.6.3. The transient-state kinetics and catalytic mechanism of PRMT1

Transient state is at the very beginning of a reaction when the enzyme and the substrate is trying to meet each other and the concentration of reactive E-S complex and the reaction rate are changing as a function of time. It occurs before steady state when the formation and breakdown of E-S complex reach an equilibrium and the maximum reaction rate is constant with time.

The functions of PRMTs have been broadly studied in different biological processes and diseased states, but the molecular basis for arginine methylation is not well defined. Many

important questions about the PRMT-catalyzed arginine methylation reaction remain to be answered. For instance, it is not known whether the chemical step or a protein conformational change in the ES complex is rate-limiting for catalysis. Such a molecular level understanding of how substrate recognition is coupled to catalysis will be of great significance to evaluate the function of PRMT activity in different physiological contexts. To address these mechanistic questions, transient kinetic analyses of arginine methylation are highly desirable. Unfortunately, such studies are greatly limited by lack of assay tools appropriate for fast measurement of substrate binding and methylation on rapid time-scales. Here we studied the transient-state kinetic analysis of PRMT1 catalysis using stopped-flow fluorescence measurement with fluorescein-labeled peptide substrates. The fast association and dissociation rates suggest that PRMT1 catalysis of histone H4 methylation follows a rapid equilibrium sequential kinetic mechanism. The data give direct evidence that the chemistry of methyl transfer is the major rate-limiting step, and that binding of the cofactor SAM or SAH affects the association and dissociation of H4 with PRMT1. Importantly, from the stopped-flow fluorescence measurements, we have identified a critical kinetic step suggesting a precatalytic conformational transition induced by substrate binding. These results provide new insights into the mechanism of arginine methylation and the rational design of PRMT inhibitors.

1.6.4. The interaction between lysine acetylation and arginine 3 methylation on H4 tail

It has become an increasing recognition that multiple PTM marks at the amino-terminal tails of the core histones intercommunicate with one another to fundamentally regulate DNA functions such as transcription, replication, recombination and damage repair (5, 55). At the molecular level, how individual PTM patterns or codes are created and how they affect downstream molecular events are poorly defined. More studies are needed to address the

communicational relationship between functionally related histone modification marks. Acetylation of H4 at its N-terminal tail is commonly seen in many cell types. With 16 possible acetylation combinations, cells may benefit by utilizing such combinatorial modification tricks to fine tune and/or maximize multivalent readouts for diversified functionality. In this study, we investigated in detail the impact of individual acetylation marks at K5, 8, 12, 16, and their different combinations on type I and type II methylation at site R3. It was previously shown that H4 acetylation reduced PRMT1-mediated R3 methylation (40). However, it is not clear how individual acetylations combinatorially affect R3 methylation and which acetylation site plays a predominant role in affecting R3 methylation. Furthermore, R3 can be either asymmetrically dimethylated or symmetrically dimethylated. It remains unknown whether lysine acetylation affects these two types of methylation in the same or distinct manners. To answer these mechanistic questions, we created a library of H4 peptides containing all the possible acetylated isoforms. The concentration of each peptide was calibrated with NMR to obtain the accurate concentration prior to the enzymatic methylation experiments. Our data reveal that the effect of lysine acetylation on arginine methylation depends on the site of acetylation and the type of methylation. While certain acetylations bring a repressive impact on PRMT-1 mediated methylation, lysine acetylation generally is correlated with enhanced methylation by PRMT5. Furthermore, circular dichroism study and computer simulation demonstrate that hyperacetylation increases the content of ordered secondary structures at the H4 tail region. These findings provide new insights into the regulatory mechanism of Arg-3 methylation by H4 acetylation, and unravel that complex intercommunications exist between different PTM marks *in cis*. The divergent activities of PRMT1 and PRMT5 with respect to different acetyl-H4

substrates suggest that type I and type II PRMTs use distinct molecular determinants for substrate recognition and catalysis.

CHAPTER 2

INHIBITORY STUDY OF PROTEIN ARGININE METHYLTRANSFERASE 1 USING A FLUORESCENT APPROACH

(This work is mainly based on the published paper *Biochem. Biophys. Res. Commun.* 379 (2009) 567-72. In this project, the author is obliged to Dr. Nan Xie, Dr. Jiang Wu, and Chao Yang for their great contributions to peptide preparation.)

2.1. Introduction

Protein arginine methylation has emerged as an important regulatory mechanism for gene expression and cellular signalling (18-20). The methylation is catalyzed by protein arginine methyltransferases (PRMTs) that transfer the methyl group from S-adenosyl-L-methionine (AdoMet, SAM) to specific arginine residues in histone and nonhistone protein substrates, resulting in mono and di-methylated arginine residues and S-adenosyl-L-homocysteine (AdoHcy, SAH). It has been shown that PRMTs are involved in the regulation of diverse biological processes such as DNA transcription, RNA processing, DNA repair, and cell differentiation (24, 56-58). As the predominant PRMT protein in mammalian cells, PRMT1 (HRMT1L2) accounts for 85% of cellular PRMT activity (59). Notably, deregulation of PRMT1 has been linked to certain diseases such as breast cancer and leukaemia (60, 61), which suggests its role as a potential drug target.

Rapid, homogeneous, nonradioactive, and colorimetric or fluorescent assays are particularly needed for the kinetic analysis of PRMTs and for the identification of potent PRMT inhibitors. The design of nonradioactive PRMT assays, however, is technically challenging because the substrates and products of PRMTs exhibited little spectroscopic difference (35). Recently, several coupled colorimetric and fluorescent methods were reported to study SAM-

dependent methyltransferases, including PRMTs. In these methods, the enzymatic methylation reaction is carried out in conjugation with secondary enzymes that convert SAH to adenine and then hypoxanthine, a spectrometrically active compound (35), or to homocysteine which is subsequently detected by thiol-reactive chromogenic or fluorogenic compounds (36-38). The major advantage of the coupled methods is that they avoid using radioisotope-labeled materials and allow for the measurement of PRMT activity via absorption or fluorescent readouts. However, these methods involve multiple additional components which may potentially complicate the methylation results. Especially, when used for inhibitor screening, there is a high chance that the coupling components may also be inhibited thus leading to false positives. Therefore, new and alternative methods are highly needed to serve as research tools to elucidate the functions of PRMTs in health and disease as well as to facilitate the discovery of PRMT inhibitors.

In this paper, we report our work of designing peptide-based fluorescent reporters and using them for biochemical analysis and inhibition study of PRMT1. These fluorescent ligands are proved to be effective to probe PRMT-substrate interaction with dual modes of fluorescence intensity and fluorescence anisotropy, thus suited for studying organic inhibitors that target the substrate-binding pocket of PRMTs. By applying the fluorescent reporters in combination with radioactive methylation assay, we elucidated the inhibitory mechanism of AMI-1, the first reported small molecule PRMT inhibitor (46).

2.2. Results and discussion

2.2.1. Expression and purification of PRMT1

6×His-tagged rat PRMT1 was successfully expressed with BL21(DE3) and purified by Ni affinity chromatography. As shown in Figure 2.1, a major band of relatively pure PRMT1 was obtained, which can be used directly in the kinetic study.

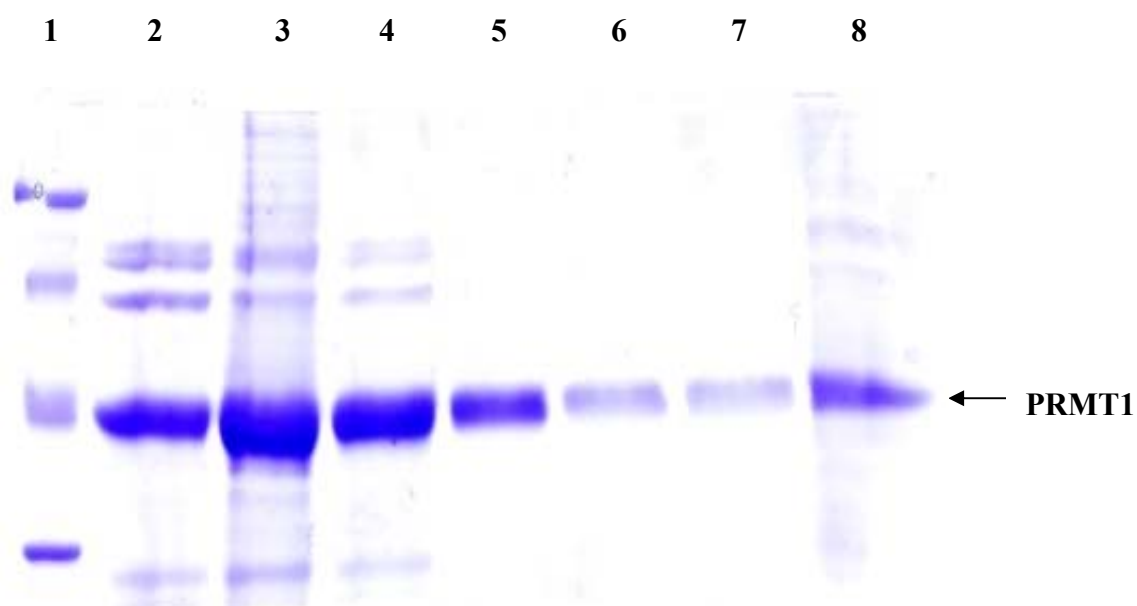


Figure 2.1. SDS-PAGE of rPRMT1 after purification

1. Marker. 2. 70 mM imidazole washing. 3. Beads before elution. 4. 200 mM imidazole eluant1. 5. 200 mM imidazole eluant2. 6. 200mM imidazole eluant3. 7. 200 mM imidazole eluant4. 8. Beads after elution.

2.2.2. Design and synthesis of the fluorescent PRMT1 reporters

To create the fluorescent reporters that can be used for nonradioactive PRMT study, we synthesized fluorescein-labeled peptides based on two different substrates of PRMT1. First, PRMT1 and several other PRMT members are reported to robustly methylate glycine and

arginine-rich (GAR) motifs which frequently occur in RGG repeats of proteins such as fibrillarin and nucleolin (23, 39). Herein, we made a fluorescent GAR-rich peptide (R4-FL) which is labeled with fluorescein through a lysine residue (Table 2.1). Apart from methylating GAR motifs, PRMT1 also methylates histone H4 at the R3 site (26, 40, 41). We synthesized a labeled H4 peptide, H4-FL (42), by modifying the N-terminal 20-aa sequence of histone H4 with fluorescein at position 10 through a 2,3-diaminopropionic acid residue (Dpr). Fluorescein was selected as the reporter group because it has long absorption and emission wavelengths and its photophysical properties are relatively sensitive to the local microenvironment. We envisioned that the fluorescent signals (e.g., intensity, anisotropy) of fluorescein might change accordingly when the peptide ligands bind to and/or are methylated by PRMT1. Synthesis of these peptidyl compounds was achieved using the Fmoc-based solid phase peptide synthesis protocol.

Table 2.1. Sequences of H4, H4-FL, R4, and R4-FL

Peptide	Sequence	Expected mass	Observed mass
H4	Ac-SGRGKGGKGLGKGGAKRHRK	2034.4	2034.1
H4-FL	Ac-SGRGKGGKGDpr(FL)GKGGAKRHRK	2366.7	2366.4
R4	Ac-GGRGGFGGRGGKGGRRGGFGGRGGFG	2223.4	2223.2
R4-FL	Ac-GGRGGFGGRGGK(FL)GGRGGFGGRGGFG	2582.4	2581.3

2.2.3. Fluorescence response of the PRMT1 reporters

We first tested whether the fluorescence intensity of fluorescein can change upon ligand-enzyme interaction. His₆x-tagged recombinant rat PRMT1 was expressed in *E. coli* and purified on Nickel-NTA beads. As shown in Figure 2.2, the fluorescence intensity of both H4-FL and R4-FL decreases at increasing concentrations of rPRMT1. The magnitude of the change at the

maximum emission wavelength (524 nm) is approximately 25%. Such a fluorescence intensity change most likely reflects that the microenvironment surrounding the fluorescein group is altered after ligand-PRMT1 binding. The molecular factors causing such alteration may include hydrophobicity variation, prototropic shift, and the presence of new hydrogen bonding with PRMT1 (62, 63).

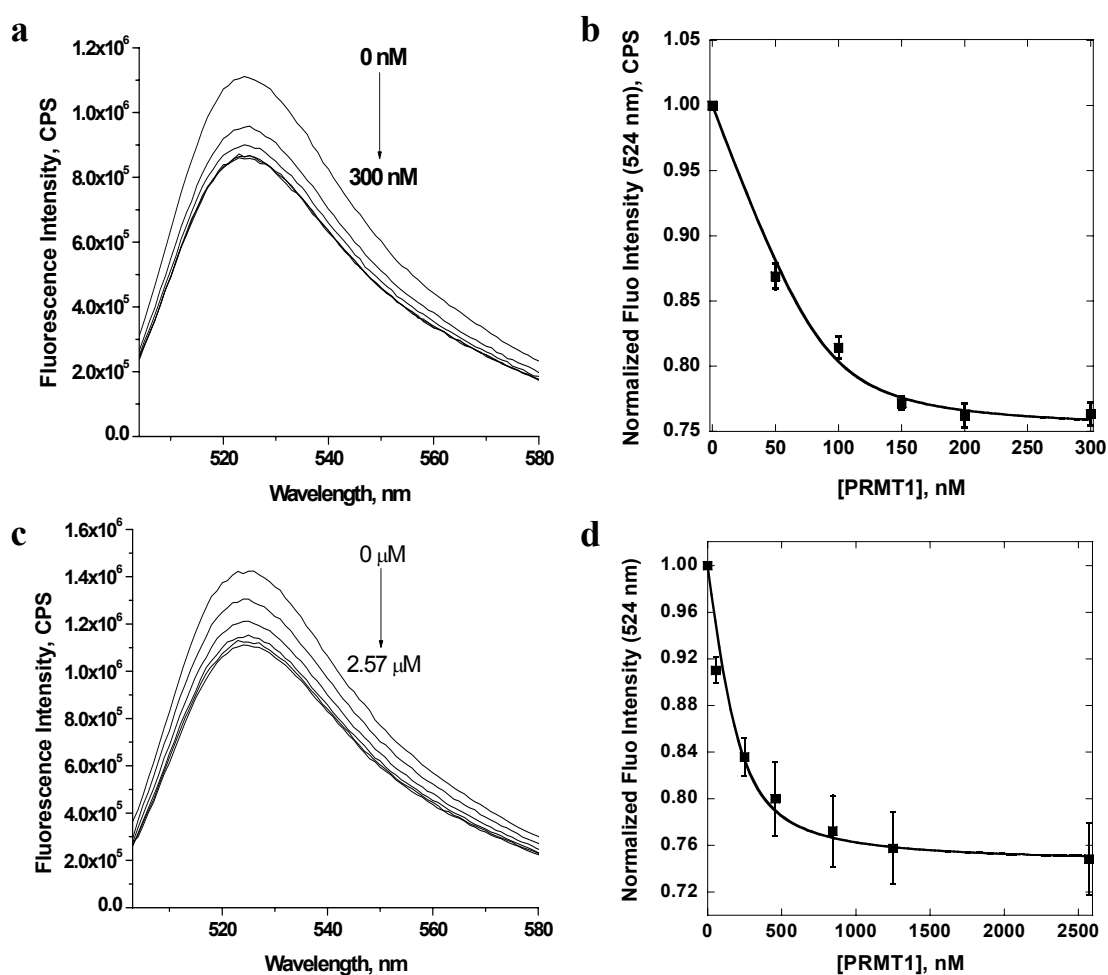


Figure 2.2. Fluorescence intensity changes of H4-FL and R4-FL upon interaction with PRMT1. (a) Emission spectra obtained for H4-FL (0.20 μM) with increasing concentrations (0, 0.05, 0.10, 0.15, 0.20, and 0.30 μM) of PRMT1. (b) Plot of the fluorescence

intensity of H4-FL at 524 nm as a function of PRMT1 concentration. (c) Emission spectra obtained for R4-FL (0.20 μM) with increasing concentrations (0, 0.05, 0.25, 0.84, 1.25, and 2.57 μM) of PRMT1. (d) Plot of the fluorescence intensity of R4-FL at 524 nm as a function of PRMT1 concentration.

It is an intriguing question whether the reporter molecules can be used to probe the catalytic process of PRMT1. To investigate this possibility, we mixed R4-FL with PRMT1 in the presence of AdoMet and monitored the fluorescence emission at 524 nm at different time points. As shown in Figure 2.3, the fluorescence intensity of R4-FL first decreases rapidly and then gradually goes up. It is quite likely that the first phase (*i.e.* the rapid fluorescence decrease) corresponds to substrate binding and the second phase (*i.e.* the gradual fluorescence increase) corresponds to the methyl transfer and/or product release. A detailed stopped flow study will reveal more information about this complex process. To our knowledge, this is the first example of reporting a simple fluorescent approach that can be used to examine the pre-steady state kinetics of PRMT catalysis. Interestingly, the analog inhibitor, sinefungin, is only able to inhibit the methylation step, suggesting that its inhibition of PRMT1 is not competitive against the peptide substrate.

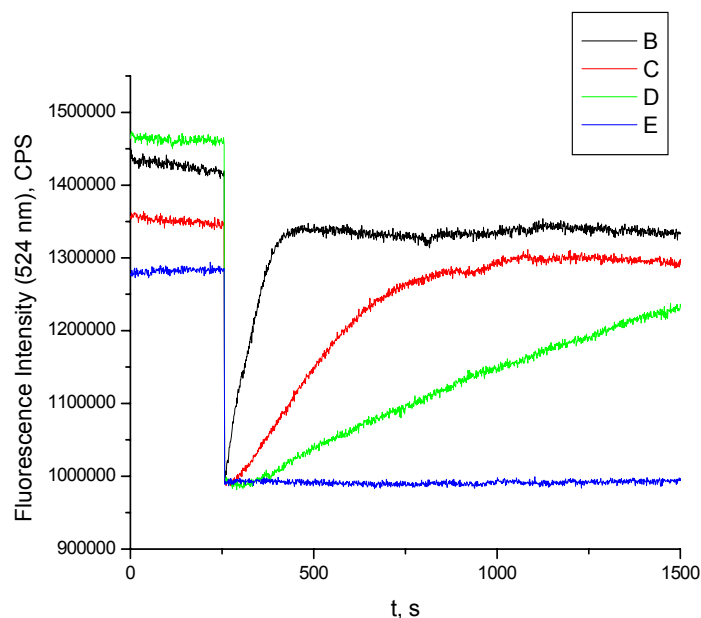


Figure 2.3. Inhibition Effect of Sinefungin on PRMT1 methylation.

B: 0 μM sinefungin, C: 5 μM sinefungin, D: 15 μM sinefungin, E: 50 μM sinefungin. 0.4 μM of PRMT1 is added to the mixed solution of R4-FL (0.2 μM) and Sinefungin (0 μM , 5 μM , 15 μM or 50 μM). The dropping curve shows the binding of R4-FL and PRMT1, and the raising curve shows the methylation of R4-FL.

We next examined the fluorescence anisotropy of H4-FL and R4-FL in the presence of PRMT1. It is expected that, when bound to PRMT1, the molecular mobility of the organic ligands will be in a more restricted state due to the complex formation, which will give rise to larger anisotropy readouts. Indeed, our data showed that the fluorescence anisotropy of both H4-FL and R4-FL increases as a function of PRMT1 concentration (Figure 2.4). The maximal magnitudes of the anisotropy enhancement are 100% and 300% for H4-FL and R4-FL, respectively, which are much larger than that of the fluorescence intensity change. Thus, the

fluorescence anisotropy or polarization of H4-FL and R4-FL is better suited than fluorescence intensity for use in screening PRMT1 inhibitors. It should be noted that the dynamic range in anisotropy could be further increased by using recombinant PRMT1 that contains more bulky tags such as GST or by reducing the size of the reporter ligands.

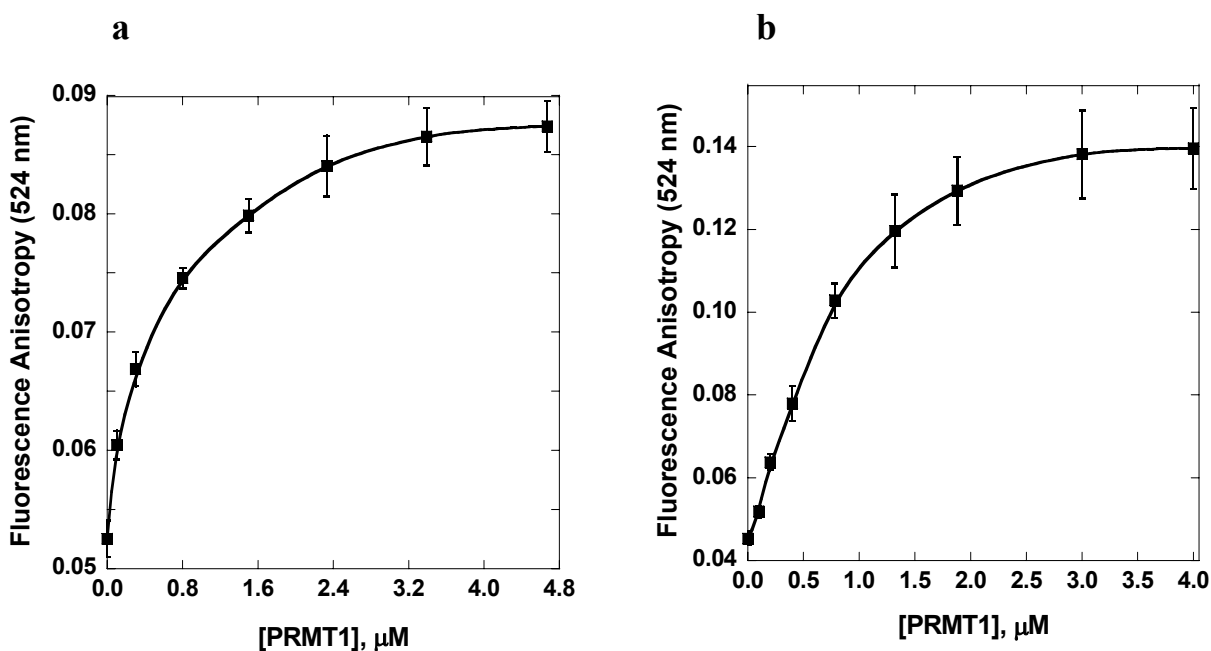


Figure 2.4. Fluorescence anisotropy titration. (a) Fluorescence anisotropy (524 nm) of H4-FL solution at different PRMT1 concentrations. The concentration of H4-FL is 0.20 μM. The K_d is calculated to be 0.31 ± 0.04 μM. (b) Fluorescence anisotropy (524 nm) of R4-FL solution at different PRMT1 concentrations. The concentration of R4-FL is also 0.20 μM. The K_d is calculated to be 0.40 ± 0.07 μM.

A minor concern is that the added fluorophore might interfere with the interaction of H4 and R4 peptides with PRMT1, thus compromising the methylation reaction. To investigate this

effect, we measured the steady state kinetic parameters of PRMT1 for both the labeled and non-labeled peptides. ^{14}C -labeled AdoMet was used as the methyl donor in the assay. The methylated products were loaded onto P81 paper and quantified by scintillation counting. As shown in Table 2.2, the K_m of H4-FL and R4-FL, respectively, doubled that of H4 and R4, while the k_{cat} values decreased by half. The largest effect was only a 3-4 fold difference in the specificity constants (V/K). The comparisons of these kinetic parameters suggest that the attached fluorescein group moderately affects the methylation of the peptide substrates by PRMT1, and overall, these labeled ligands are still reasonably good substrates of PRMT1.

Table 2.2. Steady state kinetic parameters of rPRMT1 in the methylation of H4, R4 and their fluorescent derivatives. The concentration of PRMT1 and AdoMet is 0.01 μM and 30 μM , respectively.

substrate	K_m , μM	k_{cat} , min^{-1}	k_{cat}/K_m , $\text{min}^{-1}\mu\text{M}^{-1}$
H4	0.64 ± 0.04	0.81 ± 0.01	1.27 ± 0.08
H4-FL	1.14 ± 0.13	0.43 ± 0.01	0.38 ± 0.04
R4	0.90 ± 0.06	0.69 ± 0.01	0.77 ± 0.05
R4-FL	1.84 ± 0.56	0.45 ± 0.05	0.24 ± 0.08

2.2.4. Inhibitory study of AMI-1 using the fluorescent strategy

After having assessed the fluorescent responses of H4-FL and R4-FL upon interaction with PRMT1, we applied the reporters to probe the interaction of PRMT1 with AMI-1, the first reported small-molecule PRMT inhibitor that was discovered by Bedford and co-workers.⁽⁴⁶⁾ AMI-1 inhibits several PRMTs (PRMT1,-3,-4,-6 and Hmt1p) and bears no similarity to AdoMet

analogues. The mechanism by which AMI-1 inhibits the enzymatic activity of PRMTs is still not identified. Due to certain structural similarity to peptidyl arginine, it was speculated that AMI-1 may bind to the substrate-binding pocket of the PRMT enzymes (46), but a recent docking study suggested that AMI-1 might interact with residues of the AdoMet binding pocket (48). To elucidate the inhibitory mode of AMI-1, we examined the interaction of AMI-1 with PRMT1 using our fluorescent reporters. As shown in Figure 2.5, the fluorescence anisotropy of both H4-FL/PRMT1 and R4-FL/PRMT1 mixtures decreases at increasing concentrations of AMI-1, indicating that the fluorescent ligands are displaced from binding to PRMT1 by the inhibitor. The inhibition constant (K_i) of AMI-1 in these two competitive assays is calculated to be $15.8 \pm 3.5 \mu\text{M}$ and $19.8 \pm 3.1 \mu\text{M}$, respectively, using the method of Nikolovska-Coleska, *et al.*(64). This evidence demonstrates that AMI-1 targets the same binding pocket in PRMT1 with the H4 and R4 substrates. It also suggests that histone H4 and RGG-rich substrates may bind to PRMT1 in a similar structural manner.

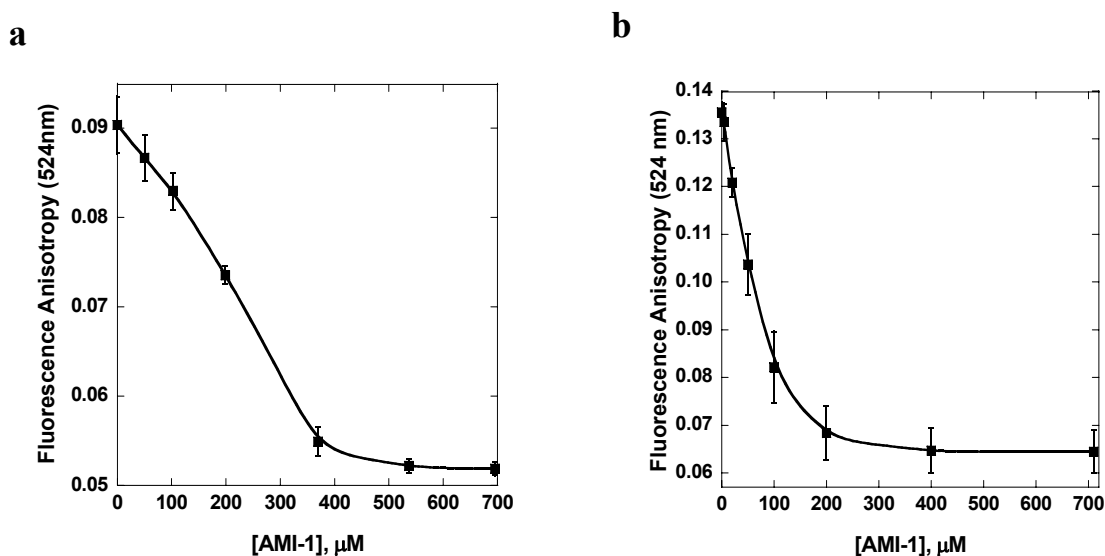


Figure 2.5. Competitive inhibition assays of AMI-1 against H4-FL (a) and R4-FL (b) using the mode of fluorescence anisotropy. The reporter and PRMT1 concentration is 2.00 μM and 4.00 μM for H4-FL assays and 0.20 μM and 2.00 μM for R4-FL assay.

To further substantiate the inhibitory mode of AMI-1, we investigated the inhibition pattern of AMI-1 versus AdoMet and the peptide substrates using radioisotopic assay. Initial velocities of PRMT1 were determined, and the data were plotted in double-reciprocal form with $E/\text{velocity}$ versus $1/[\text{H4}]$, $1/[\text{R4}]$, and $1/[\text{AdoMet}]$, respectively, at several fixed concentrations of AMI-1 (Figure 2.6). The results show that AMI-1 is a linear competitive inhibitor versus H4 (and also R4, data not shown), while is noncompetitive (mixed type) versus AdoMet. The K_i of AMI-1 from the competitive kinetic assay (Figure 2.6a) is calculated to be 17.7 μM , which is consistent with the results obtained from the fluorescence anisotropy competitive binding measurement. These data indicate that AMI-1 competes with the protein/peptide substrate, but not AdoMet, for the same form of PRMT1 and the same mutually exclusive binding site, thus further validating the conclusion that AMI-1 inhibits the methylase activity of PRMT1 by blocking the access of protein/peptide substrates.

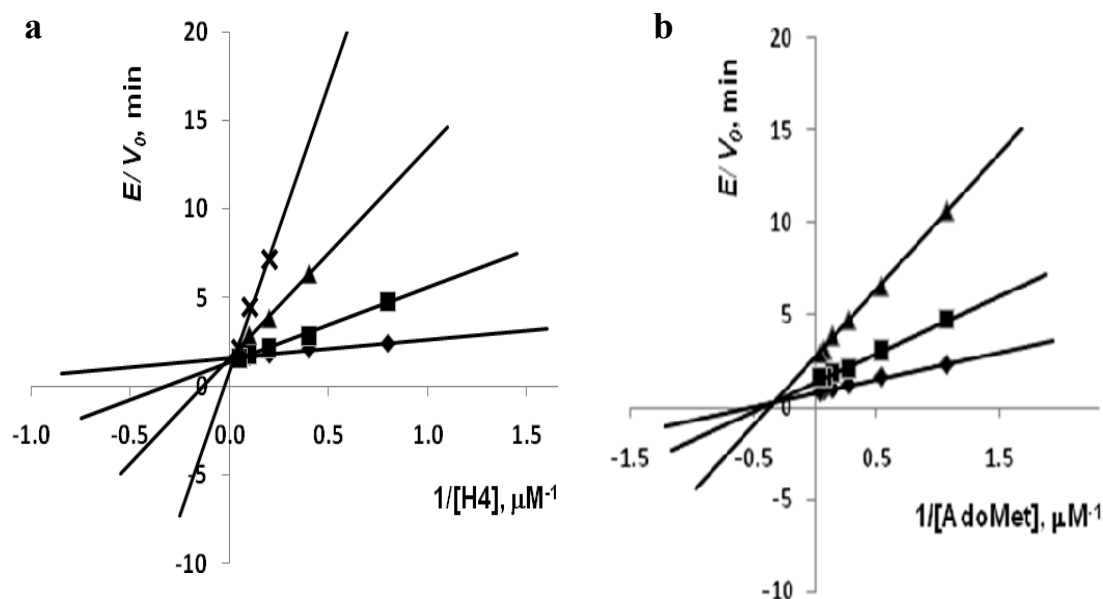


Figure 2.6. Inhibition pattern analysis of AMI-1 to PRMT1 plotted as reciprocal plots. a. E/V_0 versus $1/[H4]$ at fixed AdoMet ($5 \mu\text{M}$) and varying AMI-1: $0 \mu\text{M}$ (\blacklozenge), $50 \mu\text{M}$ (\blacksquare), $100 \mu\text{M}$ (\blacktriangle), and $200 \mu\text{M}$ (\times). The inhibition plot of AMI-1 against R4 was similar to that of H4 and is not shown. b. E/V_0 versus $1/[AdoMet]$ at fixed H4 ($2 \mu\text{M}$) and varying AMI-1: $0 \mu\text{M}$ (\blacklozenge), $50 \mu\text{M}$ (\blacksquare), and $100 \mu\text{M}$ (\blacktriangle).

There are several valuable merits about the fluorescent competitive binding assay developed herein. First, it is simple, thus avoiding complications caused by using coupling components. Second, this displacement strategy is geared to target compounds that block PRMT-substrate interaction, which is directly associated with methylase activity. Since GAR motif-containing sequence is a known common feature of substrates for many PRMTs,⁽²³⁾ R4-FL is not only a fluorescent reporter of PRMT1, but will be applicable to other PRMT members as well. Third, since the assay is independent of the enzymatic activity, the strength of the methylase activity of PRMTs does not directly influence the assay. This catalytic activity-

independent feature is particularly important for PRMTs since many recombinant PRMT enzymes exhibited very weak methylase activities, so that it is difficult to characterize the PRMT enzymatic reaction in a practical manner. For example, recombinant mouse PRMT4/CARM1 also methylates a RGG-repeat sequence,(65) but its activity is so low that no adequate readable signals would be produced using a coupled assay method within regular assay time frame (usually less than one hour). Therefore, although the fluorescence anisotropy/intensity measurement is not a direct detection of PRMT enzymatic activity, our strategy complements and offers unique advantages over the current PRMT assay toolkits, and will be particularly useful to study and screen potent PRMT inhibitors.

2.3. Conclusion

We demonstrated the use of single fluorophore-labeled reporters to examine the substrate binding and methylase activity of PRMT1. This method will be of wide application in studying protein-substrate interactions and in screening PRMT inhibitors. By combining the fluorescent assay with radioactive measurement, we established the inhibitory mechanism of AMI-1; *i.e.*, it inhibits the enzymatic activity of PRMT1 by dislodging protein/peptide substrates out of the binding pocket in the enzyme. Furthermore, we showed that the fluorescence intensity of R4-FL is sensitive to the progression of both substrate binding and methylation, suggesting that it will be a useful fluorescent probe to investigate the transient kinetic mechanism of PRMT catalysis.

2.4. Experimental

2.4.1. Synthesis of the fluorescent reporters.

Solid Phase peptide synthesis (SPPS) was performed on a PS3 peptide synthesizer (Protein Technologies) using the Fmoc (N-(9-fluorenyl) methoxycarbonyl) strategy. Fmoc-

protected amino acids, Rink amide resin and Pre-loaded Wang resin were purchased from NovaBiochem. All the synthetic reactions were performed at room temperature unless indicated otherwise. Removal of Fmoc was performed with 20 % v/v piperidine/DMF. For the coupling of each amino acid (AA), 4 eq. of AA/HBTU/HOBt (N-Hydroxybenzotriazole) were used. N-methylmorpholine (NMM) was used as the catalytic base. The N-terminal amino group was acetylated with Ac₂O unless indicated otherwise. The Dde (dimethyldioxocyclohexylidene) group on the lysine residue was removed with a solution of 2% hydrazine in DMF (66), and then the free amino group reacted with fluorescein-OSu for fluorophore labeling. After solid phase synthesis, the resins were subsequently washed with DMF, dichloromethane and then dried in vacuum for at least 2h before cleavage. Peptides were cleaved from resin by treatment with 95% TFA, 2.5% H₂O and 2.5 % triisopropylsilane (handling of TFA must be performed in a secure hood) for 3-4h. Cold ether was used to precipitate the products. Crude products were collected by centrifugation and were washed with cold diethyl ether. After lyophilization, the compounds were re-dissolved in water and purified with reverse-phased (RP) HPLC (C18, Varian) on a Varian Prostar HPLC system using linear gradients of H₂O/0.05% TFA (solvent A) vs. acetonitrile/0.05% TFA (solvent B). Analytical HPLC and MALDI-MS were used for characterization.

2.4.2. Enzymatic methylation assay.

Recombinant His₆x-tagged rat PRMT1 enzyme was expressed using a pET28b vector in *E. coli* and purified on nickel-NTA beads. The methylation buffer contained 50 mM HEPES (pH = 8.0), 0.5 mM DTT, 1 mM EDTA, and 50 mM NaCl. Methylation assays of H4 and R4 were carried out in 0.5 mL plastic tubes at 30°C with a reaction volume of 30 µL. To measure the kinetic parameters, the concentration was 10 nM for PRMT1 enzyme and 30 µM for ¹⁴C-AdoMet

(GE Healthcare), and the concentration of peptide ranged from 0 to 20 μM . Reactions were initiated with PRMT1 after the other components were incubated at 30°C for 5 min. The reaction was quenched by loading the mixtures onto the surface of a P81 filter paper disc. After washing and drying the paper, the amount of product was quantified by liquid scintillation. The inhibition pattern analysis of AMI-1 was determined by measuring initial velocities of PRMT1 at different concentrations of one substrate, a fixed concentration of the second substrate, and selected concentrations of AMI-1. The data were displayed in double reciprocal format and fitted to competitive or noncompetitive kinetic equations (67).

2.4.3. Fluorescence assay

The fluorescence intensity and anisotropy were measured using a Fluoro-Max 4 fluorimeter (Horiba Jobin Yvon). The buffer was the same as that of the radioactive assay. A 450 μL reaction mixture with 0.2 μM H4-FL or R4-FL was made in a 0.5 mL plastic tube and incubated at 30 °C in the chamber for 5 min. Then increasing amount of PRMT1 was added while keeping the reporter concentration constant. The fluorescence spectra of each sample were taken and the temperature of the sample chamber was maintained at 30 °C throughout the measurement. The excitation wavelength was chosen at 498 nm, the emission wavelength ranged from 500 nm to 650 nm, and the excitation and emission slit widths were both set at 2 nm. The wavelength of maximum emission was found to be 524 nm for both fluorescein-labeled peptides. The maximum fluorescence intensity data at 524 nm was extracted and plotted as a function of PRMT1 concentration. For the kinetic fluorescent methylation analysis of R4-FL by PRMT1 and the effect of sinefungin, a mixture containing 0.2 μM R4-FL, 15 μM AdoMet and varied concentrations of sinefungin (0 μM , 5 μM , 15 μM , and 50 μM) was prepared and incubated at 30 °C for 5 min, then, 0.4 μM of PRMT1 was added and fluorescence intensity was monitored at

different time points. The kinetic curves were normalized to the same starting point for comparison. Fluorescence anisotropy was tested under similar conditions as described above. The excitation wavelength was fixed at 498 nm and the emission wavelength was selected as 524 nm (slit 2, 2 nm). Fluorescence anisotropy at 524 nm was acquired at different concentrations of PRMT1 and the data were fitted to a quadratic equation as a function of PRMT1 concentration. The inhibition effect of AMI-1 was analyzed using fluorescence anisotropy titration in similar conditions. For H4-FL assay, the peptide and PRMT1 concentrations were fixed at 2 μM and 4 μM respectively; For R4-FL assay, they were fixed at 0.2 μM and 2 μM respectively. Increasing concentrations of AMI-1 were added for both assays until saturation was reached.

CHAPTER 3

DISCOVERY AND MECHANISTIC STUDY OF A CLASS OF PROTEIN ARGININE METHYLATION INHIBITORS

(This work is mainly based on the published paper, *J. Med. Chem.* 53 (2010)6028-39. In this project, the author is obliged to Dr. Mingyong Li and Dr. Binghe Wang for their great contributions to inhibitor virtual screening.)

3.1. Introduction

Among different post-translational modifications, arginine methylation is catalyzed by protein arginine methyltransferases (PRMTs), which utilize the cofactor *S*-adenosyl-L-methionine (AdoMet, SAM) as a methyl donor. Thus far, eleven PRMT members have been identified and are categorized into two major types, type I and type II, according to the substrate and product specificity.(18-20) Type I enzymes (e.g., PRMT-1, -2, -3, -4, -6, and -8) catalyze the transfer of the methyl group from AdoMet to one of the terminal nitrogen atoms of the guanidino group of specific arginine residues in a protein substrate, resulting in ω -N^G-monomethylarginine (MMA, L-NMMA) and ω -N^G,N^G-asymmetric dimethylarginine (ADMA) products.(19, 21-24) Type II enzymes (e.g., PRMT 5, 7, and 9) catalyze the formation of MMA and ω -N^G, N^G-symmetric dimethylarginines (SDMA).(24-27) The catalytic properties of PRMT-10, and -11 remain to be characterized. Protein arginine methylation is involved in a broad spectrum of biological processes, including transcriptional activation and repression, mRNA splicing, nuclear—cytoplasmic shuttling, DNA repair, and signal transduction.(29)

In recent years, the significance of PRMTs in human diseases is being increasingly recognized. As the predominant PRMT member, PRMT1 is likely to be responsible for bulk

protein arginine methylation in mammalian cells. Aberrant expression of spliced forms of PRMT1 has been observed in several tumor states, including breast cancer(61, 68) and colon cancer.(69, 70) Deregulation of the methylation of histone H4 at R3 (a major cellular substrate of PRMT1) is a suggestive marker of prostate cancer.(71) PRMT1 was recently shown to be a component of Mixed Lineage leukemia (MLL) transcription complex and the activity of PRMT1 is required for malignant transformation.(60) PRMT4 (better known as CARM1) is overexpressed in both aggressive prostate cancer and breast tumor.(72, 73) The type-II PRMT member, PRMT5, is recruited to the promoters of tumor suppressor genes such as ST7 and NM23, and its overexpression was observed in a variety of lymphoma and leukemia cells,(18, 74) in gastric carcinoma,(75) and in immortalized fibroblast cells.(76) In cardiovascular disorders, PRMT activity is associated with the up-regulation of serum ADMA, which subsequently blocks NO production and causes many cardiovascular implications such as diabetes and hypertension.(77-79) Furthermore, a number of viral proteins have been shown to be substrates of PRMTs, such as the herpes simplex virus 1 nuclear regulatory protein ICP27, the hepatitis C virus protein NS3, the Epstein-Barr virus nuclear antigen 2, adenovirus E1BAP5 and L4-100K, and the HIV-1 proteins Rev, Tat, and the nucleocapsid protein.(23, 29) Together, these multiple lines of evidence point toward the extensive roles of PRMTs in human pathogenesis and suggest that PRMT inhibitors could be very useful research tools and be of pharmacological merits for disease intervention.

Given the essential roles that PRMTs play in normal biology and in disease, quite a few efforts have been invested in developing small molecule PRMT inhibitors both as chemical genetic tools and as therapeutic agents.(43-45) The first type of chemical inhibitors for PRMTs are analogues of the AdoMet cofactor, including *S*-adenosylhomocysteine (SAH),

methylthioadenosine, and sinefungin.⁽⁴⁴⁾ Due to structural similarities to AdoMet, these analogue inhibitors target all AdoMet-consuming methyltransferases, such as DNA methyltransferases, protein lysine methyltransferases, and O-methyltransferases. In the past few years, several groups reported their work in a row on developing small molecule inhibitors specific for PRMTs. Most of these studies on PRMT inhibitor discovery adopted targeted or random screening approaches. The screening strategy is so widely accepted largely because of technical advancement in computer-aided drug design and in medium- and high-throughput inhibitor screening. Thus far, the disclosed small molecule PRMT inhibitors include **1** (AMI-1),⁽⁴⁶⁾ stilbamidine and allantodapsone,⁽⁴⁷⁾ the thioglycolic amide RM65,⁽⁴⁸⁾ pyrazole amide compounds,⁽⁴⁹⁾ and others.⁽⁵⁰⁻⁵⁴⁾ It is important to point out that past inhibitor development efforts were mostly focused on inhibition of the enzyme, presumably, through binding to the active site. This is also the case with the vast majority of enzyme inhibition work reported related to other enzymes so far. Because a single PRMT catalyzes the methylation of arginine residues in multiple proteins, inhibition of a particular PRMT inevitably results in bulky inhibition of methylations of a large number of proteins, but not on a particular substrate sequence. Herein we report our discovery of a class of inhibitors that modulate PRMT-mediated reaction through binding to the substrates, thus revealing a new way of chemical modulation of PRMT activities.

3.2. Results and discussion

3.2.1. Screening for new PRMT1 inhibitors

In an effort to discover potent and selective PRMT1 inhibitors, we conducted a virtual screening to search for novel PRMT1 inhibitors from the ChemBridge small molecule compound collection (about 0.4 million compounds) using the reported crystal structure of rat PRMT1.⁽⁸⁰⁾ Briefly, the 2D structures of individual compounds were first converted into 3D structures by

using the CONCORD program(81) and then docked to the PRMT1 structure (PDB entry: 1OR8) using DOCK 6 program.(82) From this virtual screening, fifty compounds with high consensus scores were selected and experimentally tested for PRMT1 inhibition (see Table SI-1 in the supplementary information). In a typical radioactive experimental assay, a reaction mixture contained 0.1 μM of recombinant His6x-PRMT1, 5 μM of [^{14}C]-labeled AdoMet, and 2 μM of the amino-terminal tail peptide of histone H4, *i.e.*, H4(1-20), as the substrate, and was incubated at 30°C in the presence or absence of 100 μM of individual compounds. The retained fractional activity of PRMT1 was used as a parameter to evaluate the potency of the compounds in blocking PRMT1-mediated methylation. It is notable to mention that, for all the enzymatic assays, the methylation reaction is maintained under initial condition so that the reaction yields of the limiting substrates are lower than 10%, which is to ensure that the concentrations of AdoMet and peptide substrate do not decrease significantly over the time course of methylation reaction. The experimental assays, unfortunately, showed that the accuracy of the virtual screening was rather poor. Out of the fifty tested compounds, only one weak hit, **2** (#5252870, ChemBridge product ID), was found to show inhibition potency at IC₅₀ about 1 mM. Subsequently, we searched for structural analogues of **2** from the ChemBridge small molecule collection to examine if more potent inhibitors can be found. Thirty-one compounds that bear similar structures or functional groups with **2** were selected and radioactive methylation assays were performed to evaluate this second set of compounds for inhibition of PRMT1 (Figure 3.1 and Figure SI-1). From the test, nine compounds were identified to have inhibition activity against PRMT1 and their IC₅₀ values ranged from 12 to 867 μM (Table 3.1). Interestingly, we noticed that some of the tested inhibitors bear great structural similarity to **1**, a previously reported PRMT1 inhibitor by Bedford's group.(46) All these compounds have rigid, planar,

conjugated systems, and contain one or more naphthalene aromatic rings. It is also recognized that most of them have negatively charged sulfonate groups and polar hydroxyl groups. Herein, we name these compounds as **3** (NS-1), **4** (NS-2), **5** (NS-3) and so on because of their characteristics of possessing naphthalene and sulfo groups. We also compared the inhibition potencies of these inhibitors with several PRMT1 inhibitors recently reported in the literature, including **1**, stilbamidine and allantodapson. As shown in Table 3.1, stilbamidine ($IC_{50} = 105.7 \mu\text{M}$) exhibited comparable inhibition activity with **1** ($IC_{50} = 137.1 \mu\text{M}$). The inhibition potency of the other PRMT1 inhibitors, including allantodapson, and compound 5756663 and 7280948 reported in the literature,^(47, 50) is even weaker. For example, at 2 mM of these three compounds, still 45%, 87%, and 100% of PRMT1 activity retains, respectively. By contrast, the NS-series of compounds identified here are quite stronger PRMT1 inhibitors. Four of these inhibitors, *i.e.*, **3**, **4**, **5**, and **6** (NS-4), showed stronger potency than **1** and stilbamidine. In particular, **3** exhibited the best inhibition potency with an IC_{50} of $12.7 \mu\text{M}$, which is about ten-fold lower than that of **1** and stilbamidine under the same reaction condition.

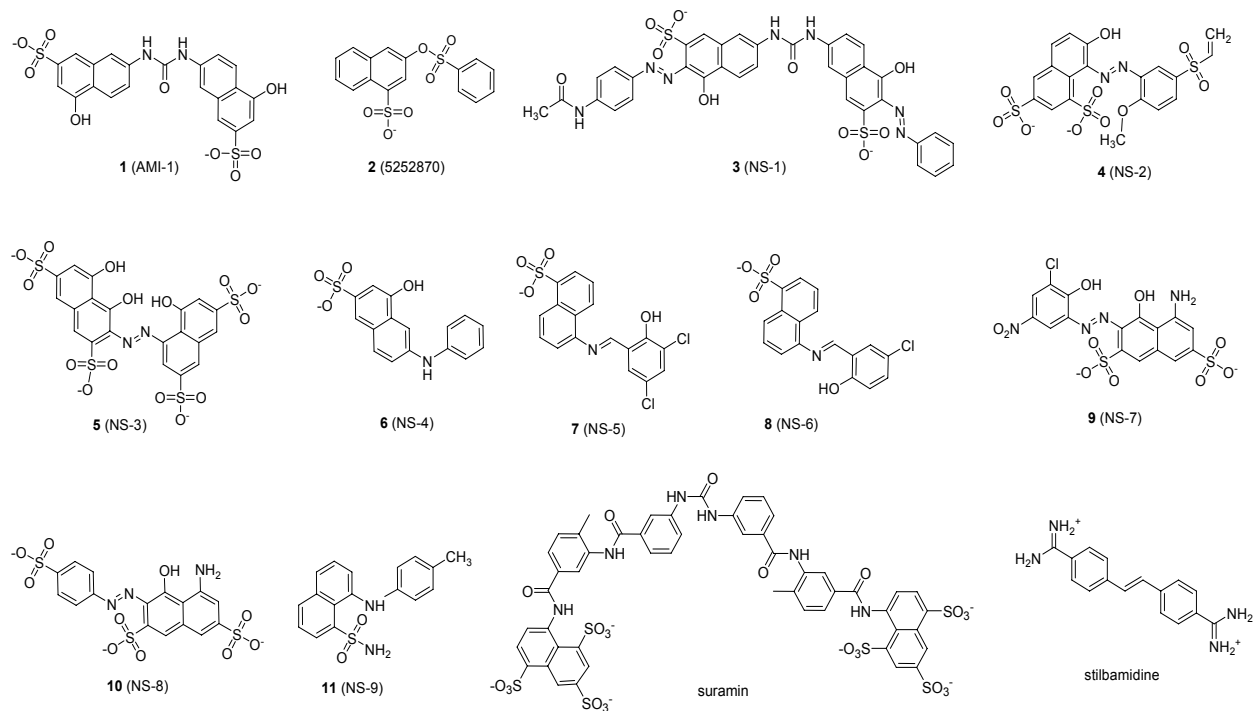


Figure 3.1. Structures of selected PRMT1 inhibitors

Table 3.1. Inhibition of PRMT1 by selected compounds.

IC₅₀ values of different NS compounds were tested in the radioactive inhibition assays with 2 μM of H4(1-20) or R4, 5 μM of [¹⁴C]-AdoMet, 0.1 μM of PRMT1, and increasing concentrations of each inhibitor.

Compounds	IC ₅₀ (μM) for H4(1-20) methylation	IC ₅₀ (μM) for R4 methylation
3	12.7 ± 0.1	741.7 ± 75.0
4	43.1 ± 1.0	108.4 ± 8.4
5	72.1 ± 1.0	463.1 ± 99.2
6	104.2 ± 3.9	227.8 ± 7.8
7	205.9 ± 25.2	1200 ± 16
8	234.1 ± 10.1	595.8 ± 37.5
9	280.6 ± 27.1	No inhibition at 2 mM

10	325.0 ± 36.9	No inhibition at 2 mM
11	867.4 ± 13.6	No inhibition at 2 mM
stilbamidine	105.7 ± 0.7	1150 ± 33
1	137.1 ± 12.1	375.6 ± 7.8
suramin	5.33 ± 0.23	1011 ± 20

3.2.2. The kinetic pattern of PRMT1 inhibition by **3**.

To provide the biochemical basis of PRMT inhibition by this type of NS compounds, we investigated the inhibition mechanism of **3**, the most potent inhibitor in the series. First, we performed a fluorescence anisotropy binding assay to check if the inhibitor can compete with the PRMT1 substrates. In this experiment, a fluorescein-labeled amino-terminal H4 peptide, namely H4(1-20)FL, with the sequence of Ac-SGRGKGGKGDpr(FL)GKGGAKRHRK, was used as a substrate ligand for PRMT1 binding.⁽⁸³⁾ The anisotropy of H4(1-20)FL increased upon binding to PRMT1, due to formation of a large macromolecular PRMT1-ligand complex (Figure 3.2). A K_d value of $0.49 \pm 0.10 \mu\text{M}$ was calculated. Addition of **3** led to reversal of the anisotropy change, thus offering direct evidence that **3** is a competitive inhibitor versus the peptide substrate. K_i of **3** was deduced to be $1.71 \pm 0.54 \mu\text{M}$ by fitting the titration data using the DynaFit program.⁽⁸⁴⁾ Similar competitive binding between **3** and a fluorescently labeled glycine- and arginine-rich (GAR) substrate, R4FL was also observed (Figure SI-2). To further validate the results of competitive inhibition, we conducted steady-state kinetic characterization. The initial velocities of PRMT1 were measured at several selected concentrations of the inhibitor over a range of varied concentrations of one substrate while fixing the concentration of the other.

The data were plotted in the double reciprocal format with $1/\text{velocity}$ versus $1/(\text{concentration of the varied substrate})$ (Figure 3.3). The kinetic inhibition data points were analyzed by fitting to the linear competitive or noncompetitive inhibition equations.⁽⁶⁷⁾ As can be seen from the double-reciprocal plots, a series of straight lines intersected on the $1/\text{velocity}$ ordinate when the concentrations of H4(1-20) are varied, while the intersecting point moved to the western side of the ordinate when concentrations of AdoMet are varied. These data clearly demonstrate that **3** is competitive versus the peptide substrate and noncompetitive versus the methyl donor. This result is consistent with the fluorescent binding assay, and is also in agreement with our previous report showing that **1** is competitive versus peptide substrates and noncompetitive versus AdoMet.⁽⁸³⁾ In addition, **6**, another inhibitor in this class, also exhibited the same inhibition pattern (Figure SI-3 and Figure SI-4b). These combined results support that this type of naphthalene-sulfo derivatives target PRMT1 by blocking the access of the substrate to the PRMT1 active site. Interestingly, the positively charged stilbamidine also showed competitive binding pattern in respect to the peptide substrate (Figure SI-4a), which is consistent with a previous report.⁽⁴⁷⁾

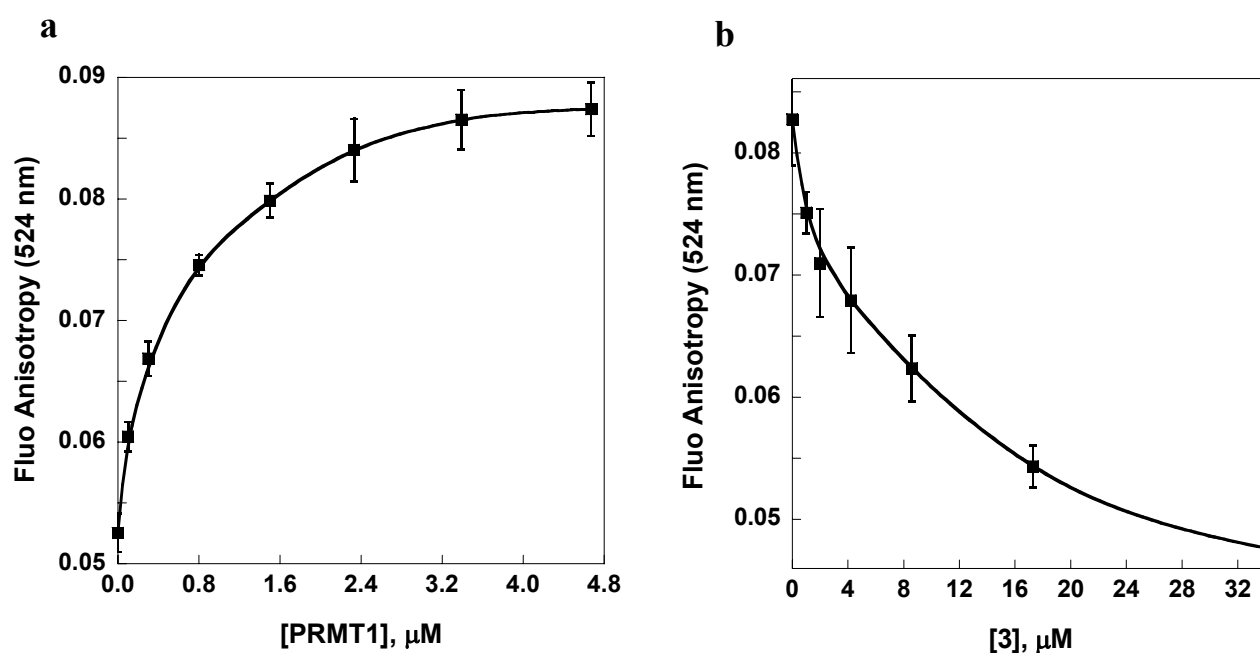


Figure 3.2. Competitive binding measurement with fluorescence anisotropy. (a) Fluorescence anisotropy of H4(1-20)FL at different concentrations of PRMT1. The concentration of H4(1-20)FL was fixed at 0.2 μM . K_d of H4(1-20)FL to PRMT1 was calculated to be $0.49 \pm 0.10 \mu\text{M}$. (b) Fluorescence anisotropy (524 nm) of H4(1-20)FL and PRMT1 complex at different concentrations of **3**. The concentrations of H4(1-20)FL and PRMT1 were kept constant at 0.2 μM and 2.0 μM , respectively. K_i of **3** was calculated to be $1.71 \pm 0.54 \mu\text{M}$ by fitting the titration data with DynaFit program.

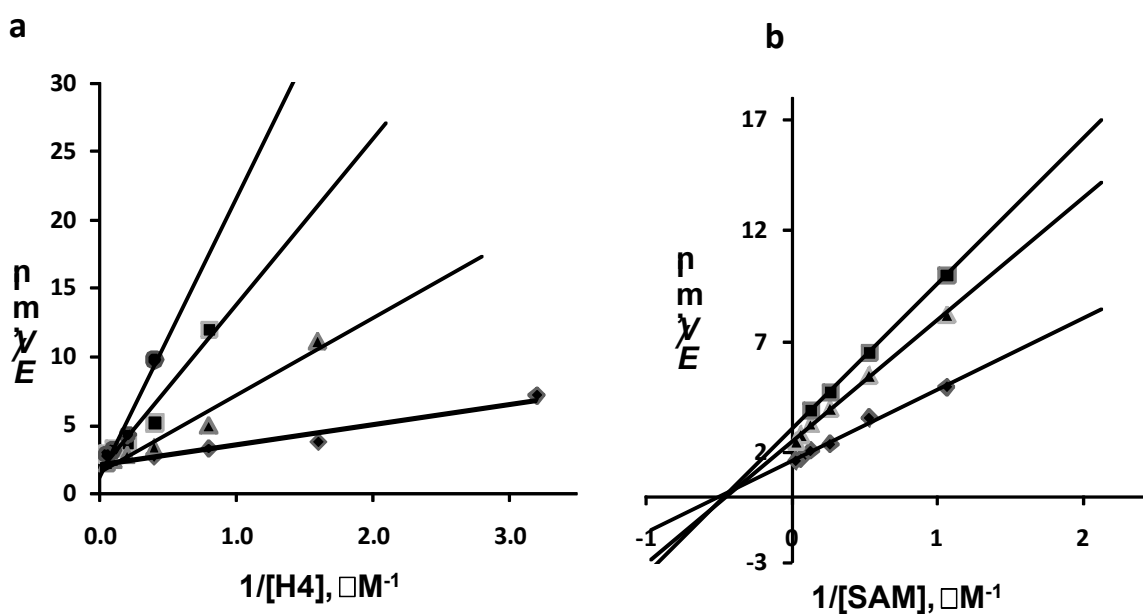


Figure 3.3. Kinetic analysis of PRMT1 inhibition by 3. a. Double-reciprocal plotting of initial velocities versus varied concentrations of H4(1-20). The concentration of $[^{14}\text{C}]$ -AdoMet was fixed at 5 μM and the concentration of **3** was selected at 0 μM (\blacklozenge), 5 μM (\blacktriangle), 10 μM (\blacksquare) and 20 μM (\bullet). b. Double-reciprocal plotting of initial velocities versus varied concentrations of $[^{14}\text{C}]$ -AdoMet. The concentration of H4(1-20) was fixed at (2 μM) and the concentration of **3**

was selected at 0 μM (\blacklozenge), 5 μM (\blacksquare) and 10 μM (\blacktriangle). 0.03 μM of His6x-rPRMT1 was used in all these assays.

3.2.3. Selectivity of **3**.

It is of interest to examine whether the NS inhibitors target PRMT1 selectively or also inhibit other PRMT members. Using radioactive methylation assays, we measured inhibitory activities of **3**, the most potent compound in this series, towards PRMT3, PRMT4/CARM1, and PRMT6 (Table 3.2). The inhibition potency of **3** for GST-tagged hPRMT1 is similar to that for His6x-rPRMT1, with an IC_{50} of $12.9 \pm 0.2 \mu\text{M}$. PRMT3 was inhibited at a lower IC_{50} of 7.1 μM . At the concentration of 500 μM , **3** showed no apparent inhibitory effect to CARM1 (5 μM of CARM1, 1 mM of H3(1-31), 30 μM of SAM). The IC_{50} for PRMT6 is about three-fold larger than that for PRMT1. It is worth mentioning that PRMT1 and PRMT3 share similar substrate specificity both of which methylate H4 and GAR peptides. On the other hand, CARM1 exhibits distinct substrate specificity from PRMT1. CARM1 targets H3 but does not methylate GAR sequences.(23) Therefore, the variation in inhibition potency is likely caused either by the differences between CARM1 and PRMT1 structures, or by the distinct nature of the substrates used. Overall, **3** inhibits PRMT1 and PRMT3 stronger than CARM1 and PRMT6.

Table 3.2. Comparison of the inhibition of PRMT-1, -3, -4, and -6 by Compound 3.

Data obtained from the results of the radioactive methylation assays. For the inhibition of His6x-rPRMT1 or GST-hPRMT1, 2 μM of H4(1-20), 5 μM of [^{14}C]-SAM and 0.1 μM of enzyme were used. For the inhibition of His6x-PRMT3, 2 μM of R4, 5 μM of [^{14}C]-SAM and 0.1 μM of enzyme were used. For the inhibition of GST-CARM1, 1 mM of H3(1-31), 30 μM of [^{14}C]-SAM

and 5 μM of enzyme were used. For the inhibition of His6x-PRMT6, 10 μM of H3(1-31), 5 μM of [^{14}C]-SAM and 0.5 μM of enzyme were used.

	Peptide substrate and its K_m (μM)	IC_{50} (μM) of 3
His6x-rPRMT1	H4(1-20); 0.64 ± 0.04	12.7 ± 0.1
GST-hPRMT1	H4(1-20); 0.69 ± 0.04	12.9 ± 0.2
His6x-PRMT3	R4; 0.92 ± 0.15	7.1 ± 0.2
GST-CARM1	H3(1-31); 796 ± 204	$\sim 2 \text{ mM}$
His6x-PRMT6	H3(1-31); 9.1 ± 1.2	39.2 ± 2.8

3.2.4. **3** directly targets the substrates, but not PRMT1.

One paradox question is that the NS-series of inhibitors bear none or little structural similarity to the arginine-containing substrates of PRMT1 such as histone H4 or GAR peptides. In particular, all the reported PRMT1 substrates are rich in positive residues, *i.e.*, arginines and/or lysines. The crystal structure of PRMT1 also reveals several large acidic grooves present at the protein surface which have been proposed to participate in the recognition of substrates.⁽⁸⁰⁾ On the other hand, most of the NS compounds are negatively charged due to the existence of one or more sulfonate groups. Therefore, it seems difficult to envision that **3** and its analogues will bind to PRMT1 at the same site as that of substrates in order to explain the competitive nature between the inhibitor and the peptide substrates. To look into these paradox problems, we hypothesized that **3** and its analogue inhibitors might bind to the PRMT1 substrate directly and that the binding subsequently prevents the substrate from accessing to PRMT1. Under this scenario, inhibitor-substrate interaction is likely facilitated by the electrostatic

interaction between the negatively-charged sulfonate groups and the cationic arginine guanidino group, as well as the van der Waals interaction between the naphthalene ring and the hydrophobic side chains in the substrate. It is conceivable that such interaction may shield the key motifs in the substrate so that they are not recognized by enzyme. To nail down the mechanistic details, we conducted several biophysical measurements to detect inhibitor-substrate and inhibitor-enzyme association.

The interaction between the inhibitors and the PRMT1 substrate was confirmed by several experiments. First, when mixing high concentrations of H4(1-20) and **3** or **1** (*e.g.*, 100 μ M of peptide and 200 μ M of inhibitor), a red or brown precipitate occurred immediately. We reasoned that the precipitation is a strong indication of the association between H4 substrate and the inhibitors. The precipitate was pelleted by centrifugation, washed with water, dissolved in 5% TFA, and analyzed with MALDI-MS. Indeed, the mass spectra revealed a peak corresponding to H4(1-20)—**1** complex (Figure 3.4). We could not observe a peak for the H4(1-20)—**3** complex on MS spectra, probably due to the instability of H4(1-20)—**3** and/or the strong anionic nature of **3**.

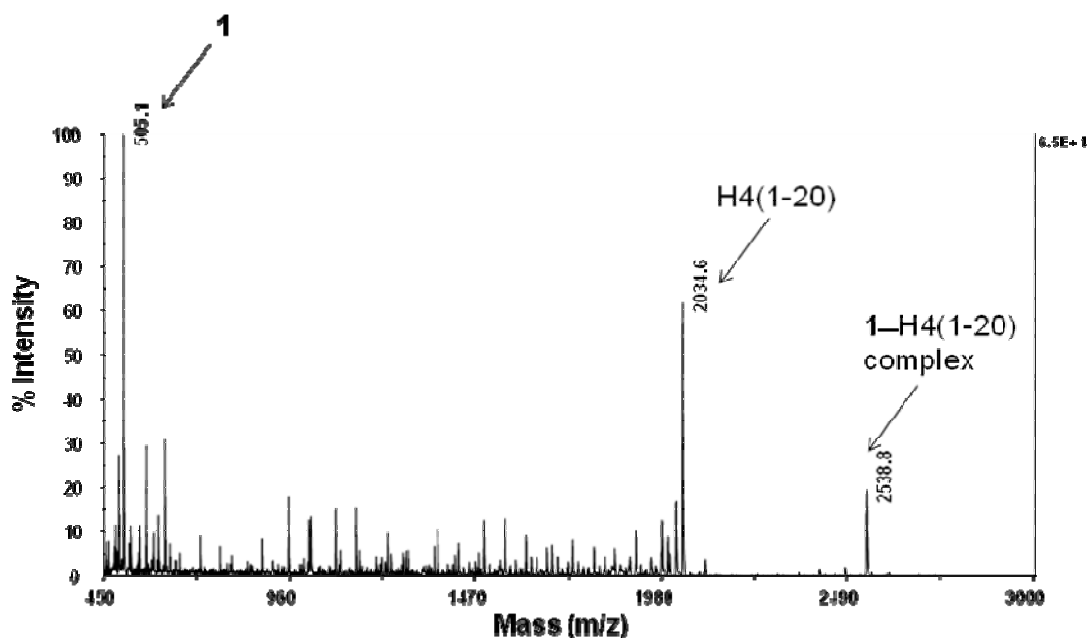


Figure 3.4. Association of 1 with H4(1-20) peptide detected by MALDI-MS. 100 μM of H4(1-20) and 200 μM of **1** were mixed in the reaction buffer. The precipitate formed was pelleted by centrifugation, washed with H_2O , dissolved in 5% TFA, and analyzed by MALDI-MS.

Next, we examined UV-Vis spectra of **3** in the presence of different concentrations of H4(1-20) or PRMT1 (Figure 3.5). **3** has a maximum absorption at 498 nm with extinction coefficient of $0.0182 \mu\text{M}^{-1}\text{cm}^{-1}$. When H4(1-20) was gradually added to a solution of **3** (**3** concentration was kept constant at 40 μM), the absorbance decreased dramatically. For instance, at 10 μM of H4(1-20), the absorbance at 498 nm decreased to 25% of the original value. By contrast, the presence of PRMT1 had a quite minor effect on the absorption of **3**. At 10 μM of PRMT1, the absorbance of **3** at 498 nm still retained 83%. These data directly pointed out that

the interaction between **3** and H4(1-20) is much stronger than **3**—PRMT1 interaction, if there is any.

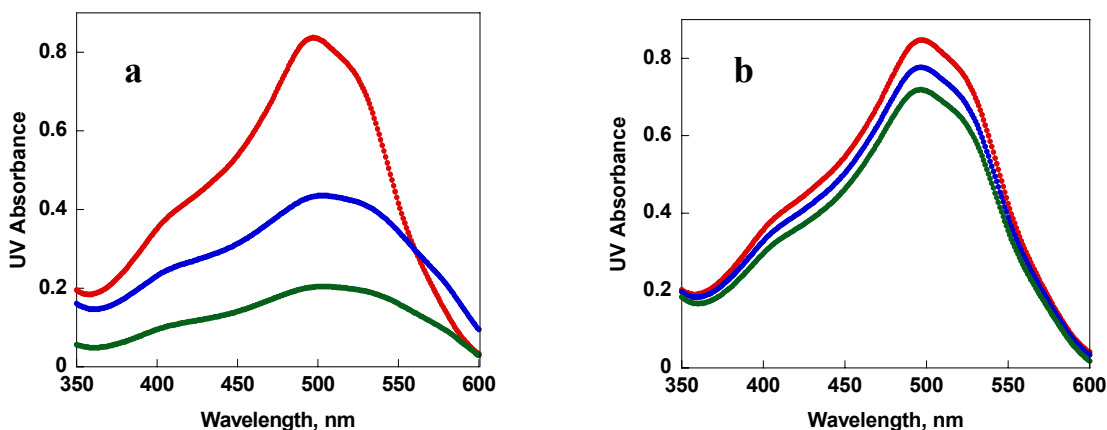


Figure 3.5. UV-Vis spectral change of **3** upon the addition of H4(1-20) or His6x-PRMT1. 40 μ M of **3** was titrated with 0 μ M (red), 5 μ M (blue) and 10 μ M (green) of H4(1-20) (a) or PRMT1 (b).

We then measured the fluorescence emission of H4(1-20)FL in the presence of **3**. Since the absorption band of **3** overlaps with the fluorescence emission peak of H4(1-20)FL, it is anticipated that fluorescence energy transfer from fluorescein (donor) to **3** (acceptor) will occur if the two molecules form a complex. Indeed, addition of the inhibitor quenched the fluorescence emission of H4(1-20)FL (Figure 3.6). On the other hand, in the control experiment, addition of the inhibitor to a fluorescein solution caused little change to its fluorescence spectra (after removing the inner filter effect). These data demonstrate that the interaction between the inhibitor and H4(1-20)FL depends on the H4 peptide itself, instead of being caused by the

attached fluorescein label. The K_d of **3** from the fluorescence binding measurement is 2.53 ± 0.64 μM , which is in the similar range as the value measured from the fluorescence anisotropy titration. Furthermore, we determined the binding stoichiometry of **3** with H4(1-20)FL by using the Job's method (Figure 3.7). The intersecting point appears at 0.5 in the plot, suggesting that **3** binds to H4(1-20)FL at 1:1 ratio.

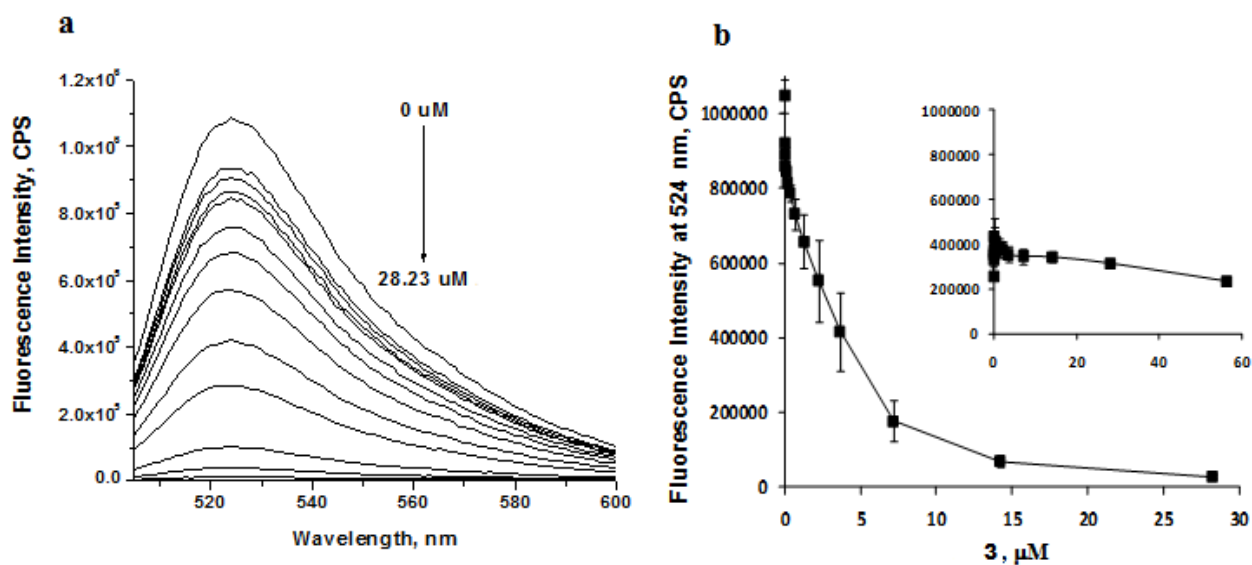


Figure 3.6. Impact of **3 on the fluorescence spectra of H4(1-20)FL.** a. Fluorescence emission spectra of H4(1-20)FL (0.2 μM) at different concentrations of **3** (0 ~ 28.2 μM). Excitation wavelength was 498 nm. Fluorescence spectrum change of NHS-fluorescein (0.2 μM) upon titration with **3** was also measured as a control (Spectra not shown). b. Fluorescence intensity of H4(1-20)FL at 524 nm as a function of **3** concentration (after removing the inner filter effect). Inlet: Fluorescence intensity of NHS-fluorescein at 524 nm as a function of **3** concentration (after correction).

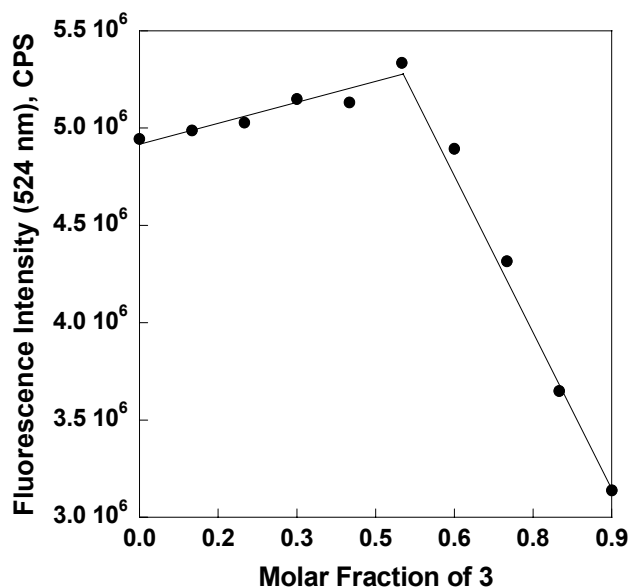


Figure 3.7. Determination of the binding stoichiometry of 3–H4(1-20)FL complex by Job’s Method. The ratio of 3/H4(1-20)FL was varied while the total concentration of H4(1-20)FL and 3 was fixed at 0.5 μ M. The fluorescence intensity (524 nm) of each solution was measured and normalized, and plotted as a function of the molar fraction of 3.

We also attempted to study 3–H4(1-20) interaction using circular dichroism (CD) spectra. In the spectra, H4(1-20) showed a pattern of absorption that is correspondent with random coil structures (Figure 3.8). Upon addition of 3, the absorption band for the random coil decreased, indicating that the inhibitor caused a structural change to H4 peptide. However, upon continuous addition of 3, a red precipitate occurred which prevented further accurate quantitative analysis of H4(1-20)—inhibitor interaction. Similar results were also observed for the interaction between 1 and H4(1-20) (data not shown).

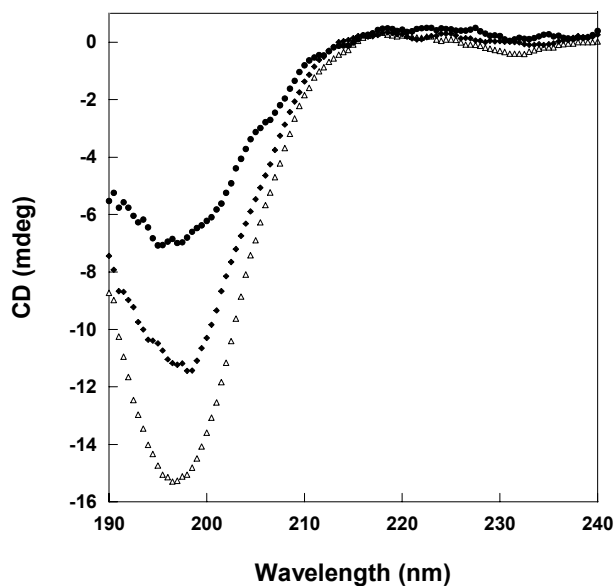


Figure 3.8. CD study of H4(1-20) association with 3. 100 μM of H4(1-20) was titrated with 0 μM (Δ), 100 μM (\blacklozenge), and 200 μM (\bullet) of **3** in 10 mM of Tris buffer (pH 7.4). CD spectrum change of H4(1-20) was monitored.

In enzyme inhibition, if an inhibitor targets the active site of an enzyme, its inhibition potency will be largely determined by the binding affinity between the inhibitor and the enzyme, with little interference by substrates. In our case, however, the experimental findings show that NS compounds target the substrate, but not the enzyme. This suggests that the potency of these inhibitors in blocking PRMT1 activity will be greatly affected by the nature of the substrate used for the assay. To investigate whether this is true, we tested PRMT1-mediated methylation on H4(1-11) and the inhibition by **3**. Indeed, **3** inhibited the methylation of H4(1-11) with an IC_{50}

(*i.e.*, 176.5 μM) significantly higher than that of H4(1-20) methylation (*i.e.*, 12.7 μM). These data indicate that the inhibition caused by the NS molecules depends on the structural sequences of the substrates used, and strongly validate the proposal that these inhibitors target substrate, instead of enzyme. On the other hand, stilbamidine inhibited the methylation of H4(1-20) and H4(1-11) with similar K_i , *i.e.*, 25.6 μM and 35.0 μM , respectively. Therefore, the inhibition mode of stilbamidine is different from that of NS compounds. Our data, in agreement with a previous study,(47) support that stilbamidine targets the active site of PRMT1 to compete with substrates.

By now, there is no structural information available regarding the nature of H4(1-20)—**3** interaction. The potency difference of **3** in inhibiting H4(1-20) methylation versus H4(1-11) methylation suggests that the inhibitor targets both the N-terminal and C-terminal residues in H4(1-20). The 1:1 stoichiometry of H4(1-20)—**3** binding indicates that the interaction is quite specific. Electrostatic interaction is likely a strong factor, but other modes of interactions such as van der Waals and hydrogen-bonding may also play significant roles. Based on the results of CD, fluorescence, and absorption spectral changes, it is quite possible that the secondary structure of the peptide substrate is altered upon inhibitor binding.

3.2.5. 3 inhibits the activity of histone acetyltransferase (HAT) p300.

The finding that **3** and its analogues inhibit PRMT1 activity by targeting its substrates implicates that **3** may also inhibit other enzymes that utilize H4 or GAR peptides as substrate. To test this possibility, we measured the acetylation of H4(1-20) by p300, a well known HAT that is able to acetylate the N-terminal tail of H4 at multiple sites.(85) The measurement was carried out with 0.02 μM of p300, 10 μM of [^{14}C]-acetyl CoA, and 10 μM of H4(1-20), at varied concentrations of **3** or **1**. Indeed, both compounds exhibited strong inhibition of p300-mediated

H4 acetylation (Figure 3.9). The IC_{50} of **3** and **1** for p300 inhibition were determined to be $21.3 \pm 2.0 \mu\text{M}$ and $118.5 \pm 6.5 \mu\text{M}$, respectively. Notably, these IC_{50} values are very similar as those obtained for PRMT1 inhibition. These data again support our conclusion that the NS-series of compounds bind to H4 directly, and the binding subsequently prevents H4 from being recognized by the H4-modifying enzymes, such as PRMT1 and p300. Thus, the inhibition caused by NS-series compounds depends on the binding between the inhibitor and the substrate, irrespective of the enzyme targets. On the other hand, although stilbamidine is a competitive inhibitor in PRMT1-catalyzed methylation, it does not inhibit significantly H4 acetylation catalyzed by p300 (Figure 3.9d); For example, at 1 mM of stilbamidine concentration, p300 still retained 84% of its HAT activity. Therefore, quite likely, stilbamidine targets the active site of PRMT1 to compete with the H4 substrate, which is in agreement with a previous study.⁽⁴⁷⁾

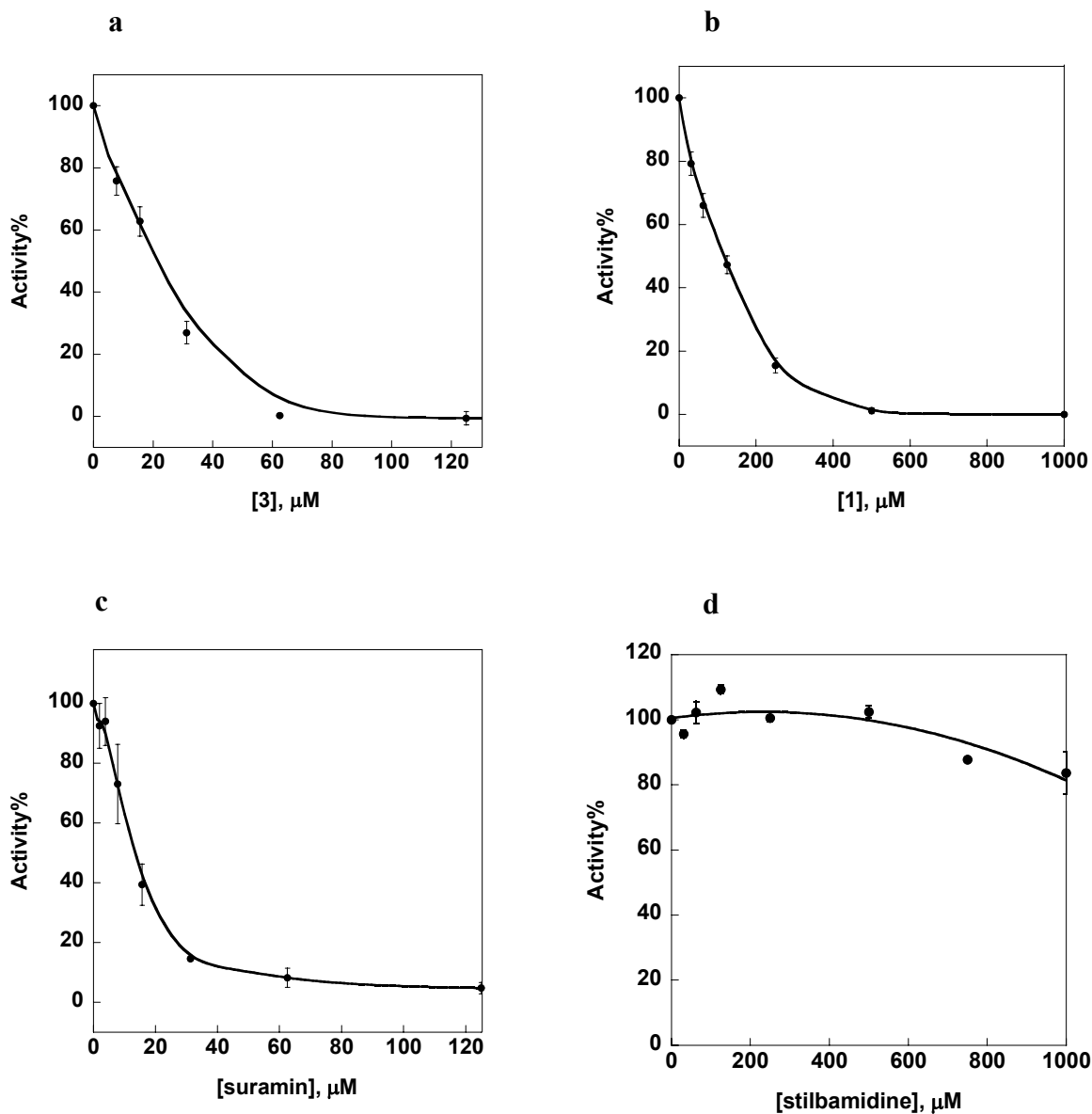


Figure 3.9. Inhibition of p300 HAT activity by 3, 1, suramin and stilbamidine. The fractional activity of p300 was plotted in respect to the concentration of **3** (a), **1** (b), suramin (c), or stilbamidine (d). The reaction buffers contained 10 μM of H4(1-20), 10 μM of ^{14}C -Acetyl CoA, and 20 nM of p300.

3.2.6. Suramin inhibits arginine methylation.

The NS-series of compounds have great structural similarity to suramin, a symmetrical polyanionic aromatic urea containing two naphthalene and six sulfonate groups (Figure 3.1). We tested whether suramin can inhibit PRMT1-mediated methylation. Indeed, suramin strongly inhibited arginine methylation on both H4(1-20) and GAR substrate R4, with IC_{50} of 5.3 μ M and 1011 μ M, respectively (Table 3.1). As a matter of fact, the inhibition potency of suramin is even stronger than that of **3**, the most potent inhibitor identified from our screening search. Furthermore, suramin also inhibited the HAT activity of p300 with an IC_{50} of 13.7 μ M (Figure 3.9c). Given their structural analogy and the similar properties in the inhibition of methylation and acetylation, suramin likely shares the same mechanism of inhibition with NS compounds; namely suramin also targets H4 and GAR proteins and blocks PTMs on the substrates. These data clearly revealed a previously unknown function of suramin.

3.3. Conclusion

In conclusion, we have discovered a type of organic compounds containing naphthalene and sulfonyl pharmacophore components that inhibit PRMT activity in the micromolar range, whose inhibition mechanism is fundamentally distinct from the other PRMT inhibitors reported so far. The biochemical and biophysical data of representative compounds (*e.g.*, **3**, **6**, **1**) show that these inhibitors are competitive versus PRMT1 substrates (*e.g.*, H4 and GAR peptides) and noncompetitive versus the methyl donor. Detailed studies illustrate that they directly target the peptide substrates instead of PRMT1, and the binding subsequently blocks the recognition of the substrates by the enzyme, which is largely responsible for the observed PRMT1 inhibition effect. We also show that the anti-parasitic drug suramin is also an effective arginine methylation

inhibitor. These NS inhibitors will be useful chemical tools for mechanistic study of arginine methylation and other epigenetic modifications. Further, illumination of the inhibitory mechanism provides a new insight for understanding the pharmacological effect of these structurally unique molecules in biological systems.

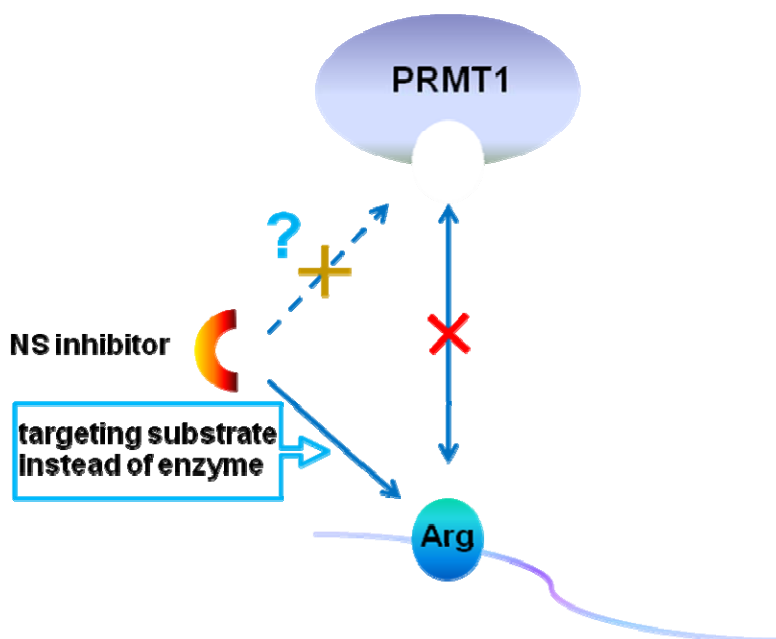


Figure 3.10. Inhibition mechanism of NS compounds.

3.4. Experimental

3.4.1. Materials

Fmoc-protected amino acids and solid phase resins were purchased from NovaBiochem. All the screening compounds were obtained from ChemBridge Corporation. Stilbamidine and allantodapsone were obtained from National Cancer Institute. Suramin was purchased from Acros Organics. For all the effective inhibitors discovered and tested, including compounds **1**, **3—11**, suramin, and stilbamidine, their purities were confirmed by analytical C18 reverse-phased HPLC with H₂O/acetonitrile gradient elution to be $\geq 95\%$. Radioactive AdoMet and

acetyl-CoA were ordered from GE Healthcare and Perkin Elmer. Other chemical reagents were purchased from Fisher, VWR, and Sigma, *etc.*

3.4.2. Peptide substrates

Peptides were synthesized using the standard solid phase peptide synthesis (SPPS) protocols, purified with C-18 reversed phase HPLC, and confirmed with MALDI-MS as previously described.⁽⁸⁶⁾ The structural sequence of the NH₂-terminal 20 aa peptide of histone H4, *i.e.*, H4(1-20), is Ac-SGRGKGGKGLGKGGAKRHRK. The structural sequence of the NH₂-terminal 11 aa peptide of histone H4, *i.e.*, H4(1-11), is Ac-SGRGKGGKGLG. The structural sequence of the GAR peptide, R4, is Ac-GGRGGGFGGRGGKGGRGGGFGGRGGGFG. The underlined Rs designate for the methylation sites. The NH₂-terminal tail 31 aa peptide of human H3, H3(1-31), was synthesized and used as a substrate in CARM1 and PRMT6 analyses. The structural sequence of H4(1-20)FL is Ac-SGRGKGGKGDpr(FL)GKGGAKRHRK. Dpr stands for 2,3-diaminopropionic acid. The structural sequence of R4FL is Ac-GGRGGFGGRGGK(FL)GGRGGFGGRGGFG. In both cases, the fluorescein (FL) is attached through the side chain amino group.

3.4.3. Protein expression and purification

His6x-tagged PRMT1 was expressed from pET28b vector. GST-PRMT1 is expressed from pGEX-4T1 vector. His6x-tagged PRMT3 was expressed from the pReceiver vector. GST-mCARM1 was expressed from the pGEX-4T1 vector. His6x-tagged PRMT6 was expressed from the pET28a vector. All the proteins were expressed in *E. coli* BL21(DE3). All the His6x-tagged proteins were purified on Ni-NTA beads, and the GST-tagged proteins were purified on glutathione agarose beads. Protein concentrations were determined using Bradford assay.

3.4.4. Virtual screening

The virtual screening was conducted on a 40-node Linux cluster at Georgia State University using the same protocol as described before.(87, 88) The 2D structures of ChemBridge database (about 0.4 million compounds) were first converted into 3D structures by using the CONCORD program.(81) Hydrogen atoms were then added to the 3D ligand structures and all atoms were assigned with AM1-BCC partial charges(89-91) by the QuACPAC 1.1 software.(92) These structures were firstly examined based on drug-like property by the FILTER 2.0.1 software.(93) Before docking-based virtual screening, the PRMT1 structure (PDB entry: 1OR8) was added with hydrogen atoms and assigned with Kollman-all charges by the SYBYL 7.1 program.(94) Residues including Arg 3, Arg 9, Arg 15, Ile 44, His 45, Met 48, Leu 49, Arg 54, Thr 55, Asp 76, Val 77, Gly 78, Ser 79, Gly 80, Thr 81, Gly 82, Ile 83, Leu 84, Ile 99, Glu 100, Cys 101, Ser 102, Ile 104, Gly 126, Lys 127, Val 128, Glu 129, Ser 143, Glu 144, Met 155 and Thr 158, were defined as the active site to construct a grid for the structure-based virtual screening. The position and conformation of each compound were optimized firstly by the anchor fragment orientation and then by the torsion minimization method implemented in the DOCK 6 program.(82) Fifty conformations and a maximum of 100 anchor orientations for each compound were generated, and all of the docked conformations were energy minimized by 100 iterations following procedures as described in literature.(82) The docked molecules were ranked based on the sum of the *van der Waals* and electrostatic energies implemented in the DOCK 6 program to obtain the top 1000 compounds. After collecting the top hits, the consensus scoring evaluation(95), including ChemScore,(96, 97) PLP,(98) ScreenScore,(99) ChemGauss and ShapeGauss(100) implemented in the FRED 2.2.3 program, was processed,(93) as well as hydrogen bond and hydrophobic profiles by the IDEA 8.8 software.(101) As the final step, a

manual binding orientation and conformational examination was performed to harvest the final fifty hits for biochemical evaluation.

3.4.5. Radioactive methylation assay

The inhibitory activities of small molecule compounds were tested using carbon-14 labeled radioactive methylation assays. The assays were carried out in 0.6-mL plastic tubes at 30°C in a reaction volume of 30 μ L. The reaction buffer contained 50 mM HEPES (pH = 8.0), 0.5 mM DTT, 1 mM EDTA, and 50 mM NaCl. In a typical procedure, 2 μ M of peptide substrate, 5 μ M of [¹⁴C]-AdoMet and varied concentrations of an inhibitor were preincubated in the reaction buffer for 5 min prior to the initiation by the addition of PRMT1 (0.1 μ M final). After incubating for an appropriate period of time, the reaction was quenched by spreading the reaction mixture onto P81 filter paper discs (Whatman). The paper disc was washed with 1 liter of 50 mM NaHCO₃ and dried in air for 2 hours. The amount of methylated products was quantified by liquid scintillation. IC₅₀ value is the concentration of inhibitor at which half of the maximal activity is reached. The K_i for stilbamidine was calculated from IC₅₀ by using the equation:

$$K_i = \frac{IC_{50}}{1 + [S]/K_m} . K_m \text{ was obtained by measuring the initial velocity of reaction at different}$$

concentrations of a particular substrate and fitting the kinetic data with Michaelis-Menton equation. The inhibition patterns of **3** and **6** were determined by measuring initial velocities of PRMT1 at a range of varied concentrations of one substrate, a fixed concentration of the other substrate, and selected concentrations of the inhibitors. The data were displayed in double reciprocal formats and fitted to competitive or noncompetitive kinetic equations.(102)

3.4.6. Inhibition of p300 catalysis

Recombinant p300 HAT domain (1287-1666) was a gift from Dr. Philip Cole at Johns Hopkins University and its expression was described in an earlier report.⁽¹⁰³⁾ Enzymatic activity of p300 and its inhibition by **3** and other compounds were measured by radioactive acetylation assays. A reaction mixture of 10 μM of H4(1-20), 10 μM of [^{14}C]-acetyl CoA, 20 nM of p300, and increasing concentrations of the inhibitors were incubated in the reaction buffer (50 mM HEPES (pH 8.0), 50 mM NaCl, 0.5 mM DTT, 1 mM EDTA) at 30 °C for 10 min, and the reaction was quenched by loading the mixture onto p81 filter paper. The radioactive products were quantified by liquid scintillation and the fractional activity of p300 was plotted in respect to the concentration of individual inhibitors.

3.4.7. Fluorescent binding assay.

Fluorescence intensity and anisotropy of fluorescein-labeled peptides were measured on a Fluoromax-4 spectrofluorometer (Horiba Jobin Yvon). The buffer was the same as that for the radioactive assay. The excitation wavelength and emission wavelength were selected at 498 nm and 524 nm, respectively. The competitive binding of small molecule compounds to PRMT1-substrate solution was measured using the fluorescence anisotropy mode in similar manners as described previously.⁽⁸³⁾ Typically, 0.2 μM of H4(1-20)FL and 2 μM of PRMT1 were mixed, and increasing concentrations of an inhibitor were added until the fluorescence anisotropy signals leveled off. The anisotropy values at 524 nm from several scans were plotted as a function of inhibitor concentration. Data were fitted with competitive binding model using DynaFit program to calculate the K_i value.^(84, 104) Also, fluorescence intensity changes of H4(1-20)FL at different concentrations of **3** were measured in order to detect their interaction. 0.2 μM of H4(1-20)FL at 30°C was titrated with increasing concentrations of **3** (0 ~ 28.2 μM).

NHS-fluorescein was used as a control. The fluorescence intensities of both H4(1-20)FL and NHS-fluorescein were corrected to remove the inner filter effect that was caused by **3** absorption, and the data were plotted as a function of the concentration of **3**. The Job's Method was applied to determine the binding stoichiometry of **3** with H4(1-20)FL. A series of solutions with a fixed total amount (0.225 nmol) but varied ratios (0~9) of **3** and H4(1-20)FL in the same reaction buffer were prepared. The fluorescence intensity of each sample at 524 nm was measured, which is related to the amount of binding complex. The fluorescence intensity was divided by the molar fraction of H4(1-20)FL, and then plotted as a function of the molar fraction of **3**.

3.4.8. UV-Vis spectroscopy of **3 upon titration with H4(1-20) or PRMT1.**

The UV-Vis spectra of compound **3** (40 μM in the same reaction buffer) were acquired on a Shimadzu UV-1700 spectrophotometer, in the presence of different concentrations of H4-20 or PRMT1.

3.4.9. CD measurement.

CD spectral changes of H4(1-20) upon the addition of different concentrations of **3** were measured on a Jasco J-810 spectropolarimeter. 100 μM H4(1-20) was titrated with 0 μM , 100 μM , and 200 μM of **3** in 10 mM Tris buffer (pH 7.4) in a 400 μl CD cuvette. CD spectrum of each equilibrated sample was scanned (100 nm/min) with an accumulation of 3 times.

CHAPTER 4

A TRANSIENT KINETIC ANALYSIS OF PRMT1 CATALYSIS

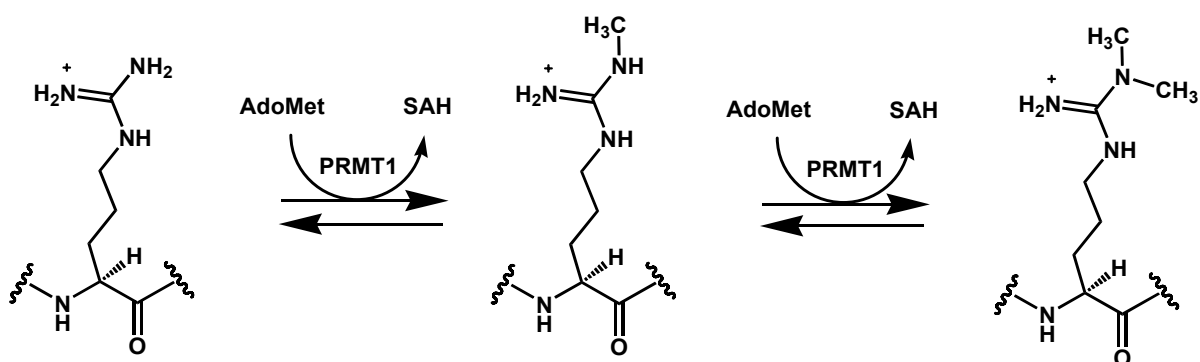
(This work is mainly based on the published paper, *Biochemistry*. 50 (2011) 7033-44. In this project, the author is obliged to Dr. Nan Xie and Miyeong Jin for their contributions to prepare the peptide compounds, and Dr. Mary R. Stahley and Dr. James T. Stivers for their assistance in stopped-flow fluorometer analysis.)

4.1. Introduction

Arginine methylation of the core histones is catalyzed by protein arginine methyltransferases (PRMTs), which transfer the methyl group from S-adenosyl-L-methionine (SAM) to the guanidino group of specific arginine residues. Thus far, about nine PRMT members have been identified at the proteomic level in mammalian cells and these have been grouped into two major types (type I and type II) according to their product specificity (18-20). Type I enzymes (PRMT1, 2, 3, 4, 6, and 8) catalyze the transfer of the methyl group from SAM to one guanidino nitrogen atom of arginine residue to produce ω -N^G monomethylarginines (MMA, L-NMMA) and ω -N^G, N^G-asymmetric dimethylarginines (ADMA) [for a review, see a ref. (21)]. Type II enzymes (*e.g.*, PRMT5) catalyze the formation of MMA and ω -N^G, N^G-symmetric dimethylarginines (SDMA) (24-27). As a result of the methyl transfer, SAM is converted to the product S-adenosyl-L-homocysteine (SAH). PRMTs can exhibit quite high substrate specificity which is correlated with their different specific functions. For instance, CARM1 (PRMT4) methylates H3R2, H3R17 and H3R26 (65, 105), while PRMT1 and PRMT5 specifically methylate H4R3 and H3R8 (40, 76). The methylation at distinct sites can affect the status of gene expression differently. For instance, asymmetric dimethylation at H3R17 and H4R3 stimulates gene activation, whereas symmetric dimethylation at H4R3 is associated with

gene repression (40, 106, 107). In general, PRMT-catalyzed arginine methylation is essential for many biological processes including gene transcriptional regulation (40, 56, 76, 105, 106, 108, 109), signal transduction (110-113), RNA transport (24, 114), RNA splicing (57, 115), DNA repair, and embryonic development and cellular differentiation (58, 116, 117).

Scheme 4.1. PRMT1-catalyzed arginine methylation.



Several studies of the kinetic mechanism of arginine methylation have been recently reported. One steady-state kinetic analysis suggested that PRMT1 utilizes a rapid equilibrium random mechanism (RER) for methyl transfer with the formation of dead-end EAP and EBQ complexes (33). In another study, PRMT6 was shown to follow an ordered sequential mechanism in which SAM binds to the enzyme first and the methylated product is the first to dissociate (34). The slight difference in these two studies may suggest that kinetics of arginine methylation can vary slightly among the individual isoforms. Nevertheless, both studies support a sequential kinetic mechanism in which a ternary complex is formed prior to the methyl transfer step.

Many important questions about the PRMT-catalyzed arginine methylation reaction remain to be answered. For instance, it is not known whether the chemical step or a protein conformational change in the ES complex is rate-limiting for catalysis. Such a molecular level

understanding of how substrate recognition is coupled to catalysis will be of great significance to evaluate the function of PRMT activity in different physiological contexts. To address these mechanistic questions, transient kinetic analyses of arginine methylation are highly desirable. Unfortunately, such studies are greatly limited by lack of assay tools appropriate for fast measurement of substrate binding and methylation on rapid time-scales. In particular, routine radioisotope-labeled methyl transfer assays do not provide information about conformational events along the reaction coordinate. Recently, we reported fluorescently labeled peptide substrates that could be useful in studies of substrate binding and methylation (118). Here we report that such substrates serve as excellent tools to dissect the transient kinetic events during PRMT1 catalysis. By using fluorophore-labeled H4 substrates in combination with stopped flow measurements, we have determined the microscopic rate constants for the key binding and methylation steps during PRMT1 catalysis. This study provides kinetic evidence that substrate recognition induces a conformational transition of the active site of PRMT1, and strongly indicates that the methyl transfer step is overall rate-limiting for arginine methylation. In addition, we find that binding of the cofactor SAM/SAH modulates the interaction between PRMT1 and the peptide substrate.

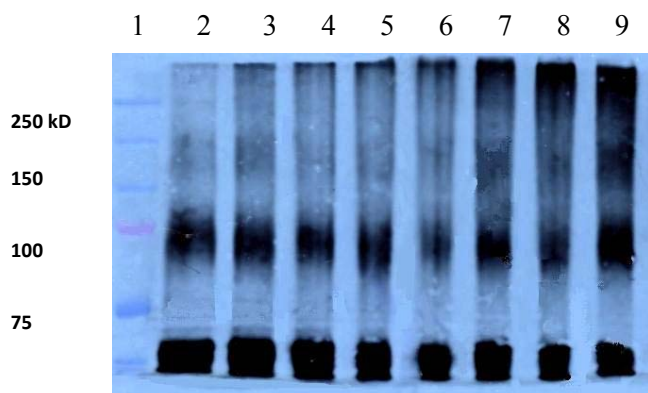
4.2. Results and Discussion

4.2.1. Oligomerization of PRMT1 stimulates its activity.

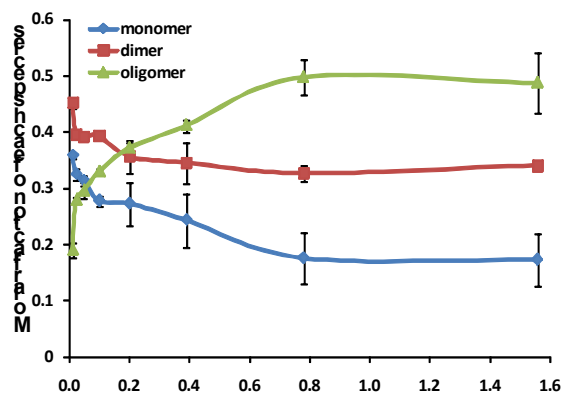
To understand the process of methylation, we first checked the oligomeric state of PRMT1, as this enzyme has been reported to function as a homo-dimer or oligomers (30). Different concentrations of PRMT1 were incubated with glutaraldehyde (0.025%, v/v) for 5 min. 0.1% Triton X-100 was added to eliminate the nonspecific interactions. The mixtures were resolved using 8% SDS-PAGE and probed with anti-PRMT1 antibody. It is clear that as the

protein concentration increases, the degree of oligomerization also increases until it reaches a plateau (Figure 4.1a and b). We further tested if there is a correlation between the activity of PRMT1 and its concentration. As Figures 4.1c and 4.1d reveal, the slope of a plot of the apparent V_{max} divided by PRMT1 concentration (*i.e.* the apparent k_{cat}) is not constant as the PRMT1 concentration changes. In other words, the turnover rate per PRMT1 monomer becomes higher as its concentration increases, and then plateaus when it rises above $\sim 0.5 \mu\text{M}$. Together, these data suggest that PRMT1 oligomerization is dependent on concentration in the range of 0 to $0.5 \mu\text{M}$, and that the final PRMT1 oligomeric complex is the most active form.

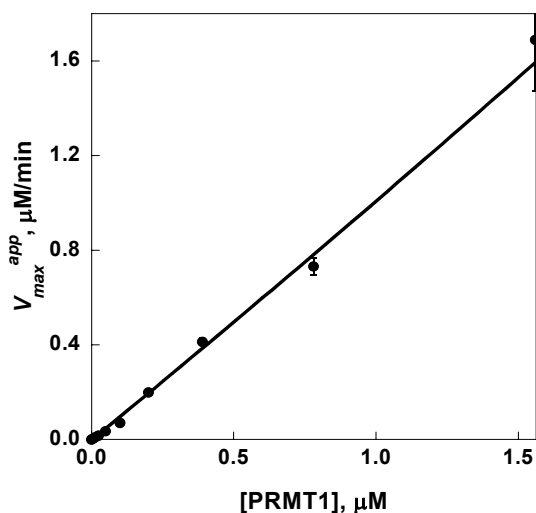
(a)



(b)



(c)



(d)

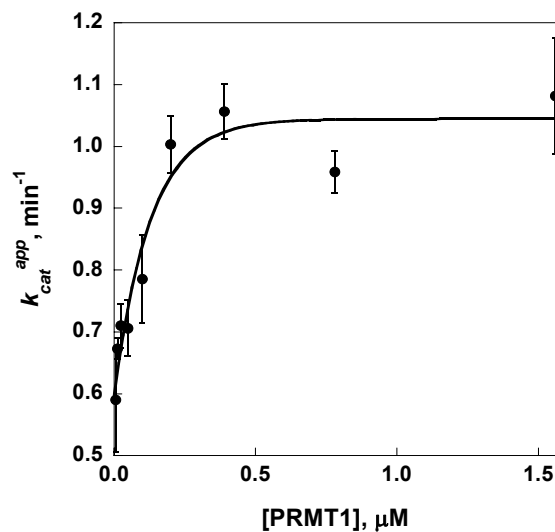


Figure 4.1. Concentration dependence of PRMT1 oligomerization and catalytic activity. (a) Western blot analysis of PRMT1 oligomerization. Different concentrations of PRMT1 (0.012 μM — 3.13 μM) were prepared in presence of 0.1% Triton X-100 and incubated with 0.025% (v/v) glutaraldehyde for 5 min. The crosslinked proteins were resolved on 8% SDS-PAGE followed by western blot detection (primary antibody: anti-PRMT1 rabbit polyclonal IgG; secondary antibody: goat anti-rabbit IgG-HRP). Lane 1 to 9: marker, 0.012 μM , 0.024 μM , 0.05 μM , 0.10 μM , 0.20 μM , 0.39 μM , 0.78 μM , and 1.56 μM of PRMT1. (b) Concentration-dependent oligomerization of PRMT1. The western blot densitometry was analyzed by *Quantity One* software, and the fractions of PRMT1 monomer, dimer and oligomer were plotted as a function of PRMT1 concentration. (c) Maximum velocity as a function of PRMT1 concentration. 0 ~ 3.13 μM of PRMT1 was added to the reaction buffer containing 18.75 μM of [^{14}C]-SAM and 18.75 μM of H4-20. The total protein concentration for each reaction was controlled at 3.13 μM by including BSA as a carrier protein, eliminating the effect of nonspecific interaction. Each reaction was quenched at less than 20% yield. (d) Apparent k_{cat} as a function of PRMT1 concentration. The data were deduced from (c) by dividing the maximum velocity with the corresponding enzyme concentration.

4.2.2. H4 peptide synthesis and steady-state kinetic characterization.

To create fluorescent probes for study of the PRMT-substrate interaction and methylation, we synthesized several peptides containing N-terminal 20 amino acids of histone H4, with 0, 1 or 2 methyl groups on Arg-3 and a fluorescein group on Dpr-10 (2,3-diaminopropionic acid residue, substituting for Leu-10) (Table 4.1). H4FL and H4FLme1 are substrates of PRMT1, and H4FLme2 is a product of PRMT1 catalysis. In this design, the

fluorescein group is placed at an optimized position relative to the methylation site, such that the label does not affect substrate methylation but might still be sensitive to the local change in microenvironment induced by ligand binding. These fluorescent peptides were synthesized with the Fmoc-based solid phase peptide chemistry strategy, purified by HPLC, and analyzed by MALDI-MS.

Table 4.1. Sequences of H4 peptides.

Dpr: 2,3-diaminopropionic acid residue; FL: fluorescein group; me: methyl group.

Peptide name	Sequence
H4(1-20)	Ac-SGR R GKGGKGLGKGGAKRHRK
H4FL	Ac-SGR R GKGGKGDpr(FL)GKGGAKRHRK
H4FLme1	Ac-SGR R _{me1} GKGGKGDpr(FL)GKGGAKRHRK
H4FLme2	Ac-SGR R _{me2} GKGGKGDpr(FL)GKGGAKRHRK

After the peptide synthesis and characterization, we measured the steady-state kinetic parameters of PRMT1 catalysis with these substrates. [¹⁴C]-SAM was used as the methyl donor for the methyltransferase reactions, enabling us to quantify the methylated products by liquid scintillation counting. In the steady-state initial rate assays, one substrate concentration was varied and the other substrate was fixed in large excess (at least five-fold higher than its K_m) to ensure pseudo first-order reaction conditions. Each reaction was quenched at an appropriate time to ensure that substrate conversion was less than 20%. As shown in Table 4.2, the K_m and k_{cat} values of peptide for H4(1-20) and H4FL vary by less than three-fold, indicating that fluorophore does not significantly affect substrate methylation by PRMT1. Also, in a competitive

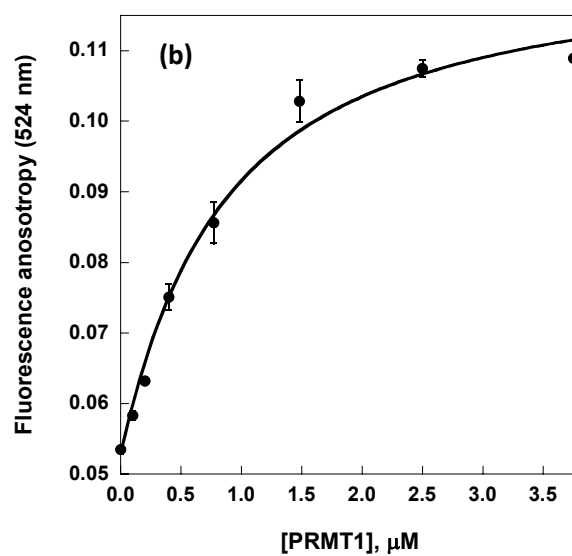
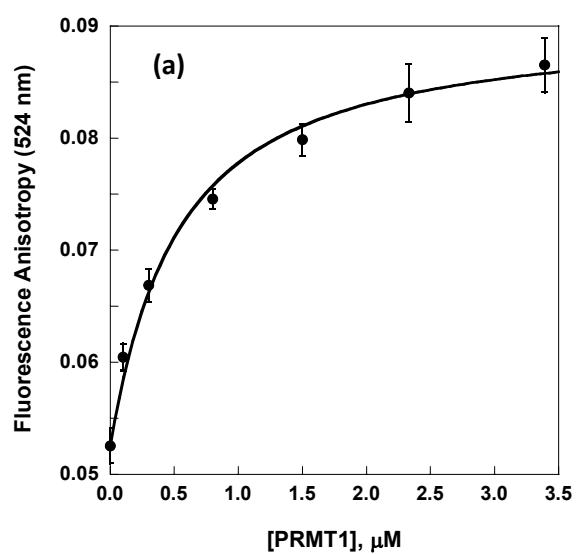
fluorescence anisotropy assay, H4(1-20) was found to completely reverse the binding of H4FL to PRMT1 (Figure 4.3), indicating that the fluorescein-labeled peptide has the same binding mode to the enzyme as the label-free peptide. In addition, these synthesized peptide substrates exhibit comparable kinetic parameters as histone H4 protein, demonstrating that they are good representatives of H4 protein. The k_{cat}/K_m values for un-methylated H4FL and mono-methylated H4FLme1 are $0.86 \pm 0.09 \mu\text{M}^{-1} \text{min}^{-1}$ and $1.6 \pm 0.29 \mu\text{M}^{-1} \text{min}^{-1}$, respectively, suggesting that PRMT1 has little preference for arginine-mono-methylated H4 peptide. The binding affinity between the fluorescein-labeled peptides and PRMT1 was measured by fluorescence anisotropy titrations (118), taking advantage of the fact that the large enzyme-peptide complex has a larger correlation time and higher anisotropy than the peptide ligand (Figure 4.2). The K_d values for the binding of H4FL, H4FLme1 and H4FLme2 to PRMT1 apoenzyme ($0.47 \pm 0.06 \mu\text{M}$, $0.74 \pm 0.13 \mu\text{M}$, and $0.44 \pm 0.09 \mu\text{M}$, respectively) are very similar, suggesting that PRMT1 does not appreciably distinguish among the three peptide forms, although the K_m of H4FLme1 ($0.17 \pm 0.03 \mu\text{M}$) is somewhat lower than the other two peptides. It is possible that binding of cofactor SAM to PRMT1 alters its interaction with the peptide substrate.

Table 4.2. Steady-state kinetic characterization of PRMT1 binding and catalysis.

The radioactive methylation assays were carried out at 30°C and pH 8.0. PRMT1 Concentration was typically 0.01 μM in the catalytic experiments. K_d values were detected in fluorescence anisotropy titration using constant fluorescent peptide (0.2 μM) and increasing concentration of PRMT1.

Substrates	K_m , μM	k_{cat} , min^{-1}	k_{cat}/K_m , $\mu\text{M}^{-1} \text{min}^{-1}$	K_d , μM

H4 protein	1.69 ± 0.39	0.50 ± 0.03	0.30 ± 0.07	-
H4(1-20)	0.64 ± 0.04	0.81 ± 0.01	1.27 ± 0.08	-
H4FL	0.50 ± 0.05	0.43 ± 0.01	0.86 ± 0.09	0.47 ± 0.06
H4FLme1	0.17 ± 0.03	0.27 ± 0.01	1.60 ± 0.29	0.74 ± 0.13
H4FLme2	-	-	-	0.44 ± 0.09
SAM (for H4FL methylation)	3.10 ± 0.46	0.48 ± 0.02	0.15 ± 0.02	-
SAM (for H4FLme1 methylation)	1.59 ± 0.37	0.33 ± 0.02	0.21 ± 0.05	-



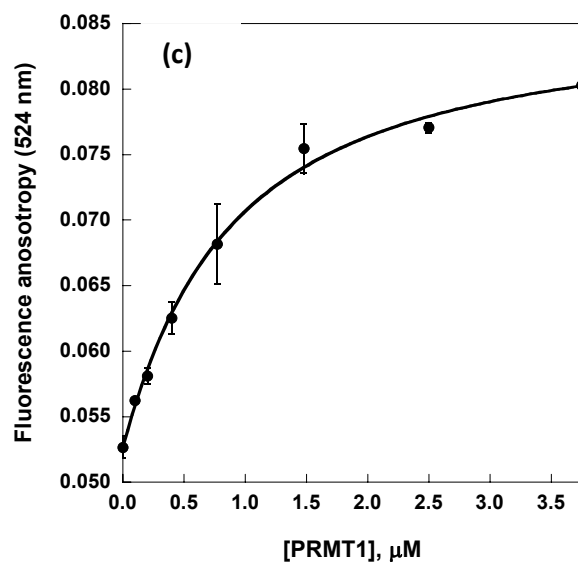


Figure 4.2. Fluorescence anisotropy titration of fluorescent peptides with PRMT1.

0.2 μM of H4FL (a), H4FLme1 (b) or H4FLme2 (c) was titrated with increasing concentration of PRMT1 at 30°C in the reaction buffer mentioned above, and the anisotropy change due to large ES complex formation was recorded, with 498 nm excitation and 524 nm emission. Data were fit to eq 1 to calculate the K_d values.

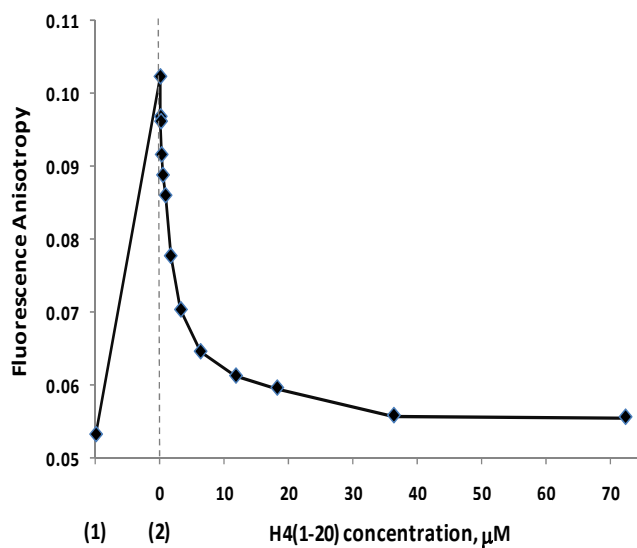


Figure 4.3. Fluorescence anisotropy change of H4FL binding to PRMT1 followed by H4(1-20) competitive titration. Data were collected on a Fluoro-Max 4 fluorimeter (Horiba Jobin Yvon) with the excitation and emission at 498 nm and 524 nm respectively. 0.2 μM of H4FL (1) and 2 μM of PRMT1 (2) were added into the reaction buffer sequentially to show the anisotropy increase. Then increasing concentration of unlabeled H4(1-20) were titrated into the H4FL-PRMT1 mixture to show the anisotropy decay due to the competitive binding of H4(1-20) and H4FL to PRMT1.

4.2.3. Measurement of the binding rate constants of the H4 peptides with PRMT1.

Our fluorescein-labeled H4 peptide showed an appreciable fluorescence decrease when mixed with excess amounts of PRMT1, which was reversed by adding increasing concentrations of unlabeled H4(1-20) (Figure 4.4). This indicates a change in the environment for the fluorescein group upon substrate-enzyme interaction, and provides a signal to measure the association rate constant of the fluorescent peptide with PRMT1 using stopped flow fluorescence. In the transient kinetics experiments, the fluorescent peptide was rapidly mixed with increasing concentrations of PRMT1 (in large excess over the substrate), and the time-dependent fluorescence signal change was monitored to obtain the observed rate constants (k_{obs}). Typical time courses for H4FL, H4FLme1 and H4FLme2 are shown in Figures 4.5a, 4.5b, and 4.5c. Each averaged data curve was fitted well to a single-exponential function, suggesting no more than a simple single-step process. The k_{obs} data were calculated and plotted against PRMT1 concentration (Figure 4.5d and Figure 4.6). The association rate constant (k_{on}) was obtained from the slope of the plot of k_{obs} against PRMT1 concentration to be $40 \pm 1 \mu\text{M}^{-1}\text{s}^{-1}$ for H4FL, $23 \pm 1 \mu\text{M}^{-1}\text{s}^{-1}$ for H4FLme1, and $26 \pm 1 \mu\text{M}^{-1}\text{s}^{-1}$ for H4FLme2.

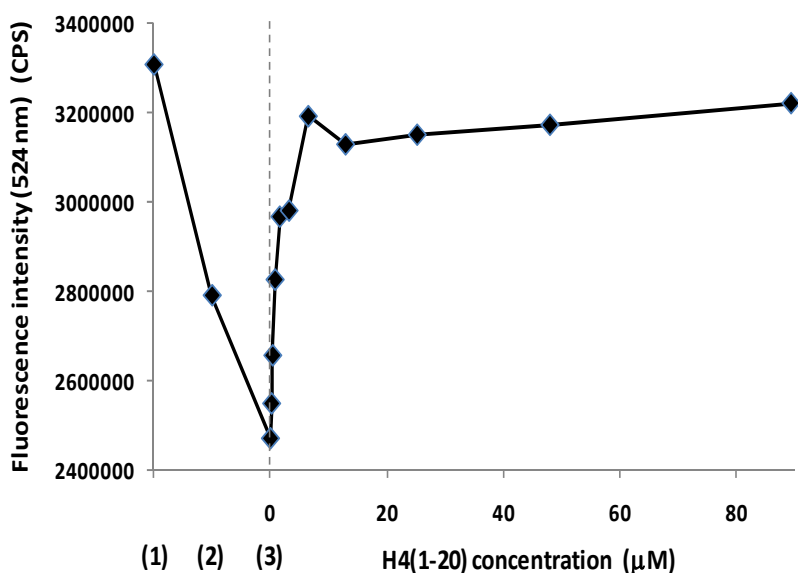


Figure 4.4. Fluorescence change of H4FLme1 association followed by H4(1-20) competitive titration. Data were collected on a Fluoro-Max 4 fluorimeter (Horiba Jobin Yvon) with the excitation and emission at 498 nm and 524 nm respectively. 2 μM of PRMT1 and 100 μM of SAH were added into the reaction buffer containing 0.4 μM of H4FLme1 sequentially to show the fluorescence decrease. Then increasing concentration of unlabeled H4(1-20) were titrated into the bi-substrate-enzyme mixture to show the fluorescence recovery due to competitive binding of H4(1-20) and H4FLme1 to PRMT1. (1) H4FLme1 (0.4 μM); (2) H4FLme1 (0.4 μM) + PRMT1 (2 μM); (3) H4FLme1 (0.4 μM) + PRMT1 (2 μM) + SAH (100 μM).

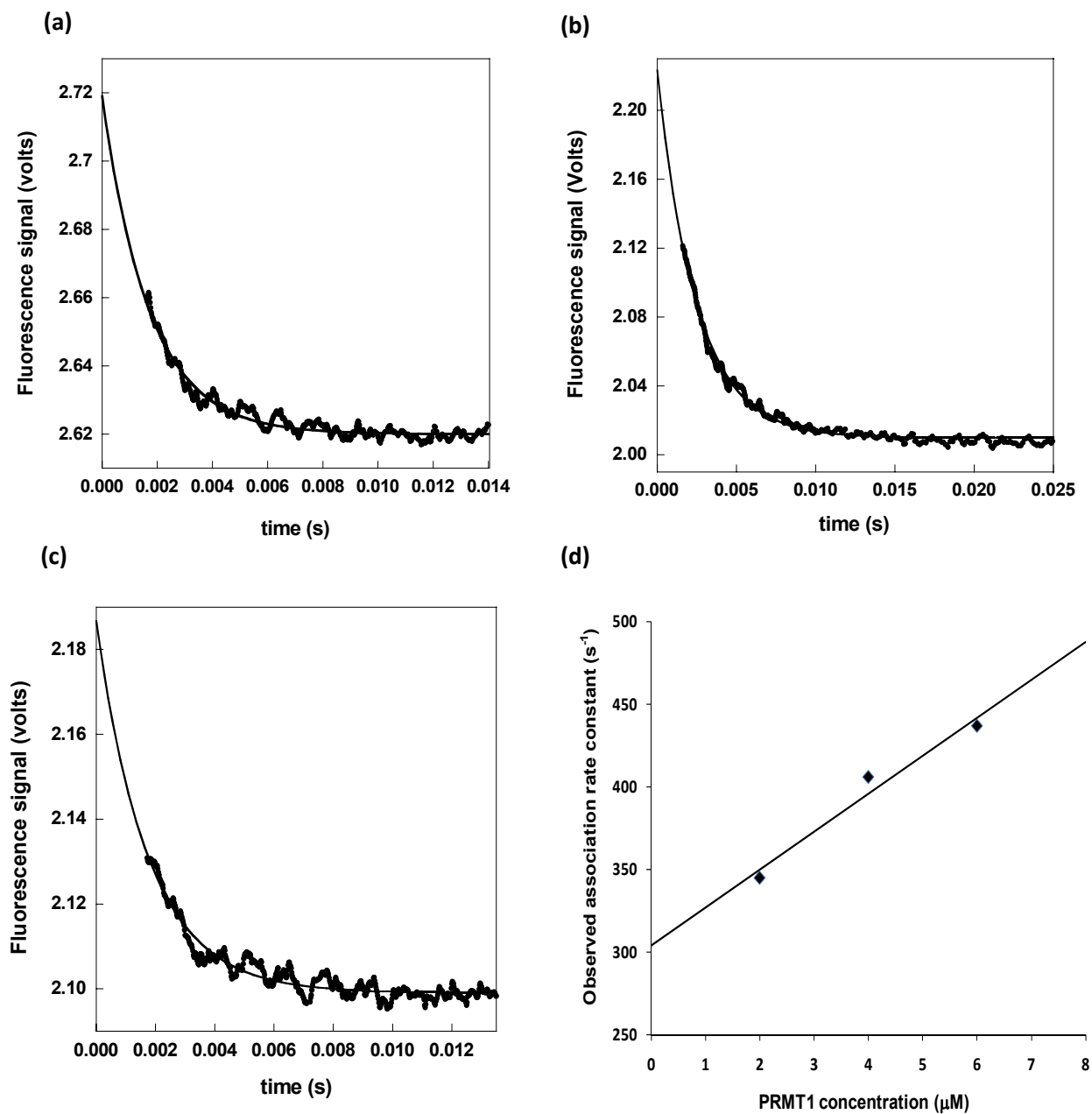


Figure 4.5. Stopped-flow measurements of peptide association with PRMT1. Panel (a), (b), and (c) show the fluorescence change of H4FL, H4FLme1, and H4FLme2 (0.4 μM) upon mixing with PRMT1 (4 μM) at 30 °C in the reaction buffer, respectively. Excitation wavelength was selected at 495 nm and emission ≥ 510 nm was detected. Each sample was

injected 4 to 6 times. The black dots show the averaged data points, and the curves are fit with eq 2. Panel (d) shows the observed association rate constant of H4FLme1 plotted against the concentration of PRMT1. The data were fit to linear eq 4.

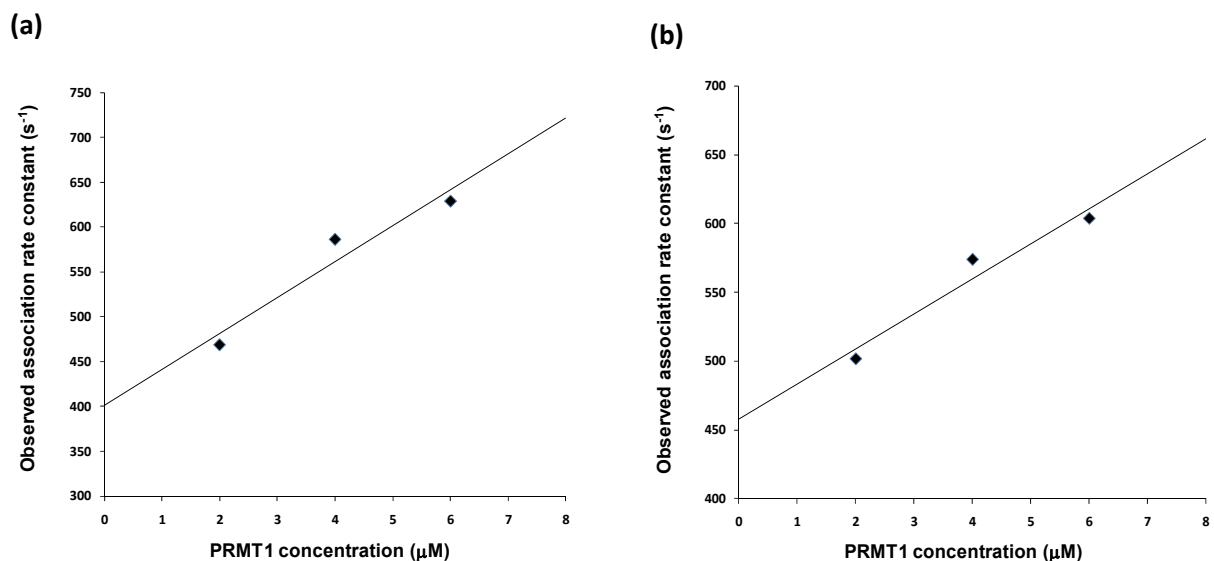


Figure 4.6. Plot of k_{obs} versus protein concentration obtained from stopped-flow fluorescence measurements. Panel (a) and (b) show the linearity between the observed association rate constant and PRMT1 concentration for H4FL and H4FLme2, respectively. 0.4 μM fluorescent peptide was mixed with increasing concentration of PRMT1 (2, 4 and 6 μM) at 30 °C in the reaction buffer. Excitation was 495 nm and emission was ≥ 510 nm. Each sample was injected 4~6 times.

4.2.4. Measurement of dissociation rate constants of peptides from PRMT1.

We next measured dissociation rate constants (k_{off}) of H4FL, H4FLme1, H4FLme2 from PRMT1. A trapping experiment was designed as previously described (**119**). In this measurement, one solution containing 0.4 μM fluorescent ligand and 2 μM PRMT1 was rapidly

mixed with the other solution containing a large excess of unlabeled H4 peptide, *i.e.*, 50 μM of H4(1-20). Following mixing, the fluorescent ligand dissociated from the PRMT1 complex, and the free PRMT1 was trapped with excess H4(1-20). The single-exponential time course reflects this dissociation process, with the expected recovery of fluorescence of the labeled peptide as it is released to bulk solution (Figure 4.7). The dissociation rate constants obtained from these measurements are $333 \pm 9 \text{ s}^{-1}$ for H4FL, $292 \pm 3 \text{ s}^{-1}$ for H4FLme1, and $319 \pm 6 \text{ s}^{-1}$ for H4FLme2.

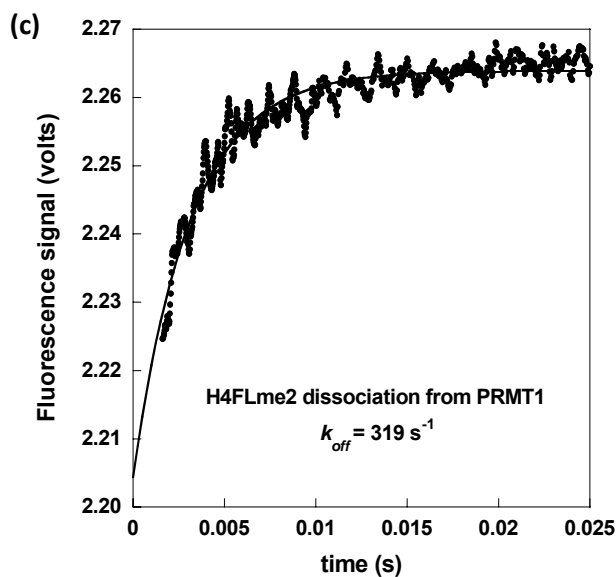
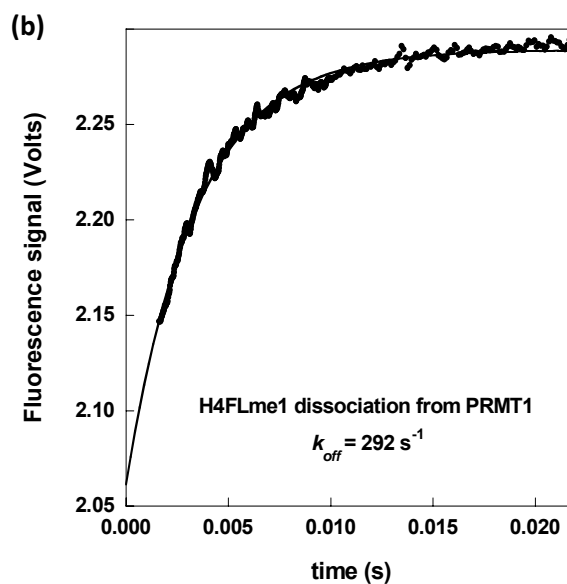
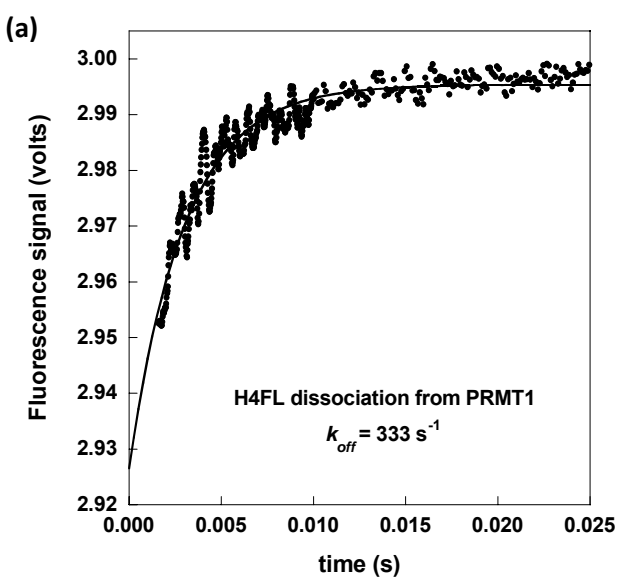


Figure 4.7. Stopped-flow measurements of peptide dissociation from PRMT1. 0.4 μM fluorescent peptide was premixed with 2 μM PRMT1 in the reaction buffer. The solution was then rapidly mixed with 50 μM H4(1-20) on stopped-flow instrument at 30 $^{\circ}\text{C}$. Each sample was injected 4 to 6 times. The black dots show the averaged data points, and the curves are fit with eq 2. (a), (b), and (c) show the dissociation time courses of H4FL, H4FLme1, and H4FLme2 from PRMT1, respectively.

4.2.5. Effect of SAH on enzyme binding and dissociation of H4FLme1.

We also examined how the cofactor analog SAH affects the association and dissociation of the fluorescent substrate H4FLme1 with PRMT1. For the binding experiment, 100 μM of SAH was preincubated with PRMT1 (2, 4, and 6 μM) prior to rapid mixing with H4FLme1. The time course for PRMT1-SAH binding with H4FLme1 was monitored with stopped-flow fluorescence (Figure 4.8a). It is noted that the magnitude of the fluorescence change of H4FLme1 upon association with PRMT1-SAH is 2-fold larger than its binding with apo PRMT1 under the same condition (Figure 4.5b), and the association rate constant is two-fold higher (Table 4.3), indicating that SAH modulates the microenvironment of the fluorophore in the ES complex. More importantly, the time course data can only be fitted to a double exponential function, rather than a single exponential function as observed above, suggesting that the binding is not a single-step process and that minimally two steps are involved (Scheme 4.2b). The double exponential fitting produces two sets of k_{obs} , one for a fast phase and the other for a slow phase (phase 1 and phase 2 in Figure 5a, 5b). The rate constant values can be further fit to a two-step binding model (eq 5) (120). The first-step binding rate constant k_1 was determined from the slope of the fast phase as $48 \pm 1 \mu\text{M}^{-1}\text{s}^{-1}$. The plateau of the slow phase ($36 \pm 2 \text{ s}^{-1}$) corresponds to the sum of k_2 and k_{-2} , and the difference on the ordinate axis between this plateau and the intercept of

the fast phase yields $117 \pm 3 \text{ s}^{-1}$ for k_{-1} . Also, we measured the dissociation progression course for H4FLme1 from PRMT1 in the presence of $100 \text{ }\mu\text{M}$ SAH (Figure 5c). Similar to the dissociation experiment for the H4FLme1—PRMT1 complex, excess H4(1-20) was used as the trapping ligand. Again, the dissociation time course could not be fitted to a single exponential function, confirming that the binding of H4FLme1 with PRMT1-SAH is not a single-step process. The two rate constants obtained from the double exponential fit ($109 \pm 1 \text{ s}^{-1}$ and $19 \pm 0.2 \text{ s}^{-1}$) correspond to the two reverse rate constants in the two-step binding model (k_{-1} and k_{-2} in Scheme 4.2b). Of note, the k_{-1} value from the trapping experiment is very close to that obtained from the binding experiment, supporting the validity of the two-step model. Combining the kinetic data for binding and dissociation, all the four rate constants of Scheme 4.2b were calculated. The k_{off} for H4FLme1 dissociation from PRMT1-SAH complex is about three-fold lower than that of apo-PRMT1 (Table 4.3). In addition, the presence of $100 \text{ }\mu\text{M}$ SAH or SAM was found to have a similar effect on the dissociation of H4FLme2 from the PRMT1-cofactor complex as described above (Figure 4.8d and Figure 4.9), lowering its k_{off} to $204 \pm 3 \text{ s}^{-1}$ or $163 \pm 3 \text{ s}^{-1}$, respectively. The kinetic difference between H4 peptide binding to holo-PRMT1 and to apo-PRMT1 suggests that the presence of the cofactor modulates the PRMT1-substrate interaction.

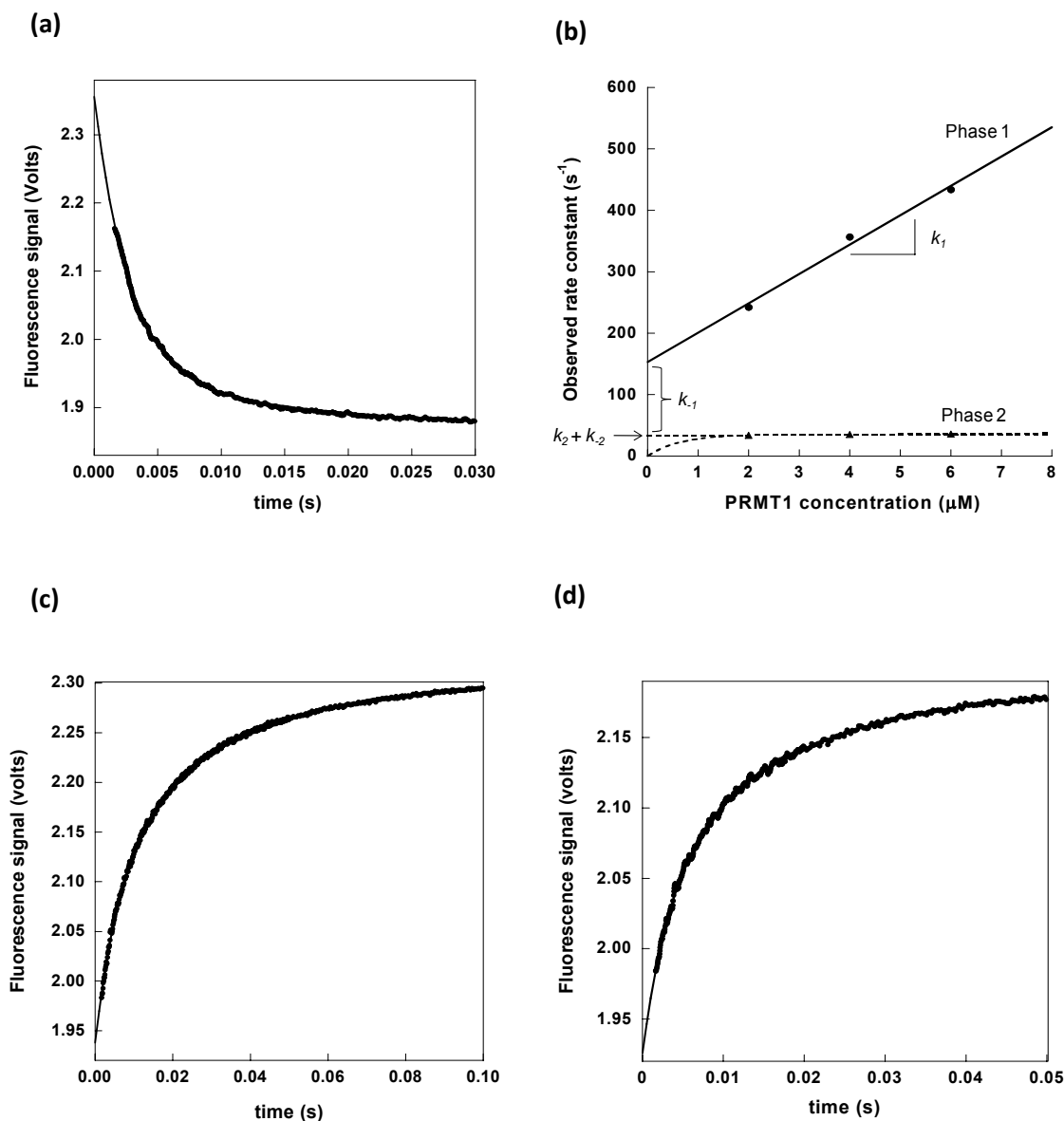


Figure 4.8. Effect of SAH on the binding and dissociation of H4 substrate. Panel (a) shows the fluorescence change of H4FLme1 ($0.4 \mu M$) upon mixing with a solution containing $4 \mu M$ PRMT1 and $100 \mu M$ SAH at $30 \text{ }^\circ C$ in the reaction buffer. The data are fit with a double-exponential function (eq 3). The observed rate constants for phase 1 and phase 2 are plotted against the concentration of PRMT1 (or PRMT1-SAH complex), and the data are fit to eq 5 to

get the four rate constants for the two phases, as shown in panel (b). Panel (c) and (d) show the dissociation time course of H4FLme1 and H4FLme2 from PRMT1-SAH complex, respectively. 0.4 μM fluorescent peptide was premixed with 2 μM PRMT1 and 100 μM SAH in the reaction buffer. The solution was then rapidly mixed with 50 μM H4(1-20) on stopped-flow instrument. The data are fit to eq 3.

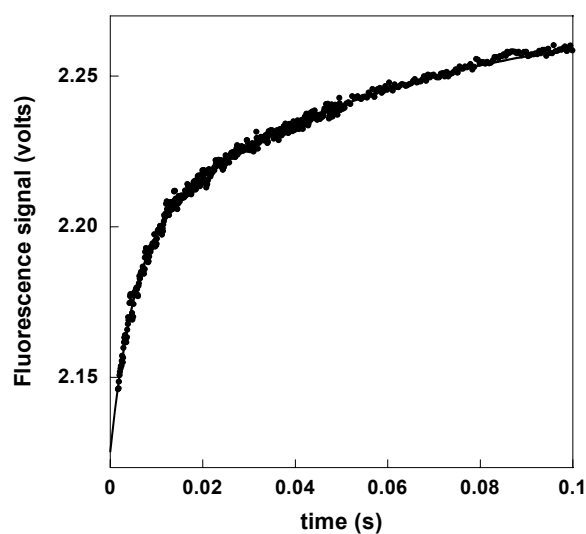
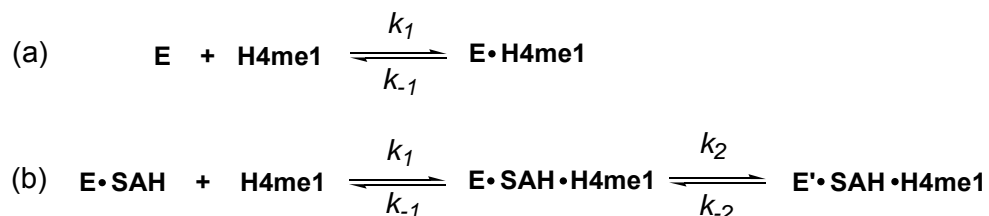


Figure 4.9. Stopped-flow measurement of H4FLme2 dissociation from PRMT1-SAM complex. 0.4 μM fluorescent peptide was premixed with 2 μM PRMT1 in presence of 100 μM SAM in the reaction buffer. The solution was then rapidly mixed with 50 μM H4(1-20) on stopped-flow instrument at 30°C. The sample was injected 4~6 times. The black dots show the averaged data points, and the curve is fit with a double exponential equation (eq 3).

Scheme 4.2. Two different kinetic models of substrate association with PRMT1

apoenzyme and holoenzyme. (a) Single-step binding model between H4FLme1 and PRMT1.

(b) Two-step binding model between H4FLme1 and PRMT1-SAH complex. E: open-state PRMT1. E': closed-state PRMT1.



4.2.6. Progression of arginine methylation probed by stopped-flow fluorescence.

Having determined the binding and dissociation rate constants of H4 substrates and products, we then investigated possible fluorescence signal changes that reflect PRMT1-mediated methylation. Toward this end, we measured the fluorescence changes of H4FL and H4FLme1 over the entire methylation reaction course (Figure 4.10a and 4.10b). In the stopped-flow experiments, a solution containing 2 μM PRMT1 and 100 μM SAM was mixed with a solution containing 0.4 μM fluorophore-labeled substrate to initiate the methylation. Such single-turnover conditions increase the chance of identifying active enzyme intermediates. Interestingly, a biphasic time course was observed. The fluorescence signal for the first phase decreased (phase I), and then gradually increased until a plateau was reached (phase II). A double exponential function was applied to determine the rate constants for the two phases ($0.14 \pm 0.01 \text{ s}^{-1}$ and $0.022 \pm 0.001 \text{ s}^{-1}$ for the methylation of H4FL, and $7.2 \pm 0.2 \text{ s}^{-1}$ and $0.034 \pm 0.001 \text{ s}^{-1}$ for the methylation of H4FLme1). The second phase, *i.e.* the slower phase, likely reflects the methyl transfer step because the rate constants are in the same range as the k_{cat} values measured from the steady-state experiments ($0.43 \pm 0.01 \text{ min}^{-1}$, $0.27 \pm 0.01 \text{ min}^{-1}$, Table 4.2). Also, product release

cannot contribute to the slow phase given that the dissociation rate constants of H4FLme1 and H4FLme2 (Table 4.3) are several thousand-fold larger than the rate constants for the slow phase. On the other hand, the fast phase observed in the time course is of great interest. It does not relate to the substrate binding, because the observed first-order rate constants for binding of the substrate (*e.g.*, $248 \pm 3 \text{ s}^{-1}$ for H4FLme1 at $2 \mu\text{M}$ of PRMT1 in presence of the cofactor) are significantly greater than the rate constants for phase I in the methylation experiments (*i.e.*, $0.14 \pm 0.01 \text{ s}^{-1}$, $7.2 \pm 0.2 \text{ s}^{-1}$). Indeed, if a closer look is taken at the very early part of the first phase (Figure 4.10a and 4.10b, insets), an even faster phase can be discerned, which likely corresponds to the substrate binding step. Therefore, the first phase in the methylation course reveals a new step existing after the ternary complex formation, and prior to the methyl transfer step. Most likely, the newly discovered step corresponds to an enzyme isomerization step towards a catalytically active form in preparation for methyl transfer.

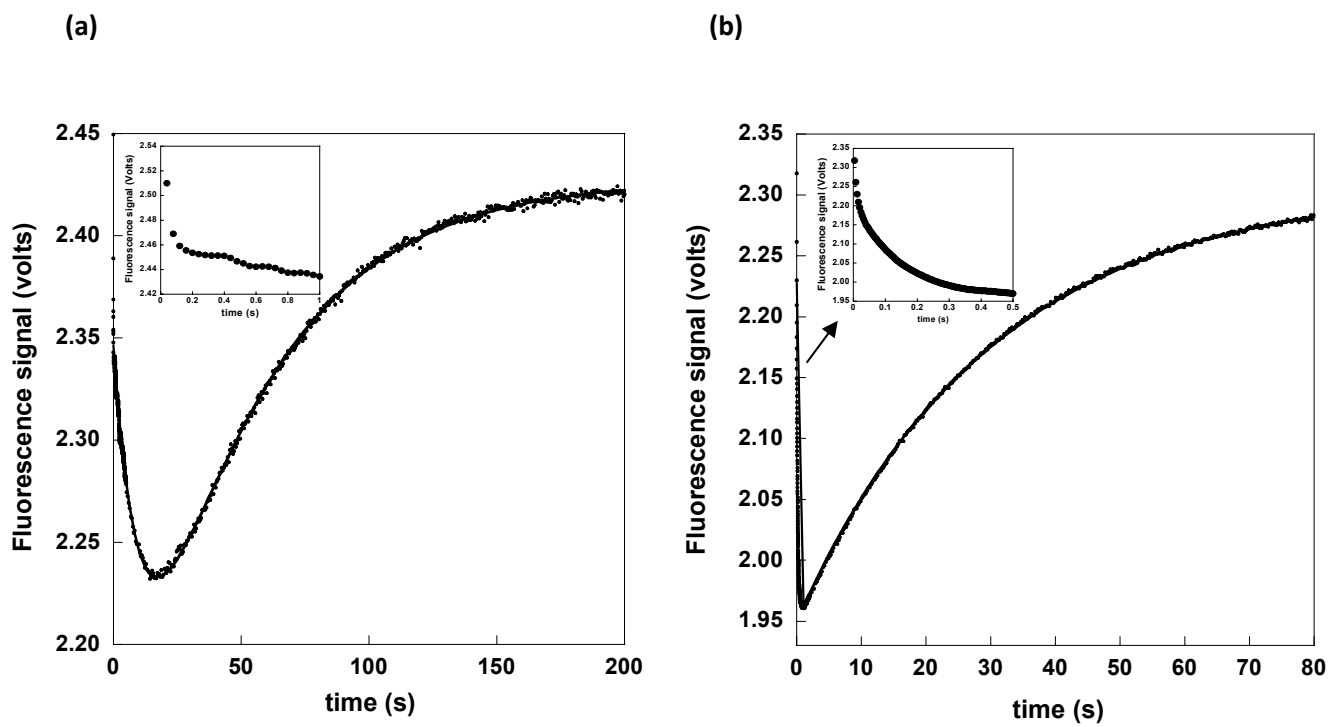


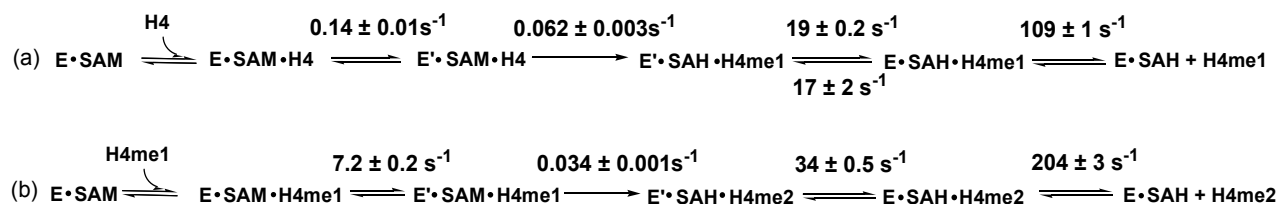
Figure 4.10. Time course of PRMT1 catalysis probed by stopped-flow fluorescence.

(a) H4FL was used to probe the progression of two methyl transfer; and (b) H4FLme1 was used to detect the progression of the second methyl transfer. In both measurements, 0.4 μM fluorescent peptide was mixed with a solution containing 2 μM PRMT1 and 100 μM SAM at 30°C in the reaction buffer. Each reaction was performed 4 to 6 times, and the black dots show the averaged data points. The data are fit with eq 3. Inset graphs magnify the data points at the very early stage of the reaction.

Table 4.3. Summary of rate constant data obtained from stopped-flow fluorescence measurements. * indicates the rate constant for the fast phase (phase 1) calculated from double-exponential fitting.

Rate constants Peptides	Association with PRMT1 ($\mu\text{M}^{-1}\text{s}^{-1}$)	Association with PRMT1-SAH ($\mu\text{M}^{-1}\text{s}^{-1}$)*	Dissociation from PRMT1 (s^{-1})	Dissociation from PRMT1-SAH (s^{-1})	Dissociation from PRMT1-SAM (s^{-1})	First phase in the course of methylation (s^{-1})	Second phase in the course of methylation (s^{-1})
H4FL	40 ± 1	-	333 ± 9	-	-	0.14 ± 0.01	0.022 ± 0.001
H4FLme1	23 ± 1	48 ± 1	292 ± 3	$109 \pm 1^*$	-	7.2 ± 0.2	0.034 ± 0.001
H4FLme2	26 ± 1	-	319 ± 6	$204 \pm 3 \text{ s}^*$	$163 \pm 3^*$	-	-

Scheme 4.3. Proposed minimal kinetic model of PRMT1 catalysis. (a) first methylation and (b) second methylation of H4. The chemical step is rate-limiting. E: open-state PRMT1. E': closed-state PRMT1.



4.3. Conclusion

Our stopped-flow fluorescence data provide a detailed view of arginine methylation catalyzed by PRMT1. Under this scheme, the methyl transfer step is the major rate-limiting step which proceeds much more slowly than substrate association/dissociation. Binding of cofactor SAM/SAH appreciably affects the interaction between H4 peptide and the enzyme, probably due to a conformational change upon enzyme-cofactor complex formation. Importantly, the transient kinetics data reveal a conformational transition step following the substrate binding and prior to the chemical step. This protein isomerization likely reorganizes the active site of PRMT1 from an open state to a closed state, activating the side-chain terminal nitrogen of H4R3 and/or the reactive methyl group of SAM to facilitate the methyl transfer. Further structural studies will be essential to validate this kinetic proposition.

4.4. Experimental

4.4.1. Design and synthesis of modified H4 peptides

The amino-terminal peptide of histone H4 containing the first 20 amino acid residues with different methylation patterns and a fluorescein group were synthesized using Fmoc [N-(9-fluorenyl) methoxycarbonyl]-based solid phase peptide synthesis (SPPS) protocol on a PS3

peptide synthesizer (Protein Technology, Tucson, AZ) as described previously (86). Each amino acid was coupled to the solid phase with 4 equivalents of amino acid/HCTU [O-(1H-6-Chlorobenzotriazole-1-yl)-1,1,3,3-tetramethyluronium hexafluorophosphate] (Novabiochem, Darmstadt, Germany). The Fmoc group was deprotected with 20% v/v piperidine/DMF, and the N-terminal amino acid was acetylated with acetic anhydride. The peptide was cleaved from the Wang resin by a cleavage solution consisting of 95% trifluoroacetic acid (TFA), 2.5% H₂O and 2.5% triisopropylsilane. It was then precipitated in cold ether and pelleted by centrifuge. Crude peptides were collected and purified using a Varian Prostar instrument equipped with a C18 Reversed-phase High Performance Liquid Chromatography (RP-HPLC) column, where 0.05% TFA-containing water and 0.05% TFA-containing acetonitrile were two mobile phases used in gradient purification. The purity and identity of peptides were confirmed by MALDI-MS. For the peptides linked to a fluorescein group, their concentrations were calibrated according to the absorption of fluorescein at 492 nm.

4.4.2. Expression and purification of PRMT1

Recombinant His-tagged rat PRMT1 was expressed in *E. coli* and purified with Ni-charged His₆x-tag binding resin as reported previously (121). Briefly, the PRMT1-pET28b plasmid was transformed into *BL21(DE3)* (Stratagene). Transformed bacteria were incubated in LB media at 37°C for growth, and then 16°C for protein expression which was induced by 0.3 mM IPTG. Cells were harvested by centrifuge and lysed by French Press. The supernatant containing PRMT1 protein was loaded onto the Ni-charged His₆x-tag binding resin (Novagen) that was equilibrated with column buffer (25 mM Na-HEPES, pH 7.0, 300 mM NaCl, 1 mM PMSF, and 30 mM imidazole). Beads were washed thoroughly with column buffer, followed by washing buffer (25 mM Na-HEPES, pH 7.0, 300 mM NaCl, 1 mM PMSF, and 70 mM

imidazole), and protein was eluted with elution buffer (25 mM Na-HEPES, pH 7.0, 300 mM NaCl, 1 mM PMSF, 100 mM EDTA, and 200 mM imidazole). Different eluent fractions were checked by 12% SDS-PAGE, and PRMT1 concentration was determined by Bradford assay.

4.4.3. Chemical crosslinking and Western blotting of PRMT1 oligomers

To study the relationship between PRMT1 oligomerization and concentration, His6x-rPRMT1 was diluted in the range of 0.012 μM ~ 3.13 μM with storage buffer (25 mM HEPES (pH 7.0), 250 mM NaCl, 1 mM EDTA, 10% glycerol, and 1 mM DTT) containing 0.1% Triton X-100, and incubated at 4 °C overnight. Then PRMT1 was cross-linked with 0.025% (v/v) glutaraldehyde at room temperature for 5 min. The reactions were quenched by addition of SDS loading buffer, and PRMT1 proteins were separated by 8% SDS-PAGE followed by western blot detection, with anti-PRMT1 rabbit polyclonal IgG (Upstate) as the primary antibody and goat anti-rabbit IgG-HRP (Millipore) as the secondary antibody. After washing away the unbound probes, PRMT1 bands were visualized using the SuperSignal West Pico Trial Kit (Thermo Scientific). The film image was analyzed by Quantity One, and the molar fraction of PRMT1 monomer, dimer and oligomer were plotted against PRMT1 concentration.

4.4.4. Radioactive methyltransferase assay

The methylation assays of different H4 peptides or protein were performed using ^{14}C -isotope labeled SAM at 30 °C. The reaction buffer contained 50 mM HEPES (pH 8.0), 50 mM NaCl, 1mM EDTA and 0.5 mM DTT. H4 substrate and [^{14}C]-SAM were preincubated in the reaction buffer for 5 min prior to initiation of the methyl transfer reaction by adding PRMT1 (0.01 μM typically). The reaction time was controlled under initial rate conditions such that typical reaction yields were less than 20%. The reaction was quenched by spotting the reaction mixture on P81 filter paper disc (Whatman). After the paper discs were washed with 50 mM

NaHCO₃ (pH 9.0) and air dried, liquid scintillation counting was performed to measure the amount of methylated products. Values for K_m and k_{cat} were obtained by measuring the initial velocity of the reaction at various concentrations of one substrate and fixed saturating concentration of the other substrate (cofactor). The kinetic data were fitted to the Michaelis-Menton equation using non-linear regression methods.

4.4.5. Equilibrium fluorescent titration

The K_d value for PRMT1 and the fluorescent peptide binding was measured by fluorescence anisotropy methods. Increasing concentrations of PRMT1 were added to a constant concentration of fluorescent peptide (0.2 μ M) at 30°C in the same buffer mentioned above. The anisotropy increase due to the formation of large ES complexes was recorded with a Fluoro-Max 4 fluorimeter (Horiba Jobin Yvon). The excitation and emission wavelengths were set at 498 nm and 524 nm, respectively. Data were fit to eq 1, where P is the fluorescence anisotropy at a given concentration of PRMT1, A is the amplitude, and k_d is the observed dissociation constant between PRMT1 (E) and H4 peptide (S).

$$P = A * \frac{(E + S + K_d) - \sqrt{(E + S + K_d)^2 - 4 * E * S}}{2 * S} + C \quad (1)$$

4.4.6. Stopped-flow fluorescence measurements

The transient-state kinetics of association, dissociation and catalytic turnover were determined by stopped-flow fluorescence assays using several fluorescein-labeled H4 peptides (H4FL, H4FLme1, H4FLme2) as probes. Binding of the fluorescent peptide to PRMT1 (or PRMT1-cofactor complex) quenches the peptide fluorescence, while release of the peptide restores the fluorescence. The transient fluorescence signal change was detected at 30°C on an

Applied Photophysics stopped-flow equipment using an excitation wavelength of 495 nm and a long pass emission filter centered at 510 nm. Four to six shots were collected and averaged for each curve. For the association measurements, increasing concentrations of PRMT1 (2, 4, 6 μM), with or without 100 μM SAH were mixed with 0.4 μM of fluorescent peptide in the reaction buffer (50 mM HEPES (pH 8.0), 50 mM NaCl, 1 mM EDTA, 0.5 mM DTT). After averaging the shot data, the association time courses were fitted to a single exponential function (eq 2) when the cofactor was absent, or to a double exponential function (eq 3) when the cofactor was present. In eq 2 and 3, F is the fluorescence intensity at time t , A is the amplitude of the fluorescence change, and k_n are the rate constants. The observed rate constants were plotted against PRMT1 concentration, and the data were fit to eq 4 (in the absence of SAH) or eq 5 (in the presence of SAH) to derive the association rate constants k_{on} or k_1 , respectively. For eq 5, k_1 and k_{-1} are the association and dissociation rate constants, and k_2 and k_{-2} are the forward and reverse rate constants of phase 2.

$$F = A * \exp(-k * t) + C \quad (2)$$

$$F = A_1 * \exp(-k_1 * t) + A_2 * \exp(-k_2 * t) + C \quad (3)$$

$$k_{obs} = k_{on} * [\text{PRMT1}] + k_{off} \quad (4)$$

$$k_{obs} = k_1 * [\text{PRMT1}] + k_{-1} + k_2 + k_{-2} \quad (5)$$

For the dissociation rate constant measurements, 0.4 μM fluorescent peptide was prebound to 2 μM PRMT1 (with or without 100 μM SAH/SAM), and the complex was rapidly mixed with 50 μM unlabeled H4(1-20) peptide to trap the free PRMT1. The averaged shot data were fitted to eq 2 when the cofactor is absent or to eq 3 when the cofactor is present. Here k (or

k_1) is the dissociation rate constant (k_{off}), and k_2 reflects the rate constant for a putative conformational change before substrate release.

For PRMT1 methylation kinetics in single turnover conditions, H4FL or H4FLme1 peptides were used to probe the reaction rate for transfer of both methyl groups (H4FL) or only the second methyl group (H4FLme1). In these reactions, 2 μM PRMT1 and 100 μM SAM were mixed with 0.4 μM H4FL or H4FLme1 in the reaction buffer mentioned above. The methylation time course exhibited two distinct kinetic phases, and was fitted to a double exponential function (eq 3), where the observed k_2 likely reflects the methyl transfer rate constant. The rate constant for transfer of the first methyl group (k_1') is calculated from eq 6, where k_{tot} (the total rate constant for transfer of two methyl groups) is obtained from H4FL methylation time course, and k_2' (the rate constant for transfer of the second methyl group) is obtained from H4FLme1 methylation time course.

$$1/k_{tot} = 1/k_1' + 1/k_2' \quad (6)$$

CHAPTER 5

HISTONE H4 ACETYLATION DIFFERENTIALLY MODULATES ARGININE METHYLATION BY AN *IN CIS* MECHANISM

(This work is mainly based on the published paper, *J. Biol. Chem.* 286 (2011) 20323-34. In this project, the author is obliged to Dr. Juxian Wang for her contribution to NMR calibration of the peptide concentrations and part of PRMT1 activity tests, to Sabrina Asher for her contribution to the peptide preparation, and to Dr. Ivaylo Ivanov and Carlo Guardiani for the molecular modeling of peptide structures.)

5.1. Introduction

The nucleosome is the fundamental structural unit of chromatin, in which 146 base pairs of DNA are wrapped around an octamer of two molecules of each of the four core histones (H2A, H2B, H3 and H4 proteins). Widespread post-translational modifications (PTMs) of the histone proteins have been identified, including acetylation, phosphorylation, methylation, ubiquitination, and ribosylation (5, 122). The types and sites of modifications and the specific functions of these PTM marks in modulating chromosomal remodeling and DNA function have been intensively studied in recent years. In particular, significant amounts of data have pointed out the functional correlation of histone modification with transcriptional regulation (123, 124). While certain modifications are shown as representative marks of active transcription (*e.g.*, H3K4 methylation, H3K36 methylation, H3 and H4 lysine acetylation, and H2B ubiquitylation), some others are correlated with transcriptional repression (*e.g.*, H3K9 methylation, H3K27 methylation, H4K20 methylation, and H2A ubiquitylation) (44, 125). Of importance, many histone PTM marks co-occurring in the same histones can be synergistic or antagonistic with one another, forming complicated combinatorial histone modification patterns which have been

proposed to function as a set of multivalent “histone codes” that promote or repress various chromosomal transactions that occur in the cell (5, 126, 127). Histone PTM patterns provide a biochemical index for individual cell type and disease state, and correlate with particular biological phenomena of the cell (128-131). Given the abundance of histone modification marks and the dynamic changes of histone modification patterns in response to cell types and differentiation contexts, it remains a challenging biological theme to illuminate the molecular basis of how histone codes and code networks are biochemically created and manifest their downstream impacts on chromatin function (127).

The N-terminal tail of histone H4 is heavily modified at several sites, including Ser-1 phosphorylation, Arg-3 methylation, Lys-5, -8, -12, -16, -20 acetylation (*i.e.*, K5ac, K8ac, K12ac and K16ac), and lys-20 methylation (40, 132-138). These modifications have been shown to be very dynamic, and distinct histone modification patterns have been observed in different cell types, or at different developmental stages of life, or in different phases of cell cycle (128, 129, 139, 140). For example, Pesavento *et al.* (140) characterized H4 modification by using Top-down mass spectrometric approaches coupled with two-dimension liquid chromatography and identified 42 forms of H4 in HeLa cells each of which contains different modification patterns. Coon and coworkers used mass spectrometry methods to identify 74 histone H4 isoforms in differentiating human embryonic stem cells (139). There is a strong need to understand how these combinatorial PTM patterns are established at the histone tail.

Acetylation represents one of the most frequent modifications at the H4 tail. The acetylation is introduced by several histone acetyltransferases (HATs), including p300/CBP (134, 141), Tip60 (142, 143), and yeast protein Esa1 (144). For example, both p300/CBP and Esa1 acetylate H4 at K5, 8, 12, and 16 *in vitro*, and in the context of a nucleosome, acetylation of

K5 and K8 by p300 is preferred (134, 141). K16 is a preferred acetylation site by the MOF subunit of the MSL and NSL complexes (145, 146). Histone acetylation is reported to affect the assembly of higher order nucleosome structures (147) and is generally proposed to coactivate gene expression. Since there are four major acetylation sites at the H4 tail, *i.e.*, K5, 8, 12, 16, HAT catalysis can produce a total of 16 acetylated H4 isoforms. Effort is needed to address which acetylation site and which acetylation combination play predominant roles in determining the transcriptional status of gene loci. H4K16 acetylation has been particularly shown to be a hallmark of open chromatin and transcriptional activation (148). It is noteworthy to point out that different acetylation patterns may be correlated with different functions. For example, K5 and K12 acetylations are known to be predeposition marks, highly enriched prior to chromatin assembly during S-phase (149, 150). Possibly, the acetylation event may affect gene expression by influencing or even determining other modifications at the histone tail. This is especially true given that histone acetylation has been demonstrated in several studies to be an early event and occur upstream of other modifications (140, 151).

Here, we investigated how different H4 acetylations and their combinations affect methylation of H4 at Arg-3 (*i.e.*, H4R3me) at the biochemical level. Protein arginine methylation is catalyzed by protein arginine methyltransferases (PRMTs) which are S-adenosyl methionine (AdoMet, SAM)-dependent enzymes and generally classified into type I and type II families. PRMT1 is the predominant member of type I PRMTs and PRMT5 is a representative member of type II PRMTs in mammalian cells (Figure 5.1). Type I PRMTs are able to transfer up to two methyl groups from the cofactor AdoMet to one single terminal nitrogen of the guanidino group of specific arginine residues in a protein substrate, resulting in ω -N^G-monomethylarginine (MMA) and ω -N^G,N^G-asymmetric dimethylarginine (ADMA) products (19, 21, 23, 24). In

contrast, Type II PRMT enzymes place one methyl group on each of the two terminal guanidino nitrogens to form MMA and ω -N^G, N^G-symmetric dimethylarginine (SDMA) products (24, 26, 27). Due to the lack of structural information, it is still poorly understood how the regiospecificity in methylated products is achieved. At the H4 tail, both PRMT1 and PRMT5 are able to methylate H4R3 *in vivo*. Of significance, the biological impact of H4R3 methylation by PRMT1 is opposite to that of PRMT5: PRMT1-mediated dimethylation of R3 is correlated with gene activation (40), but the methylation of H4R3 by PRMT5 is in many cases associated with gene repression (76). Our biochemical data show that PRMT1 recognizes and methylates H4 substrates that contain different acetyl marks in a very distinct manner from that of PRMT5, thus providing a molecular insight into the mechanism of how PRMT1 and PRMT5 target the chromatin template and how acetylation contributes to the establishment of H4 modification patterns or codes by an *cis*-acting mechanism. This finding also unveils a clear distinction between type I PRMT and type II PRMT with respect to the mode of substrate specificity regulation.

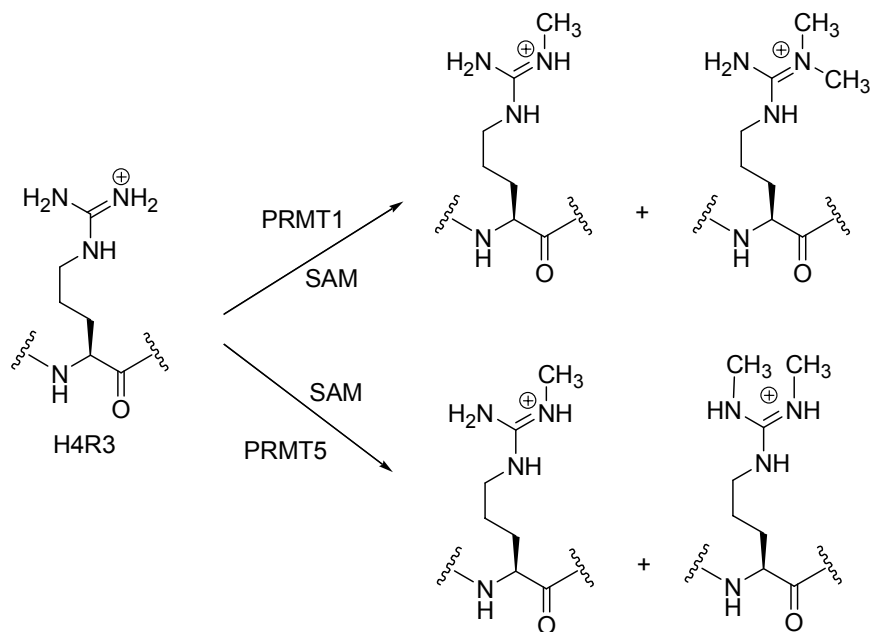


Figure 5.1. Methylation of H4R3 by PRMT1 and PRMT5.

5.2. Results

5.2.1. Design, synthesis, and characterization of modified H4 peptide library.

The N-terminal tail of H4 is subject to many PTMs including R3 methylation and acetylation at K5, 8, 12, and 16 sites. To quantitatively evaluate the *in-cis* effect of acetylation marks on R3 methylation, we designed a library of H4 peptides containing the first 20 amino acids that incorporate all the 16 possible acetylation combinations, including 1 uncetylated, 4 monoacetylated, 6 diacetylated, 4 triacetylated, and 1 tetraacetylated forms (Table 5.1). All peptides are N-terminally capped with acetic anhydride because virtually all H4 proteins are N-terminally acetylated *in vivo* (129, 139, 140, 152). These peptides are used as substrates of PRMT1 and PRMT5 to evaluate how different acetylation combinations affect the methylation of R3 catalyzed by these two enzymes. It is worthwhile to stress that our data and others have fully determined that the N-terminal peptide sequence represents an authentic substrate of PRMTs and its catalytic properties are very similar to that of the full-length H4 protein (33). All the peptides were synthesized using the standard Fmoc SPPS protocols, purified on C-18 reversed phase HPLC column, and confirmed with MALDI-MS as previously described (86).

Table 5.1. Sequences of synthetic H4 peptides. The ac symbol stands for acetyl group.

Abbreviation	Sequence	MW calculated	MW measured
A. wt H4	ac-SGRGKGGKGLGKGGAKRHRK	2034.2	2034.1
B. H4K5ac	ac-SGRGK _{ac} GGKGLGKGGAKRHRK	2076.2	2076.1
C. H4K8ac	ac-SGRGKGGK _{ac} GLGKGGAKRHRK	2076.2	2076.2
D. H4K12ac	ac-SGRGKGGKGLGK _{ac} GGAKRHRK	2076.2	2076.2
E. H4K16ac	ac-SGRGKGGKGLGKGGAK _{ac} RHRK	2076.2	2076.3
F. H4K5ac8ac	ac-SGRGK _{ac} GGK _{ac} GLGKGGAKRHRK	2118.2	2118.1
G. H4K5ac12ac	ac-SGRGK _{ac} GGKGLGK _{ac} GGAKRHRK	2118.2	2118.4

H. H4K5ac16ac	ac-SGRGK _{ac} GGKGLGKGGAK _{ac} RHRK	2118.2	2118.2
I. H4K8ac12ac	ac-SGRGKGGK _{ac} GLGK _{ac} GGAKRHRK	2118.2	2118.5
J. H4K8ac16ac	ac-SGRGKGGK _{ac} GLGKGGAK _{ac} KRHRK	2118.2	2118.1
K. H4K12ac16ac	ac-SGRGKGGKGLGK _{ac} GGAK _{ac} RHRK	2118.2	2118.3
L. H4K5ac8ac12ac	ac-SGRGK _{ac} GGK _{ac} GLGK _{ac} GGAKRHRK	2160.2	2160.6
M. H4K5ac8ac16ac	ac-SGRGK _{ac} GGK _{ac} GLGKGGAK _{ac} RHRK	2160.2	2160.7
N. H4K5ac12ac16ac	ac-SGRGK _{ac} GGKGLGK _{ac} GGAK _{ac} RHRK	2160.2	2160.3
O. H4K8ac12ac16ac	ac-SGRGKGGK _{ac} GLGK _{ac} GGAK _{ac} RHRK	2160.2	2160.6
P. H4K5ac8ac12ac16ac	ac-SGRGK _{ac} GGK _{ac} GLGK _{ac} GGAK _{ac} RHRK	2202.2	2202.4

Since synthetic peptides typically contain varying amounts of TFA counter ions as a result of HPLC purification, we sought to determine the accurate concentration of each H4 peptide prior to enzymatic analysis. The NMR spectra of H4 peptides show two very characteristic peaks at 7.4 and 8.7 ppm which come from the imidazole side chain of His-18 (Figure 5.2). We used the integration ratio between these two peaks and the methyl peak of standard reagent DSS to calibrate the concentration of each H4 peptide. A typical 1D ¹H-NMR spectrum used for calibration of H4 peptide concentration is shown in Figure 5.2. The use of NMR calibration to obtain the accurate concentration of H4 peptides is technically critical for accurately quantifying and comparing the effect induced by individual acetylation marks. As a matter of fact, varying degrees of difference were observed between weight-based concentrations and NMR-calibrated concentrations (data not shown).

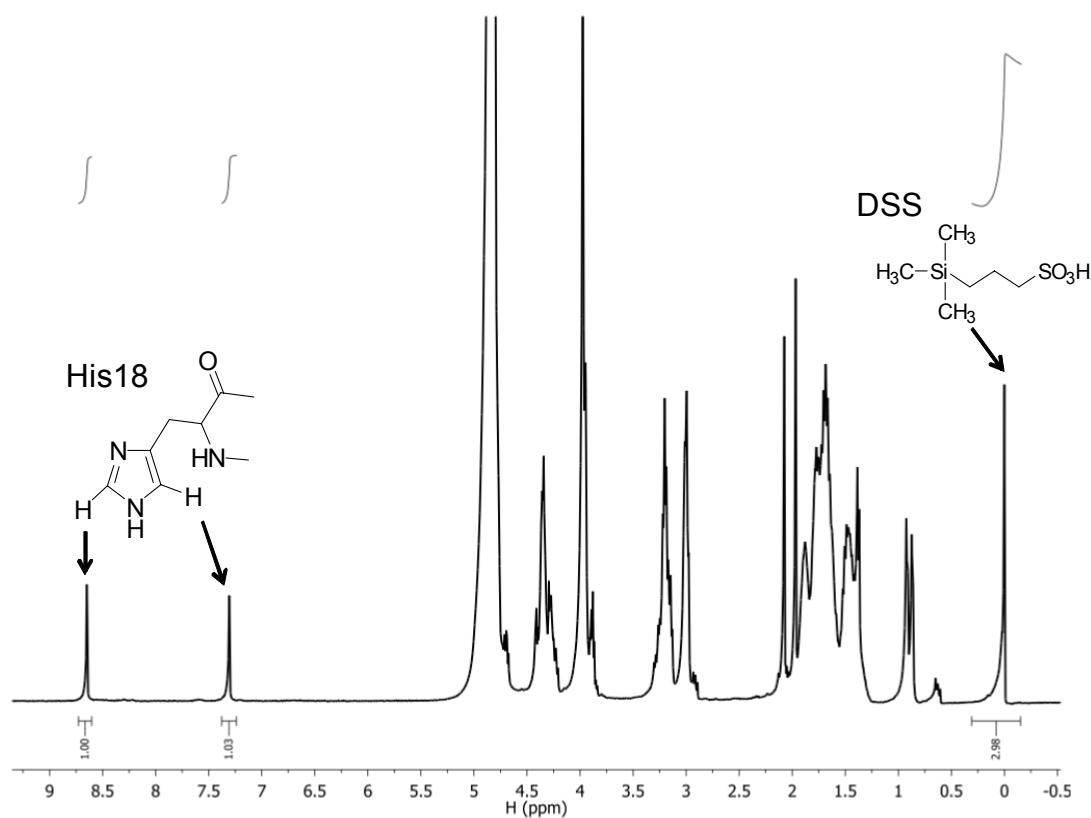


Figure 5.2. A typical NMR spectrum used for calibration of H4 peptide concentration. The NMR solution contained 4.5 mM of H4K16ac peptide and 1 mM of DSS in D₂O.

5.2.2. Impact of H4 acetylation on PRMT1-catalyzed R3 methylation.

Arginine 3 of H4 is methylated by PRMT1. However, the potential effect of acetylation at K5, 8, 12, and 16 on R3 methylation is not clear. The four acetylations at K5, 8, 12, 16 generate multiple combinations. It remains to determine whether individual combination marks affect R3 methylation differentially or in a similar manner and which acetyl mark predominantly modulates R3 methylation.

With the purified H4 library peptides, we tested PRMT1-catalyzed methylation of individual H4 peptides each of which contains a unique acetylation pattern. The methylation

reaction was composed of 0.1 μM of PRMT1, 20 μM of [^{14}C]-AdoMet and 100 μM of each substrate, and the reaction was allowed to proceed for 10 min. The reaction mixtures were resolved on 16% SDS-PAGE and the methylated products were visualized by phosphorimaging and quantitated using ImageQuant software (Figure 5.3). At first glance of the experimental data, it is apparent that some acetylation combinations decrease but some others increase the level of R3 methylation. In particular K5 acetylation is detrimental to R3 methylation, which alone decreases R3 methylation by 30%. In combination with other lysine acetylations, *e.g.*, with K8ac, or K8ac and K12ac, the repressive effect of K5ac is even stronger; the degree of repression reaches 3 and 5 folds, respectively. On the other hand, K16ac leads to a positive impact on R3 methylation. K16 acetylation alone increases the PRMT activity by 30%. The majority of H4 peptides that contain the K16ac mark (except **M** and **P**) are slightly better substrates of PRMT1. For instance, if K16ac coexists with K5ac, K8ac or K12ac, the activation effect is dominant. Compared to K5ac and K16ac, the effect of K8ac and K12ac in regulating R3 methylation seems quite marginal by itself and is influenced by the presence of K5ac or K16ac mark. For example, a repressive effect is observed when K8ac co-presents with K5ac, but a positive effect is observed when K8ac co-presents with K16ac. Overall, these data support that K5ac and K16ac are two counteractive modification marks that affect R3 methylation in opposite ways: K5ac is the predominant factor that negatively impacts R3 methylation, and K16ac positively modulates R3 methylation by PRMT1.

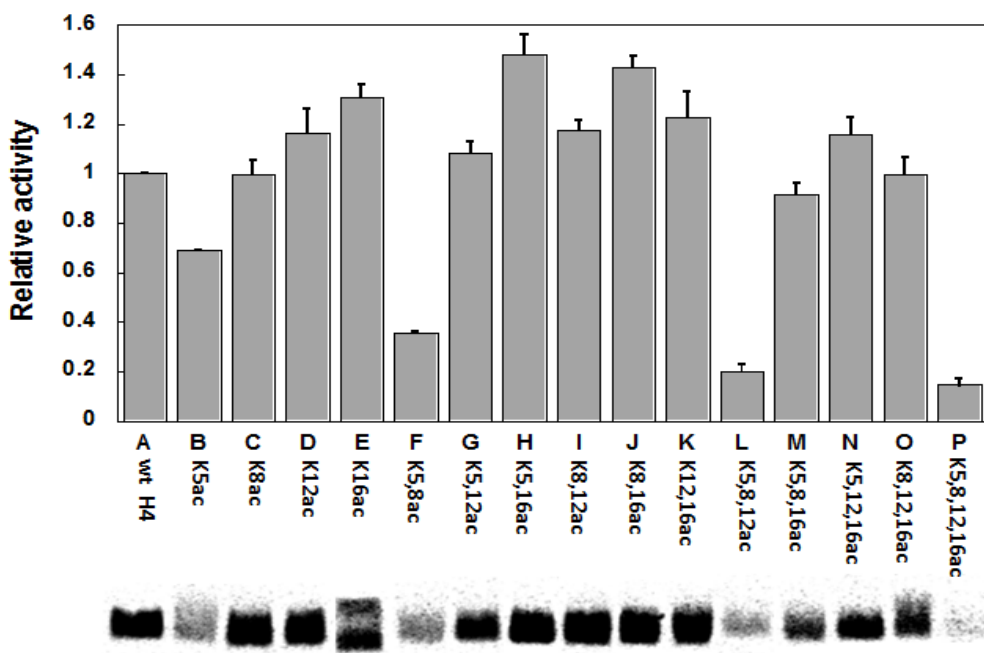


Figure 5.3. Effects of lysine acetylation on Arg-3 methylation by PRMT1. The reaction buffer contained 50 mM of HEPES (pH 8.0), 10 mM of NaCl, and 1 mM of DTT. The concentration of PRMT1, [14 C]-AdoMet and H4-20 were 0.1 μ M, 20 μ M and 100 μ M, respectively. The reaction time was 10 min.

To understand the mechanism by which K5ac and K16ac affect R3 methylation by PRMT1, we measured the steady-state kinetic parameters of unacetylated and several acetylated H4 peptides. The data shown in Table 5.2 reveal that for the methylation of H4K5ac peptide, the k_{cat} decreases by half but there is little change in K_m . These data suggest that acetylation of K5 does not cause explicit changes in the substrate binding and recognition by PRMT1. Likely, the positively charged K5 is required for a methyl transfer step in the catalytic pathway of PRMT1 and acetylation of K5 blocks this key step in the methyl transfer reaction as reflected in its effect on k_{cat} . On the other hand, acetylation of K16 affects K_m more than k_{cat} and V/K is increased from

1.78 to 3.22 $\text{min}^{-1}\mu\text{M}^{-1}$. Thus, K16ac appears to increase the affinity of enzyme-substrate association, but has little effect on the catalytic step.

Table 5.2. Steady-state kinetic parameters of PRMT1 catalysis. The methylation of each peptide by PRMT1 was tested with the radioactive filter binding assay. Varied concentrations of peptide (0 to 20 μM) and 15 μM of [^{14}C]-AdoMet were incubated at 30°C for 5 min in the reaction buffer (50 mM HEPES, pH 8.0, 10 mM NaCl and 1 mM DTT). The reaction was initiated with PRMT1. The methylated products were purified on to P81 filter paper and quantified by liquid scintillation. Calculated methylation rate was plotted as a function of peptide concentration and the data were fitted with Michaelis-Menton equation.

	Substrates	K_m, μM	k_{cat}, min^{-1}	V/K, $\text{min}^{-1}\mu\text{M}^{-1}$
A	wt H4-20	0.34 ± 0.05	0.64 ± 0.13	1.78 ± 0.69
B	H4(1-20)K5ac	0.37 ± 0.06	0.32 ± 0.01	0.86 ± 0.14
C	H4(1-20)K8ac	0.58 ± 0.10	0.50 ± 0.02	0.86 ± 0.15
D	H4(1-20)K12ac	0.27 ± 0.05	0.47 ± 0.01	1.74 ± 0.32
E	H4(1-20)K16ac	0.23 ± 0.05	0.74 ± 0.06	3.22 ± 0.75
H	H4(1-20)K5acK16ac	3.29 ± 0.53	1.02 ± 0.07	0.31 ± 0.05
J	H4(1-20)K8acK16ac	1.11 ± 0.17	1.33 ± 0.06	0.84 ± 0.19
K	H4(1-20)K12acK16ac	0.38 ± 0.07	0.77 ± 0.03	2.06 ± 0.38

Our biochemical data reveal that the impact of H4 acetylation on PRMT1-mediated R3 methylation depends on the individual pattern of acetylation combination. The clear observation is that K5ac is the predominant modification mark that negatively impacts on R3 methylation by PRMT1 (Figure 5.3). The lower k_{cat} of H4K5ac methylation with regard to that of the wild type H4 suggests that the acetyl group on K5 produces a steric or hydrophobic hindrance in the active site, reducing the ability of PRMT1 in methylating H4R3. Acetylation at K8 and K12 seems to have minimal effects on R3 methylation, but their presence can augment the impact of K5ac or

K16ac. Interestingly, K16ac enhances R3 methylation, and to some degree antagonizes the effect of K5 acetylation. This is slightly different from the result of a previous study showing that all forms of H4 acetylation repress R3 methylation (40). The difference is likely caused by the methods used in peptide concentration determination. In our experiments, the peptide concentrations were accurately calibrated by NMR technique, but in the previous study peptide concentrations were weight-based. Despite this technical difference, the repressive impact of H4 acetylation on type I methylation of R3 was clearly observed in several acetylated H4 forms containing the K5ac mark. It is important to mention that our biochemical results coincide well with the *in vivo* data that methylated R3 was found to be present with K16ac mark in many H4 isoforms (139, 140) and coexistence of K16ac with R3me was observed in higher histone H4 population than any other acetylated H4 isoforms (140).

The observed acetylation effect also suggests valuable clues about PRMT1-H4 interaction. It seems reasonable that K16ac affects K_m , but not k_{cat} , given the remoteness of this residue to R3 along the H4 backbone chain. The prominent impact of K16 acetylation on R3 methylation is in good agreement with a previous study showing that the amino acid residues on the H4 tail distal from R3 (i.e., aa 16-20) interact with PRMT1 and contribute to substrate recognition (153). The crystal structure of PRMT1 highlights that an acidic area exists on the surface of PRMT1 (80) and suggests that positive charges of substrates are needed for binding to the enzyme. Here, our data demonstrate that electrostatic interaction does not seem to be the sole factor determining the PRMT1—substrate interaction since K16 acetylation favors the methylation at R3. This is also supported by the fact that, in H2A, a PRMT1 substrate with similarity to H4, threonine is placed at the equivalent position of H4K16.

5.2.3. Impact of H4 acetylation on PRMT5-mediated R3 methylation.

In addition to asymmetric dimethylation by PRMT1, H4R3 can be symmetrically dimethylated by PRMT5 *in vivo*. Of great interest is that these two types of dimethylation in many cases are correlated with opposite functions in gene transcriptional regulation: PRMT1 activates gene expression but PRMT5 represses transcription (40, 76). To understand the molecular basis of such functional oppositeness, we have examined how H4 acetylation affects symmetric dimethylation of H4R3 by PRMT5. First, we subjected the 16-mer H4 library peptides to PRMT5 catalysis under the similar condition as the methylation by PRMT1. Concentrations of PRMT5, [¹⁴C]-AdoMet and H4 peptide were maintained at 0.1 μM, 30 μM and 200 μM respectively, and the reaction proceeded for 1 h. The methylated products were resolved on SDS-PAGE and analyzed by phosphorimaging. As shown in Figure 5.4, intriguingly, most acetylated H4 peptides are better methylated by PRMT5 than the unacetylated H4. This is in stark contrast with the methylation catalyzed by PRMT1, in which the fully acetylated H4 is a poor substrate. The preference of acetylated H4 by PRMT5 is further validated by the data of k_{cat} and K_m measurement (Table 5.3). In particular, K5ac upregulates the value of k_{cat} , suggesting that this modification mark provides favorable contact with the active site of PRMT5 to facilitate methyl transfer. Also, K16ac increases K_m , suggesting that this distal modification mark weakens the binding affinity of H4—PRMT5. Thus, the impacts of K5ac and K16ac are opposite to that of PRMT1 catalysis.

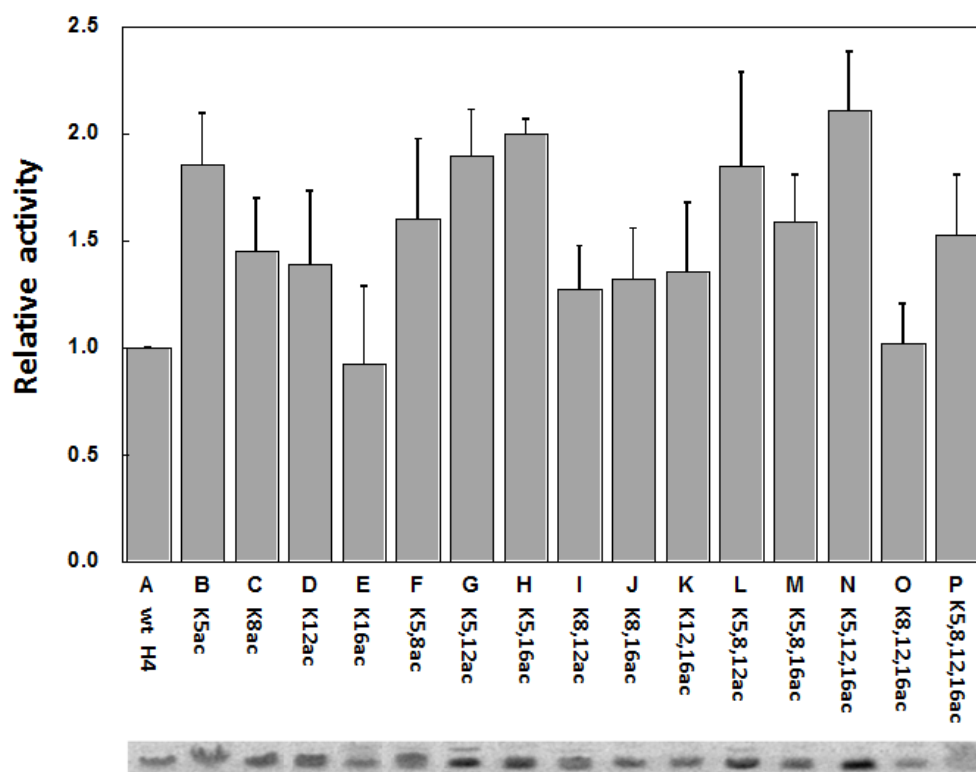


Figure 5.4. Effects of acetylation on R3 methylation catalyzed by PRMT5. Reaction buffer contained 50 mM of HEPES (pH 8.0), 10 mM of NaCl, and 1 mM of DTT. Concentration of PRMT5, [^{14}C]-AdoMet and H4 peptide were 0.1 μM , 30 μM and 200 μM respectively. The reaction time was 1 h.

Table 5.3. Kinetic parameters of PRMT5 catalysis. The catalytic activity of PRMT5 on each peptide was tested with the radioactive filter binding assay. Varied concentrations of peptide (0 to 10 μM) and 30 μM of [^{14}C]-AdoMet were incubated at 30°C for 5 min in the reaction buffer (50 mM HEPES (pH 8.0), 50 mM NaCl, 1 mM EDTA and 0.5 mM DTT) prior to the addition of PRMT5. The methylated products were loaded onto P81 filter paper and quantified by liquid scintillation. Calculated methylation rate was plotted as a function of peptide concentration and the data were fitted with Michaelis-Menton equation.

Substrates		K_m , μM	k_{cat} , min^{-1}	V/K , $\text{min}^{-1}\mu\text{M}^{-1}$
A	wt H4-20	0.63 ± 0.11	0.043 ± 0.002	0.068 ± 0.012
B	H4(1-20)K5ac	0.38 ± 0.08	0.079 ± 0.003	0.21 ± 0.044
C	H4(1-20)K8ac	0.66 ± 0.14	0.042 ± 0.003	0.064 ± 0.014
D	H4(1-20)K12ac	0.52 ± 0.13	0.049 ± 0.003	0.094 ± 0.024
E	H4(1-20)K16ac	1.20 ± 0.16	0.048 ± 0.002	0.040 ± 0.006

5.2.4. Impact of H4 acetylation on PRMT1 and PRMT5 activity using H4 protein and nucleosome as substrates.

So far, we used a 16-mer H4 peptide library comprising different acetylation patterns to dissect the detailed effects of H4 acetylation on the activity of PRMT1 and PRMT5. To further confirm these results, we investigated methylation of H4 at the protein level by these two PRMT members. In the experiment, acetylation of recombinant H4 protein was first introduced by incubation with acetyl-CoA and HAT proteins p300 or MOF. Next, the acetylated H4 protein was subject to PRMT1 and PRMT5 catalysis using [^{14}C]-AdoMet as the methyl donor. The reaction mixtures were then resolved on SDS-PAGE and the methylated H4 band was visualized by storage phosphor imaging. As seen in Figure 5.5, it is clear that acetylation on H4 protein inhibited its methylation catalyzed by PRMT1, but promoted PRMT5-mediated methylation. These data coincide well with the peptide methylation data showing that hyperacetylation of H4 inhibited PRMT1 activity but potentiates PRMT5 activity. We also attempted to test such effects by using nucleosomal substrates. The reconstituted nucleosome was assembled from the recombinant core histone proteins and a 208-bp 5SrDNA by using the EpiMark protocol (Figure 5.6). However, we found that H4 protein in the context of nucleosome or even in the presence of DNA (2:1 ratio as is in the nucleosome) was not appreciably methylated by PRMT1 or PRMT5 in our reaction conditions (Figure 5.7). This important observation implicates that DNA

(especially the unassembled free DNA) poses a physical barrier between nucleosomal histone and PRMTs, preventing the N-terminal tails of the core histones from being methylated by PRMTs. Quite likely, arginine methylation of the chromatin template by PRMTs would require additional accessory proteins or factors *in vivo*. Another possibility is that the 5SrDNA used here is not well-suited for nucleosome assembly. If we switch to another nuclear DNA fragment the methylation result could be different. This DNA effect should be further investigated.

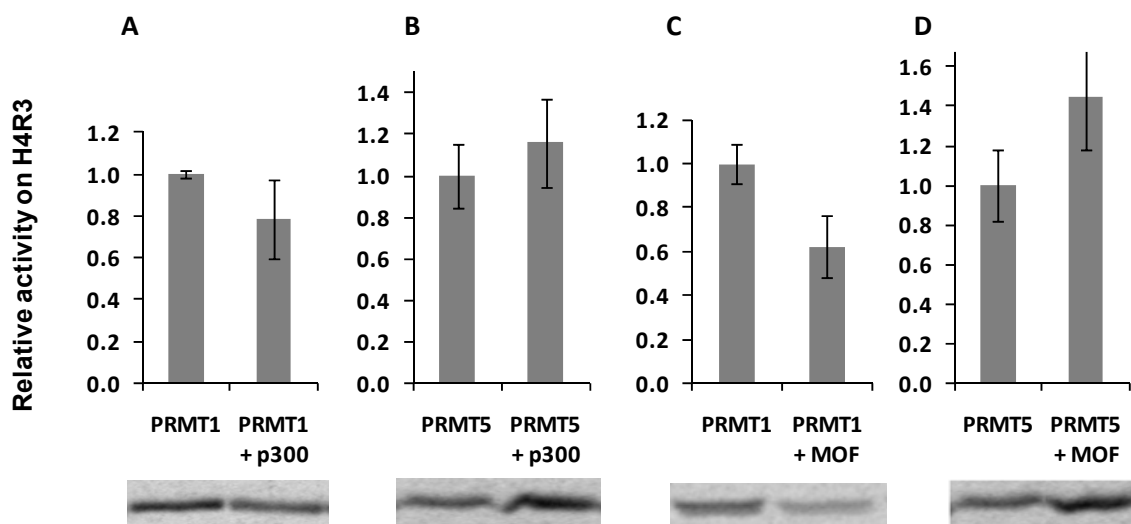


Figure 5.5. Acetylation on H4 protein inhibits its methylation by PRMT1, while promotes its methylation by PRMT5. (A) p300-acetylation inhibits H4 methylation by PRMT1. H4 protein was incubated with Acetyl-CoA in the absence or presence of p300 before submission to PRMT1 methylation with [^{14}C]-AdoMet. Methylated H4 bands were separated by 15% SDS-PAGE and visualized by storage phosphor scan, which is the same method as for B, C, and D. (B) p300-acetylation promotes H4 methylation by PRMT5. H4 protein was incubated with Acetyl-CoA in the absence or presence of p300 before submission to PRMT5 methylation. (C) MOF-acetylation inhibits H4 methylation by PRMT1. H4 protein was incubated with Acetyl-CoA in the absence or presence of MOF before submission to PRMT1 methylation. (D) MOF-

acetylation promotes H4 methylation by PRMT5. H4 protein was incubated with Acetyl-CoA in the absence or presence of MOF before submission to PRMT5 methylation.

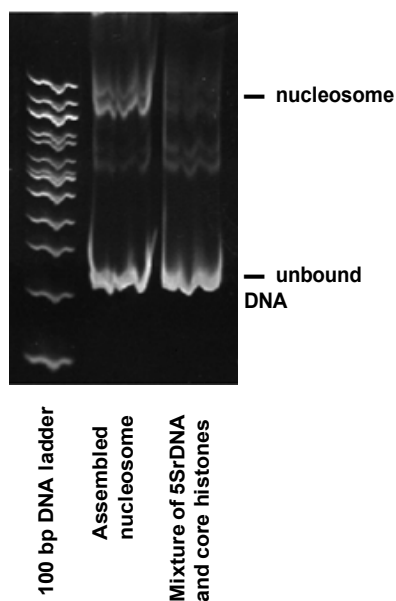


Figure 5.6. Gel shift assay of the assembled nucleosome. The nucleosomes were assembled using the EpiMark Nucleosome Assembly kit with purified recombinant core histones and 5SrDNA (208 bp) according to the manufacturer's protocol. The assembled nucleosomes were checked by the Gel Shift Assay with 6% native acrylamide gel electrophoresis.

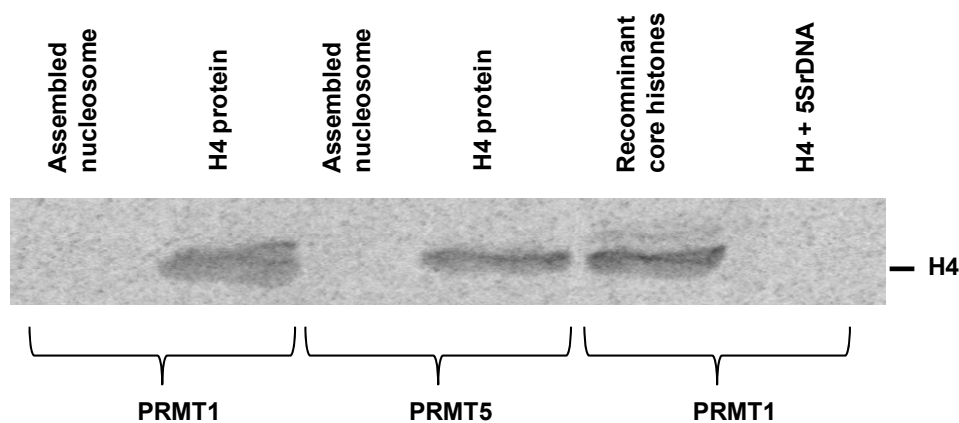


Figure 5.7. Assembled nucleosome cannot be methylated by PRMT1 or PRMT5 *in vitro*. The methylation of the nucleosome was tested with PRMT1 and PRMT5 *in vitro* and compared to H4 protein. 0.21 μM nucleosome or 0.42 μM H4 was incubated with 10 μM [^{14}C]-

SAM and methyltransferase (0.01 μM PRMT1 or 0.1 μM PRMT5) at 30°C for 65 min, then the reaction was quenched by SDS loading buffer. The PRMT1 methylation of the recombinant core histones and the mixture of H4 protein and 5SrDNA (2:1 mole ratio) were also tested as controls. The methylated protein was separated by 17% SDS-PAGE and visualized by storage phosphor scan.

5.2.5. The structural changes of H4 induced by acetylation.

It is of great interest to understand the structural basis of the distinct effect of lysine acetylation on R3 methylation, especially K16ac which is remote from the methylation site. Thus far, there is no information available on whether and how lysine acetylation changes the structure of the histone tails in the nucleosome. It could be possible that acetylation causes changes in the secondary structure of the H4 tail which affects its interaction with PRMTs. To examine whether there are any structural changes in H4 following lysine acetylation, we measured CD spectra of wild-type unacetylated H4 peptide (**A**) and the tetraacetylated H4 peptide (**P**). In particular, the CD spectra were measured at different concentrations of TFE (0—80%) to determine whether hydrophobicity of the solvent environment affects the secondary structures (Figure 5.8A and 5.8B). The collected CD spectra were analyzed by Dichroweb, an online server for protein CD spectra deconvolution (154) to calculate secondary structure contents (helix, strand, turn, and random coil) for each peptide sample. As shown in Figure 5.8C, the contents of random coils occupied a high percentage in both A and P. This is not surprising given that the N-terminal sequence of H4 is invisible in the crystal structures of nucleosome (155), suggesting it is largely in disordered states. However, we clearly noticed that for the H4 peptide with tetraacetyl marks (*i.e.* **P**), the content of helix and strand became appreciably higher than that of the unacetylated H4, namely, 36% versus 13%. This suggests that lysine acetylation renders the H4 peptide in

more structured states. Furthermore, it was observed that as TFE concentration increased, the amount of ordered secondary structures appeared to go higher (Figure 5.8D), implicating that hydrophobic environment favors formation of ordered structures in H4 N-terminal region. Overall, these data demonstrate that lysine acetylation promotes the tendency of H4 tail to form ordered secondary structures.

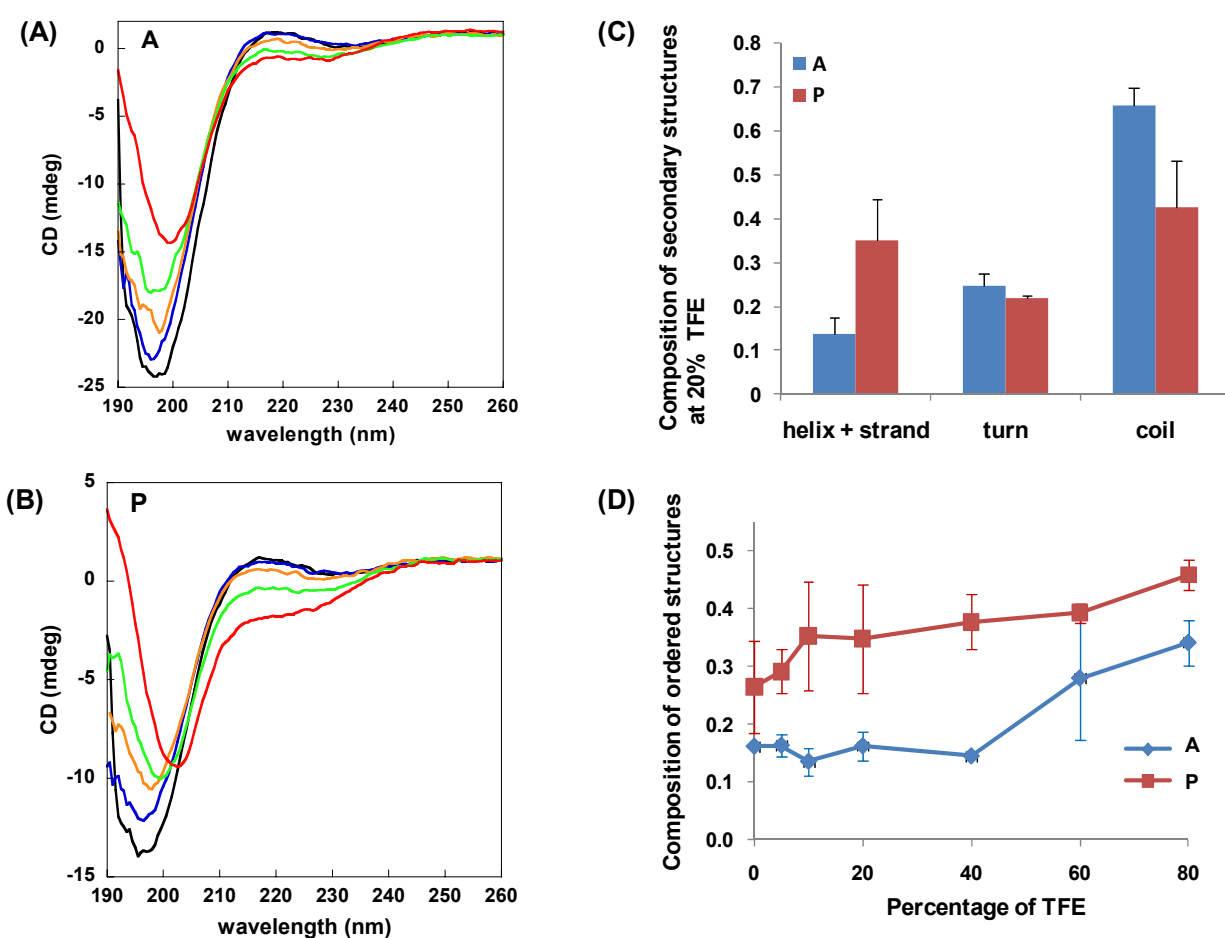


Figure 5.8. Secondary structure analysis of unacetylated H4 peptide (A) and tetraacetylated H4 peptide (P). CD spectra of unacetylated H4 (panel A) and tetraacetylated H4 (panel B) were measured at different concentrations of TFE (0 ~ 80%) in 20 mM Tris-HCl buffer

(pH 7.4): black, 0% TFE; blue, 5% TFE; orange, 20% TFE; green, 40% TFE; red, 80% TFE. The CD data were analyzed by Dichroweb to calculate secondary structure compositions. Panel C: column graph showing the distribution of secondary structures for the two peptides at 20% of TFE. Panel D: the changes in the composition of ordered structures (*i.e.* helix and strand) for each peptide with TFE concentration.

To further confirm the structural impact of lysine acetylation on the H4 sequence, we conducted a simulation analysis of the unacetylated H4 and tetraacetylated H4 peptides. The modeling was conducted on the Jaguar parallel machine by using the AMBER suite of programs. The simulations show that a dramatic structural change occurs upon lysine acetylation. The first evidence for the structuring effect of tetra-acetylation is provided by the distribution of the radius of gyration plot (Figure 5.9a). This distribution appears relatively flat and broad (average: 12.16 Å, variance: 6.06 Å²) in the case of the wild-type peptide but undergoes a shift towards lower values when the peptide is acetylated. This observation is suggestive of a transition from a population of extended, predominantly random coil peptides to a population of compact and more globular structures. Figure 5.9b shows that in the wild type peptide, the distribution of the pairwise backbone RMSD had an average of 7.67 Å and a variance of 4.20 Å². These values shift to 4.93 Å and 2.36 Å² respectively for the acetylated peptide suggesting that acetylation creates a more homogeneous population with a smaller number of structural families. This prediction is confirmed by clustering analysis where a cutoff as large as 9.0 Å was necessary to group the wild type population into 14 clusters whereas a cutoff of 6.0 Å was sufficient to generate 18 clusters in the case of the acetylated peptide.

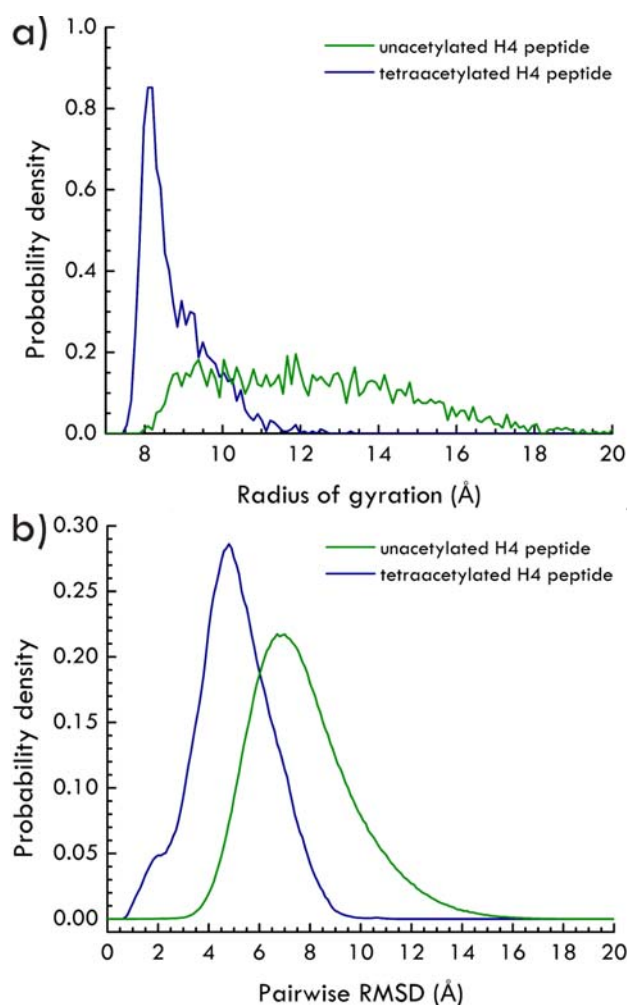


Figure 5.9. Simulated structural changes upon tetraacetylation of the N-terminal H4 tail. Panel (a): Probability distribution of the radius of gyration of the unacetylated and tetraacetylated H4 peptides. Panel (b): probability distribution of the pairwise backbone RMSD of the structures of the equilibrium population.

The clusters of the equilibrium population of the unacetylated peptide roughly belong to three main structural groups whose representative conformations can be seen in Figure 5.10. The first group (50% of structures) is mainly populated by extended conformations where lysine and arginine side chains stick out from the axis of the molecule to minimize electrostatic repulsion.

The second group (24% of structures) is populated by distorted hairpin-like conformations where the standard β -hairpin is replaced by a swollen bubble-like loop arising from the repulsion between lysines and arginines. Finally, the third group (26% of structures) comprises extended conformations featuring a small loop at one or both ends that can be regarded as intermediates in the interconversion pathway between the structures of the first two groups.

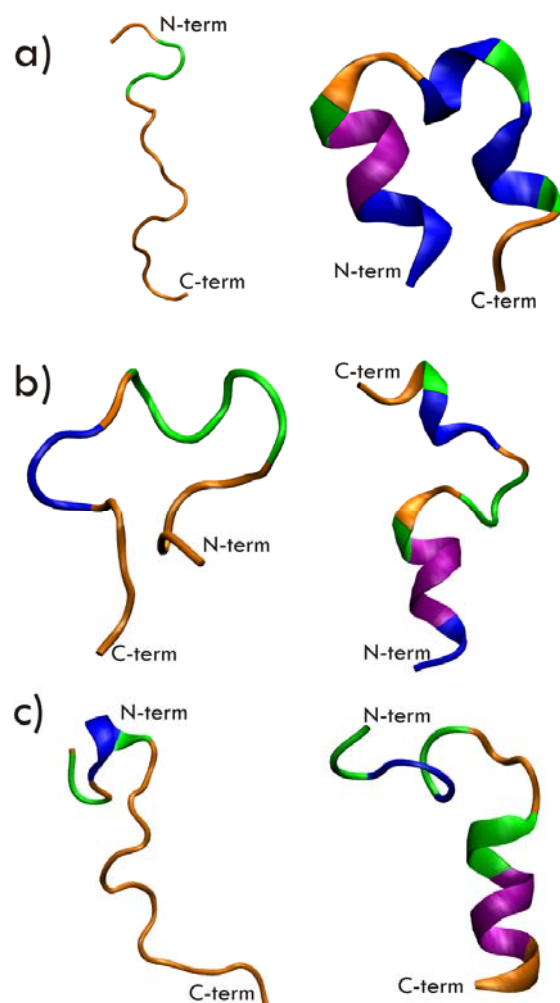


Figure 5.10. Clustering of the equilibrium population of the unacetylated (left column) and tetraacetylated (right column) H4 peptides. Rows (a), (b), (c) show the representative conformations of clusters 1, 2 and 3 respectively. The color code represents

different secondary structural elements as identified through a DSSP analysis (156). Purple: α -helix; Blue: 3_{10} -helix; Green: turn; Orange: random Coil.

Three major classes can also be detected in the equilibrium population of the tetraacetylated H4 peptide based on the results of the clustering analysis (Figure 5.10). The motif of the first class, including 59% of structures, is represented by three 3_{10} helices orthogonal to each other and is therefore somewhat reminiscent of the hairpin-like conformations of group 2 of the unacetylated peptide. It can therefore be suggested that acetylation induces the stabilization and structuring of a conformation that was already present in the population of the unacetylated species. As a final remark, we note that this motif brings the N- and C- termini of the H4 tail peptide close to one another thus suggesting a possible mechanism through which the acetylation of K16 affects the methylation propensity of R3 from a distal region of the molecule. The second class, amounting to 24% of the structures, features extended conformations composed by two or three 3_{10} helices linked by turns. The third class (17% of structures) is characterized by an L-shaped motif composed by two orthogonal 3_{10} helices linked by a central turn region, which, similarly to the case of the unacetylated peptide, can be considered as intermediates between the conformations of the former two classes. In fact, in conditions of dynamic equilibrium, it can be suggested that the extended conformations of Class 2 can bend in the L-shaped conformation of Class 3 which finally completes the folding in the orthogonal arrangement of helices of Class 1.

5.3. Conclusion

To dissect the interplaying relationship between different histone modification marks, we investigated how individual lysine acetylations and their different combinations at the H4 tail affect Arg-3 methylation *in cis*. Our data reveal that the effect of lysine acetylation on arginine

methylation depends on the site of acetylation and the type of methylation. While certain acetylations present a repressive impact on PRMT-1 mediated methylation (type I methylation), lysine acetylation generally is correlated with enhanced methylation by PRMT5 (type II dimethylation). In particular, Lys-5 acetylation decreases activity of PRMT1 but increases that of PRMT5. Furthermore, circular dichroism study and computer simulation demonstrate that hyperacetylation increases the content of ordered secondary structures at the H4 tail region. These findings provide new insights into the regulatory mechanism of Arg-3 methylation by H4 acetylation, and unravel that complex intercommunications exist between different PTM marks *in cis*. The divergent activities of PRMT1 and PRMT5 with respect to different acetyl-H4 substrates suggests that type I and type II PRMTs use distinct molecular determinants for substrate recognition and catalysis.

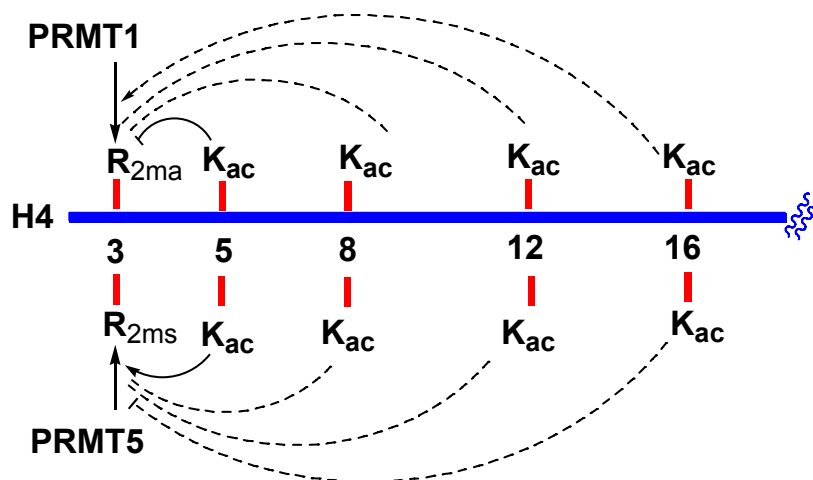


Figure 5.11. Summary of the effects of lysine acetylation on R3 methylation in H4.

Acetylation of the N-terminal H4 tail reciprocally affects PRMT1-mediated Arg-3 methylation and PRMT5-mediated Arg-3 methylation. A solid line means that the effect of acetylation is appreciably strong and a dotted line means that the effect of acetylation is relatively weak.

5.4. Experimental

5.4.1. Design and synthesis of acetylated H4 peptides

The amino-terminal peptide of histone H4 containing the first 20 amino acid residues and different acetylation patterns were synthesized using Fmoc [N-(9-fluorenyl) methoxycarbonyl]-based solid phase peptide synthesis (SPPS) protocols on a PS3 peptide synthesizer (Protein Technology, Tucson, AZ). Each amino acid was coupled to the solid phase by using 4 equivalents of amino acid/HCTU [O-(1H-6-Chlorobenzotriazole-1-yl)-1,1,3,3-tetramethyluronium hexafluorophosphate] (Novabiochem, Darmstadt, Germany). Fmoc was deprotected with 20% v/v piperidine/DMF. The N-terminal amino acid was acetylated with acetic anhydride. The peptide was cleaved from the Wang resin by incubating the resin in a cleavage solution consisted of 95% trifluoroacetic acid (TFA), 2.5% H₂O and 2.5% triisopropylsilane for 3 h. Peptides were precipitated in cold ether and then pelleted by centrifuge at 3000 RPM for 10 min. After washing with ether, crude peptides were collected and purified using a Varian Prostar instrument equipped with a C-18 Reversed-phase High Performance Liquid Chromatography (RP-HPLC) column. 0.05% TFA-containing water and 0.05% TFA-containing acetonitrile were two mobile phases used in gradient purification. The purity and identity of purified peptides were confirmed by analytical HPLC and MALDI-MS.

5.4.2. Calibration of peptide concentrations with NMR

The accurate concentration of each peptide was determined by measuring its 1D ¹H-NMR spectra with external standard on a Bruker Avance 400 MHz instrument. For each NMR sample, a D₂O solution was prepared containing 4.5 mM (weight-based) of individual H4 peptide and 1 mM of 4,4-dimethyl-4-silapentane-1-sulfonic acid (DSS), respectively. The ¹H NMR spectra were collected at room temperature. The integration ratio between the proton peak

of DSS at 0 ppm and the two proton peaks of the imidazole group of the histidine residue, i.e., His-18 ($\delta = 7\text{--}9$ ppm) was measured to calculate the real concentration of each H4 peptide sample.

5.4.3. Protein expression and purification

Recombinant His-tagged rat PRMT1 was expressed in *E. coli* and purified with Ni-charged His6x-tag binding resin (Novagen). The PRMT1-pET28b(+) plasmid was transformed into *E. coli* *BL21(DE3)* (Stratagene) by heat shock. Bacteria were incubated in LB media at 37°C for growth, and 16 °C for protein expression (induced by IPTG 0.3 mM). Cells were harvested by centrifuge and lysed by French Press. The supernatant containing PRMT1 protein was loaded to the Ni-charged His6x-tag binding resin equilibrated with column buffer (25 mM Na- HEPES, pH 7.0, 300 mM NaCl, 1 mM PMSF, and 30 mM imidazole). Beads were washed thoroughly with column buffer and washing buffer (25 mM Na- HEPES, pH 7.0, 300 mM NaCl, 1 mM PMSF, and 70 mM imidazole), and eluted with elution buffer (25 mM Na-HEPES, pH 7.0, 300 mM NaCl, 1 mM PMSF, 100 mM EDTA, and 200 mM imidazole). Different eluents were checked by 12% SDS-PAGE. After dialysis and concentrating, protein concentration was determined by Bradford assay. Active flag-tagged human recombinant PRMT5/MEP50 was purchased from BPS Bioscience, Inc.

5.4.4. Radioactive methylation assays

The methylation assays of different H4 peptide substrates were performed using ^{14}C -isotope labeled AdoMet at 30°C. The typical reaction buffer contained 50 mM HEPES (pH=8.0), 10 mM NaCl and 1 mM DTT. Peptide substrate and [^{14}C]-AdoMet were preincubated in the reaction buffer for 5 min prior to the initiation of methyl transfer reaction by the addition of PRMT. The reaction time was controlled under initial condition so that the typical reaction yields

were within 15%. The reaction was quenched either by spreading the reaction mixture onto P81 filter paper disc (Whatman) or by mixing the reaction buffer with 5x protein-loading dye. For the filter-binding assay, the paper discs were washed with 50 mM NaHCO₃ (pH 9.0) and air dried for 2 h, and then liquid scintillation was conducted to measure the amount of methylated products. For the gel-based assay, methylation mixtures were resolved on 16% SDS-PAGE and the gel was dried and exposed to phosphor film for at least 36 h in dark. The phosphorimage was scanned on Typhoon 9400 scanner and the amount of methylated products was quantitated with ImageQuant program (GE healthcare). Data of K_m and k_{cat} were obtained with the filter binding assay by measuring the initial velocity of reaction at varied concentrations of one substrate and fixed saturating concentration of the other substrate, and fitting the kinetic data with Michaelis-Menton equation.

The methylation assays were also conducted for histone H4 protein and reconstituted nucleosomes to confirm the effect of H4 acetylation on its methylation by PRMT1 and PRMT5. Recombinant human core histones were purchased from New England Biolabs and reconstituted nucleosomes were assembled using the EpiMark assembly kit. The protein substrate was incubated with acetyl-CoA (20 μ M) in the absence or presence of p300 or MOF (0.4 μ M) in the reaction buffer (50 mM HEPES (pH = 8.0), 50 mM NaCl, 1mM EDTA, and 0.5 mM DTT) at 30°C for 10 min. Then [¹⁴C]-AdoMet (15 μ M) and PRMT1 (0.01 μ M) or PRMT5 (0.1 μ M) were added into the reaction mixture to initialize H4 methylation. The methylated protein was separated on SDS-PAGE (15 % for H4 protein and 17 % for nucleosome) and visualized by storage phosphor imaging.

5.4.5. Circular Dichroism (CD) measurement and analysis

Secondary structures of unacetylated H4 peptide and tetraacetylated H4 peptide at different concentrations of TFE were studied with CD on a Jasco J-810 spectropolarimeter. A 1-mm CD cell with 200 μ L of peptide sample (in 20 mM Tris buffer, pH 7.4) with 0 ~ 80% of 2,2,2-trifluoroethanol (TFE) was loaded to the CD spectrophotometer. Nitrogen pressure was kept constant around 100 kPA. CD spectra of peptides were scanned from 260 nm to 190 nm with standard sensitivity, 0.5 nm data pitch, 1 nm band width, 100 nm/min scanning speed, and 10-time accumulation. The concentrations of peptides were selected to keep the negative peak value of ellipticity in-between -10 mdeg to -30 mdeg. CD spectra were saved as text file (Jasco 1.30) and submitted to Dichroweb, an online server for protein Circular Dichroism spectra deconvolution (154). Dichroweb incorporates five open source algorithms (Contin-LL, Selcon 3, CDSSTR, VARSSLC, and K2d) to calculate protein secondary structure content. Of these five algorithms, Provencher & Glockner Method (Contin-LL) and Self Consistent Method (Selcon 3) were chosen to determine the percentage of secondary structural components (helix, strand, turn, and random coil) of each peptide sample.

5.4.6. Structure simulation for the unacetylated and tetraacetylated H4 peptides

The modeling was conducted on the Jaguar parallel machine at the Oak Ridge Leadership Computing Facility by using the AMBER suite of programs. The wild-type and tetraacetylated H4 peptide were parameterized using the Antechamber (157) program with BCC charges. His-18 of the wild type peptide was recognized to be in the epsilon-protonation state through an H-bond network analysis carried out using the WHATIF server (158) (<http://swift.cmbi.ru.nl/servers/html/index.html>). The same protonation state was assigned to the histidine of the tetraacetylated peptide since the presence of non-standard acetylated lysine

residues prevented the use of WHATIF. Replica exchange (REMD) simulations have been performed with the Amber10 suite (159) of programs using the force field ff99SB (160) and the GB-neck solvent model (161) with a 0.2 M concentration of monovalent ions and a dielectric constant of 78.5 (corresponding to water). Both the wild type and the acetylated peptides underwent 200 steps of steepest descent minimization followed by 200 steps of conjugate gradient minimization. Twenty replicas of the minimized system were then created and gradually heated to their target temperatures in a short 1 ns NPT run using Langevin dynamics with a collision frequency of 1.0 ps⁻¹. The temperatures of the replicas were chosen in geometric progression to ensure uniform exchange probability for all pairs of temperatures (the values for the temperature T (in K) was set to 300, 314, 330, 345, 362, 380, 398, 417, 437, 458, 480, 503, 528, 553, 580, 608, 637, 668, 700 and 734). A 105 ns REMD simulation was then carried out: the first 5 ns of the simulation were discarded and analysis was performed on a set of 1976 structures for the wild type and 1722 structures for the acetylated peptide, respectively. The structures, sampled at intervals of 50 ps along the T = 300 K trajectory, were then clustered using a quality threshold clustering algorithm (162). Secondary structure analysis was performed using the DSSP algorithm (156)

CHAPTER 6

SUMMARY

Posttranslational modifications (PTMs) are important strategies used by eukaryotic organisms to modulate their phenotypes. One of the well studied PTMs, arginine methylation, is catalyzed by protein arginine methyltransferases (PRMTs) with SAM as the methyl donor. The functions of PRMTs have been broadly studied in different biological processes and diseased states like cancer and heart disease, suggesting them as potential therapeutic targets, but the molecular basis for arginine methylation is not well defined. To unravel the molecular mechanism of arginine methylation and facilitate the rational design of PRMT inhibitors, we explored several strategies to study the activity and inhibition of PRMT1, the predominant PRMT in mammalian cells.

1. New fluorescent reporters were designed and applied to perform single-step analysis of substrate binding and methylation by PRMT1. Both fluorescence intensity and anisotropy of the two reporters, R4-FL and H4-FL, were shown to effectively manifest enzyme-substrate interactions, highlighting their application in investigating PRMT inhibitors. In particular, the methylation process of R4-FL can be directly studied using fluorescence intensity readout. By combining the fluorescent measurement with radioactive analysis, we determined that AMI-1 inhibits PRMT1 activity through the mechanism of blocking peptide substrate binding. Furthermore, we showed that the fluorescence intensity of R4-FL is sensitive to the progression of both substrate binding and methylation, suggesting that it will be a useful fluorescent probe to investigate the transient kinetic mechanism of PRMT catalysis. Given that GAR motif-containing sequence is a common feature of many PRMT substrates,^(2,3) R4-

FL is not only a fluorescent reporter of PRMT1, but may also be applicable to other PRMT members.

2. Malfunction of protein arginine methyltransferases (PRMTs) is correlated with many human diseases. Thus, small molecule inhibitors of protein arginine methylation are of great potential for therapeutic development. In our study, we have discovered a type of organic compounds containing naphthalene and sulfonyl pharmacophore components that inhibit PRMT activity in the micromolar range, whose inhibition mechanism is fundamentally distinct from the other PRMT inhibitors reported so far. The biochemical and biophysical data of representative compounds show that these inhibitors are competitive versus PRMT1 substrates (e.g., H4 and GAR peptides) and noncompetitive versus the methyl donor. Detailed studies illustrate that they directly target the peptide substrates instead of PRMT1, and the binding subsequently blocks the recognition of the substrates by the enzyme, which is largely responsible for the observed PRMT1 inhibition effect. We also show that the anti-parasitic drug suramin is also an effective arginine methylation inhibitor. These NS inhibitors will be useful chemical tools for mechanistic study of arginine methylation and other epigenetic modifications. Further, illumination of the inhibitory mechanism provides a new insight for understanding the pharmacological effect of these structurally unique molecules in biological systems.

3. The biological functions of PRMTs have been shown to be involved in diverse biological processes and diseased states, yet the molecular basis for arginine methylation is unclear. In our study, we performed the transient-state kinetic analysis of PRMT1 catalysis. Our stopped-flow fluorescence data provide a detailed view of arginine methylation catalyzed by PRMT1. According to our result, the methyl transfer step is the major rate-limiting step which proceeds much slower than substrate association and product release. Binding of the cofactor

SAM/SAH appreciably affects the interaction between H4 peptide and the enzyme, probably due to a conformational change upon enzyme-cofactor complex formation. Importantly, the transient kinetics data reveal a conformational transition step following the substrate binding and prior to the chemical step. This protein isomerization likely reorganizes the active site of PRMT1, bringing the side-chain terminal nitrogen of H4R3 in close proximity to the reactive methyl group of SAM and facilitating the methyl transfer. These results provide new insights into the molecular mechanism of arginine methylation and the rational design of PRMT inhibitors.

4. Epigenetic crosstalk has become a very popular research area recently. To dissect the interplaying relationship between different histone modification marks, we investigated how individual lysine acetylations and their different combinations at the H4 tail affect Arg-3 methylation *in cis*. Our data reveal that the effect of lysine acetylation on arginine methylation depends on the site of acetylation and the type of methylation. While certain acetylations present a repressive impact on PRMT-1 mediated methylation (type I methylation), lysine acetylation generally is correlated with enhanced methylation by PRMT5 (type II methylation). In particular, Lys-5 acetylation inhibits activity of PRMT1 but promotes that of PRMT5. Furthermore, CD study and computer simulation demonstrate that hyperacetylation increases the content of ordered structures at the H4 tail region. These findings give new insights into the regulatory mechanism of Arg-3 methylation by H4 acetylation, and unravel that complex intercommunications exist between different PTM marks *in cis*. The divergent activities of PRMT1 and PRMT5 with respect to different acetyl-H4 substrates suggests that type I and type II PRMTs use distinct molecular determinants for substrate recognition and catalysis.

Our data about the divergent impacts of acetylation on R3 methylation, e.g., K5 acetylation represses while K16 acetylation enhances R3 asymmetric di-methylation, also

provide insights into the function of HATs. Many acetylated H4 isoforms, especially the one containing K16ac, favors R3 methylation by PRMT1. Therefore, certain H4 acetylation marks are compatible with type I methylation of R3. Recent MS analysis of H4 protein in differentiating human embryonic stem cells revealed that K16 was the most abundant acetylated residue and K16ac and K5ac rarely occurred on the same histone H4 molecule, indicating that to some extent, these two acetylations are mutually exclusive and likely have distinct functions (139). This is consistent with previous notions that K16 acetylation has distinct function from the acetylation of other lysine residues at the H4 tail, including K5ac (163, 164). Given that PRMT1-mediated R3 methylation is associated with gene activation, it may be that K5 acetylation has repressive and K16 acetylation has activating function in gene regulation. Although histone acetylations are generally considered as gene activation marks, they might also be able to exhibit repressive function under certain contexts by fine tuning its site specificity at the histone tail with balanced usage of counteractive PTM marks such as K5ac and K16ac. Although a quantitative correlation of the exact linkage of individual H4 acetylation marks to transcriptional on/off status needs to be investigated in the future, a few studies indeed suggest that histone acetylation may possess repressive function in gene expression regulation in certain contexts (165-168).

5. Indication from the assembled nucleosome methylation assay.

In the study of accetylation effect on histone methylation, we found that H4 protein in the context of nucleosome or even in the presence of DNA (2:1 ratio as is in the nucleosome) was not appreciably methylated by PRMT1 or PRMT5 in our reaction conditions. The physiological substrate, nucleosome, has difficulty to be methylated by PRMT1/5. This important observation implicates that DNA (especially the unassembled free DNA) poses a physical barrier between nucleosomal histone and PRMTs, preventing the N-terminal tails of the core histones from being

recognized by PRMTs. In another way, the negatively charged DNA and the acidic surface grooves on PRMT1 may compete with each other to bind the the positively charged histones. In the cells, although the histone tails extend out from its nucleosome core and adopt a free, flexible sturcutre, they can also possibly interact with link DNA from another nucleosome or another chain. Quite likely, arginine methylation of the chromatin template by PRMTs would require additional accessory proteins or factors *in vivo* to release the interaction between DNA and histones and give access for PRMT binding. Another possibility is that the 5SrDNA used in our assay is not well-suited for nucleosome assembly. If we switch to another nuclear DNA fragment the methylation result could be different. This DNA effect should be further investigated.

6. Salt effect on the interaction between NS-1 and H4-20.

The NaCl salt effect on the interaction between H4-20 and NS-1 were tested with UV-Vis spectral change and PRMT1 inhibition assay. From Figure SI-6, mixing of 5 μ M H4-20 peptide induces a big change in the UV-Vis spectrum of 40 μ M NS-1 (maximum absorption reduced nearly by half), but adding of 0 ~ 300 mM NaCl introduces very little change to the absorption of the mixture. Thus NaCl concentration has little effect on H4-20-NS-1 interaction. The inhibition effect of NS-1 on PRMT1 activity was also tested with varied NaCl concentration in the radioactive methylation assay (Figure SI-7). PRMT1 activity is negatively affected by NaCl concentration when it goes above 150 mM. If NS-1-H4-20 interaction is weakened by salt effect, we would expect to see an increase in PRMT1 activity when NaCl goes higher. Yet when NaCl ranges between 0 to 150 mM, the inhibition effect of NS-1 does not change much with NaCl concentration. Again this leads to the conclusion that the salt effect appears to be very minor, indicating that charge-change interaction is not the major driving force for H4-20-NS-1 association. The hydrophobic interactions, H-bonding, or π - π stacking may play more important

roles here. As changing the substrate to H4(1-11) increased the IC_{50} of NS-1 significantly, we propose that the C-terminal and N-terminal residues are both required for efficient binding. According to the fluorescent titration with job's method, NS-1 and H4(1-20) showed a 1:1 binding ratio, thus the association should be specific instead of nonspecific charge-charge interaction.

7. The enzyme-substrate interaction speculation from the modeled peptide and the crystal structure of PRMT1.

We think that PRMT1 competes with DNA for binding to histones. Acid residues (20 Asp and Glu) are predominant on the surface of PRMT1, forming several acid grooves which are supposed to generate an initial binding affinity for positively-charged substrates. Surface-scanning mutagenesis study indicated that some of these negatively charged residues were important for substrate specificity (E47, E129, and E236), substrate binding (E46 and D51), dimerization/oligomerization, or transcription coactivator function (31). In the crystal structure, the electron densities of bound peptide substrates were broken into three separate fragments. Other than the arginine bound in the active site, the amino acid residues of the peptide were not clearly identified due to low resolution of side chain densities. A mixture of peptide binding modes was proposed from the three disconnected densities. The fact that multiple substrate binding grooves exist on the surface of PRMT1 may explain why PRMT1 methylates diverse protein substrates. The negatively charged C terminus is close to the active site and may play an important role for substrate binding or catalysis.

Our biochemical data reveal that the impact of H4 acetylation on PRMT1-mediated R3 methylation depends on the individual pattern of acetylation. The clear observation is that K5ac is the predominant modification mark that negatively impacts R3 methylation by PRMT1. The

lower k_{cat} of H4K5ac methylation with regard to that of the wild type H4 suggests that the acetyl group on K5 produces a steric or hydrophobic hindrance in the active site, reducing the ability of PRMT1 in methylating H4R3. Interestingly, K16ac enhances R3 methylation, and to some degree antagonizes the effect of K5 acetylation. The observed acetylation effect suggests valuable clues about PRMT1-H4 interaction. It seems reasonable that K16ac affects K_m , but not k_{cat} , given the remoteness of this residue to R3 along H4 backbone. The prominent impact of K16 acetylation on R3 methylation is in good agreement with a previous study showing that the basic amino acid residues on the H4 tail distal from R3 (*i.e.*, aa 16-20) interact with PRMT1 and contribute to substrate recognition (153). The crystal structure of PRMT1 highlights that an acidic area exists on the surface of PRMT1 (80) and suggests that positive charges of substrates are needed for binding to the enzyme. Here, our data demonstrate that electrostatic interaction does not seem to be the sole factor determining the PRMT1—substrate interaction since K16 acetylation favors the methylation at R3. Upon tetra-acetylation, the structural modeling shows that H4 tail forms a more regular and bended conformation, likely bringing K16 closer to the target arginine and affecting the peptide binding with PRMT1. The extra acetyl group on K16 may increase the hydrophobic contact or provide one more H-bond to a PRMT1 binding groove compared to the unacetylated, extended H4 peptide, thus lowering the K_m .

On the other hand, the acetylation effect on R3 methylation is quite opposite for PRMT5 catalysis. We propose that PRMT5 likely has a larger binding pocket connected with the active site than PRMT1 to accommodate the acetyl group on Lys 5 close to Arg 3. This acetyl group may provide more hydrophobic or H-bond interaction with PRMT5 to increase its binding affinity. Thus compared with wild-type H4(1-20), H4K5ac become a better substrate for PRMT5 and a worse substrate for PRMT1.

An effort is put to gain the crystal structure of PRMT1 fused with H4(1-20) to analyze the detailed binding mode.

8. A discussion of type I and type II PRMT catalytic mechanism and a summary of how our discovery fits into the context of current understanding of arginine methylation.

So far the only proposed catalytic mechanism of PRMT1 according to its crystal structure is that the two invariant active site glutamates fix the positive charge on the guanidine group on the δ and one of the ω nitrogens, so that the lone pair of electrons left on the other ω nitrogen can attack the active methylsulfonium group of SAM in close proximity. The attacking guanidine nitrogen is deprotonated by a His-Asp relay system. Possibly an active site structural rearrangement can help stabilize the positively charged transition state, lowering the energy gap between the ground state and the transition state thus facilitating the reaction. The active site pH environment is important for catalysis, which puts electrostatic and steric requirements for the residues besides the target arginine. The detailed catalytic mechanism of type II PRMTs is still unknown due to lack of crystal structure of the enzyme-substrate-cofactor ternary complex. Recently the structure of *C. elegans* PRMT5 (CePRMT5) with bound SAH was reported. The mutagenesis study suggested that a conserved phenylalanine (Phe 379 for CePRMT5) in the active site of PRMT5 is critical for directing the symmetric di-methylation, as mutating of Phe 379 to methionine (as in PRMT1) led to generation of both symmetric and asymmetric dimethylated arginines. (17) Thus type I and type II PRMTs are likely to share a similar catalytic mechanism with different active site steric groups. Phe 379 is located on helix α A which becomes more structured upon the cofactor binding. The steric constraint placed by Phe 379 and possibly other residues should be important for PRMT5 product specificity. Yet we still don't know exactly how the target arginine is bound in the active site (defined by E499, E508, F379,

K385, S503, and S669 in CePRMT5). It is possible that the two essential acidic residues (E499 and E508) bind to the guanidinium δ and ω nitrogens in a similar manner as for PRMT1 to facilitate the methyl transfer. But after one methyl group is added, there is not enough space for the same ω nitrogen to accept another methyl group due to steric hindrance produced by Phe 379, *etc.* So the monomethylated arginine has to rotate the side chain and likely rebind to another enzyme active site with switched positions of the two ω nitrogens for the free one to get methylated. Therefore, with the steric restriction in the active site, type II PRMTs can only catalyze the formation of symmetrically dimethylated arginines. But with a methionine in the position of the conserved phenylalanine, PRMT1 has a more flexible active site structure to accommodate two methyl groups on one ω nitrogen. Furthermore, from the above point of view, type II PRMTs are more likely to follow a distributive mechanism rather than a processive mechanism, similar as what we experimentally suggested for PRMT1.

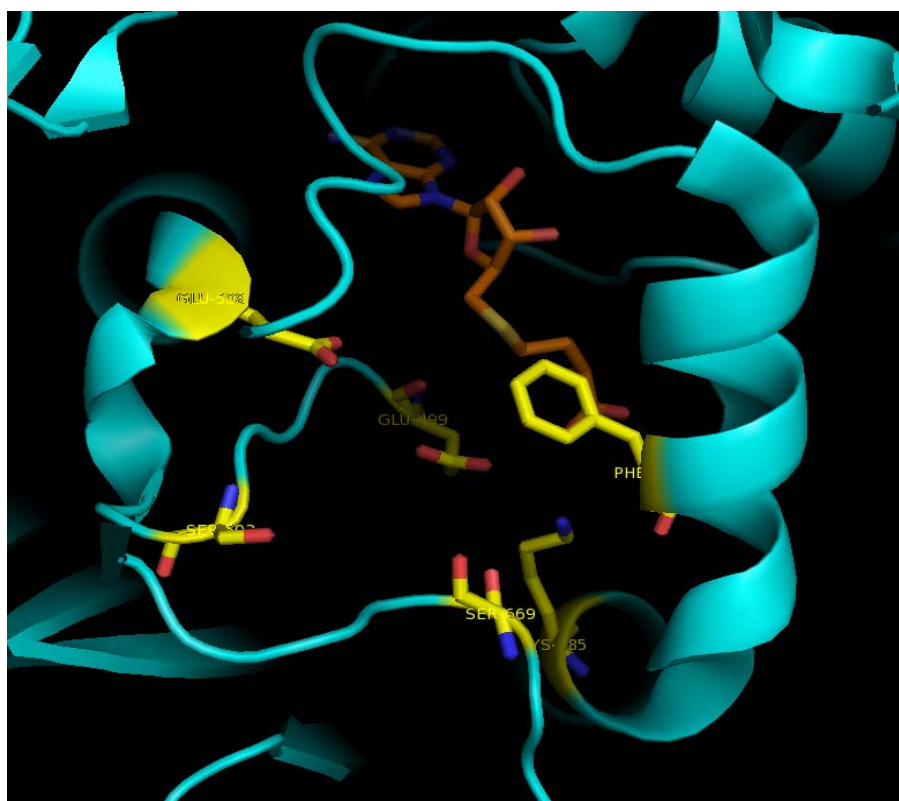


Figure 6.1. The active site of PRMT5 (PDB 3UA3).

Our kinetic data suggests that PRMT1 has to form a ternary complex with the substrate and the cofactor to transfer the methyl group. The catalytic mechanism is by bringing the two substrates in close proximity to facilitate the nucleophilic attack. The transient state kinetic data indicate that PRMT1 transfers two methyl groups following a distributive mechanism, that the chemical step of methyltransfer is rate-limiting, that cofactor binding causes an enzyme conformational change which increases its affinity for the substrate, and that substrate association leads to another conformational transition that likely covers the active site and brings the target arginine closer to the active methyl group of SAM for the nucleophilic attack. This may be accomplished by movement of the double-E loop connecting strand $\beta 4$ and helix αD towards the target arginine of the peptide to bury it in the active site. To confirm these hypotheses, the crystal structures of the apo enzyme, the holoenzyme and the enzyme-cofactor-substrate ternary complex should be compared.

APPENDIX

Table SI-1. Inhibitory data of the fifty top-ranked compounds obtained from the virtual screening. In a typical assay, the reactions were carried out at 30°C with 0.1 μ M of 6x-rPRMT1, 5 μ M of [14 C]-AdoMet, and 2 μ M of H4(1-20), in the presence of 100 μ M of individual inhibitors.

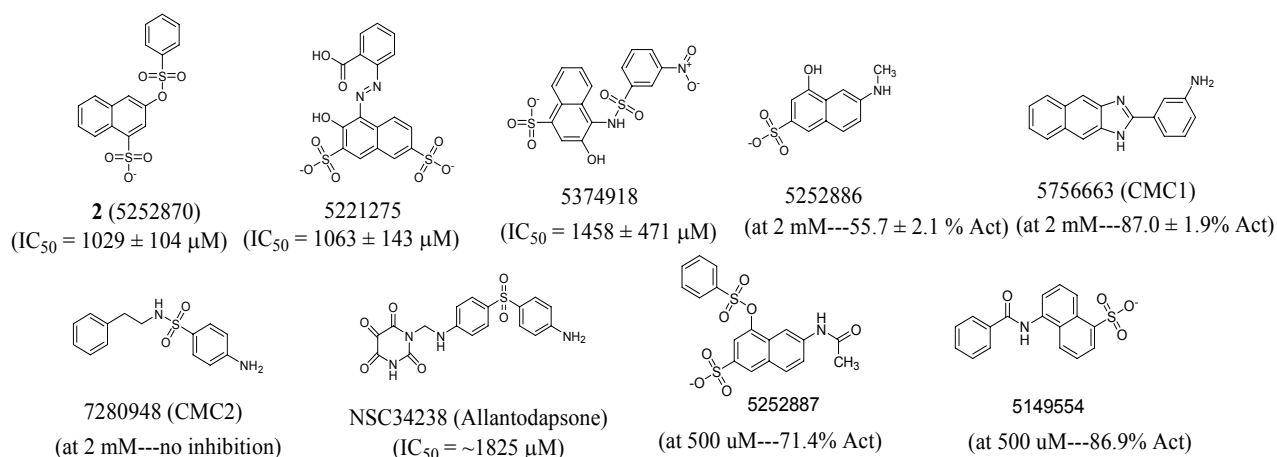
Compound ID	Retained fractional activity of PRMT1	Compound ID	Retained fractional activity of PRMT1
7395064	100	6117046	100
5310809	100	7736131	100
5794588	100	RJC 03491	100
6877387	103	7558583	100
6381790	98	5650276	93
5839065	99	5839747	98
6278455	91	5767214	100
7848611	95	7071534	100
5689130	100	6715339	100
5838031	100	HTS 06914	100
6244071	100	5845246	100
6274859	100	JFD 00459	100
6300962	120	6764997	99
5718222	100	7340109	98
6944291	100	5837758	108
7245849	100	5839847	100
5755262	100	7730013	121
6097286	100	6911199	94
7786009	120	5706616	100
5836899	100	6746073	100

CD 10984	100	7789764	100
SEW 03621	100	5847891	100
5843933	90	6722670	92
5688743	100	KM 08497	100
6498204	100	2	80

Table SI-2. IC₅₀ of selected compounds for the inhibition of GST-hPRMT1.

Radioactive methylation assay conditions were the same as described for the inhibition of His6x-rPRMT1, except for longer reaction time. The typical reaction mixture contained 2 μ M of H4(1-20), 5 μ M of [¹⁴C]-AdoMet, 0.1 μ M of GST-hPRMT1, and increasing concentrations of individual inhibitor.

compound #	IC ₅₀ (μ M) to GST-hPRMT1
3	12.9 \pm 0.2
4	50.5 \pm 0.5
5	68.2 \pm 1.0
6	121.7 \pm 7.8
stilbamidine	56.6 \pm 0.6
1	91.2 \pm 4.9



The following inhibitors did not show any inhibition at 500 μM :

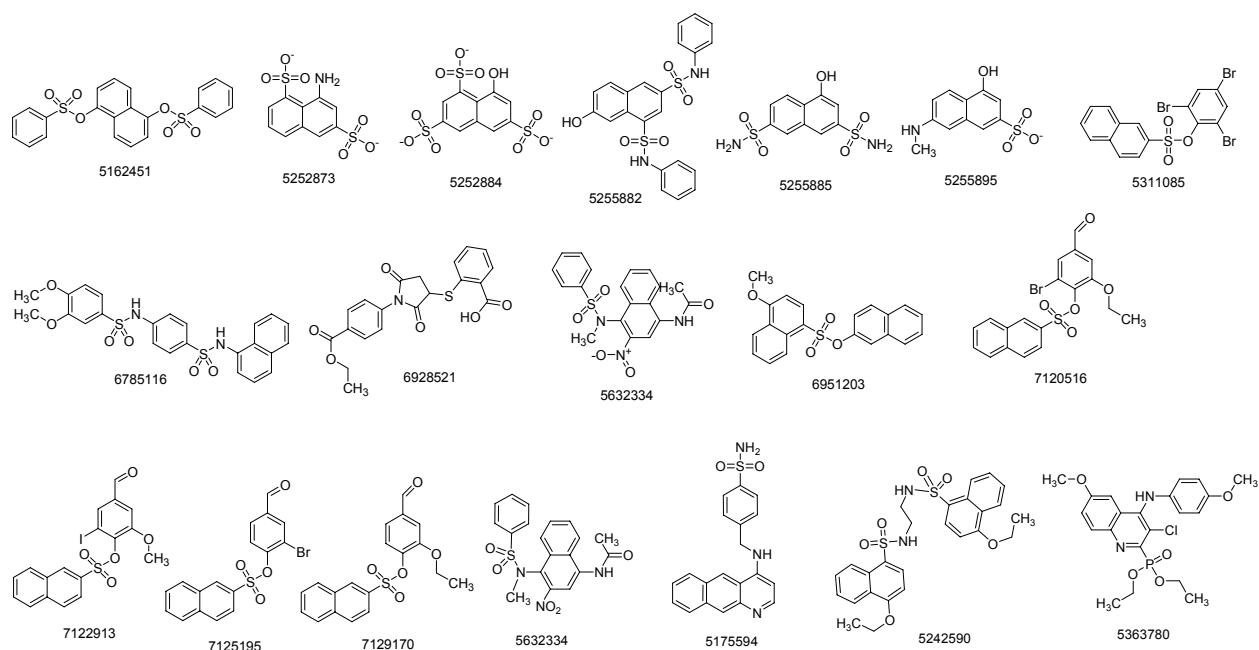


Figure SI-1. Structures and inhibition data of the rest of selected analog compounds.

The inhibition assays were performed using His6x-rPRMT1 (0.1 μM), [^{14}C]-AdoMet (5 μM), and H4(1-20) (2 μM). The potencies of these compounds are much weaker than compounds

3→11.c

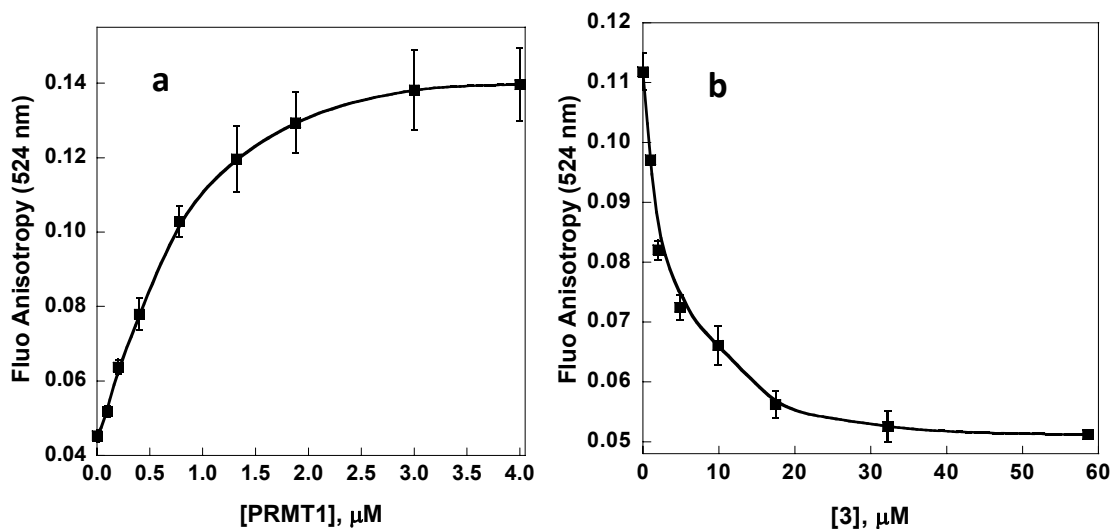


Figure SI-2. Fluorescent competitive binding of 3 to R4-FL. (a) Fluorescence anisotropy (524 nm) of R4-FL solution at different concentrations of PRMT1. The concentration of R4-FL was fixed at 0.2 μM . (b) Fluorescence anisotropy (524 nm) of R4-FL and PRMT1 complex at different concentrations of 3. The total concentration of R4-FL and PRMT1 was 0.2 μM and 2.0 μM respectively.

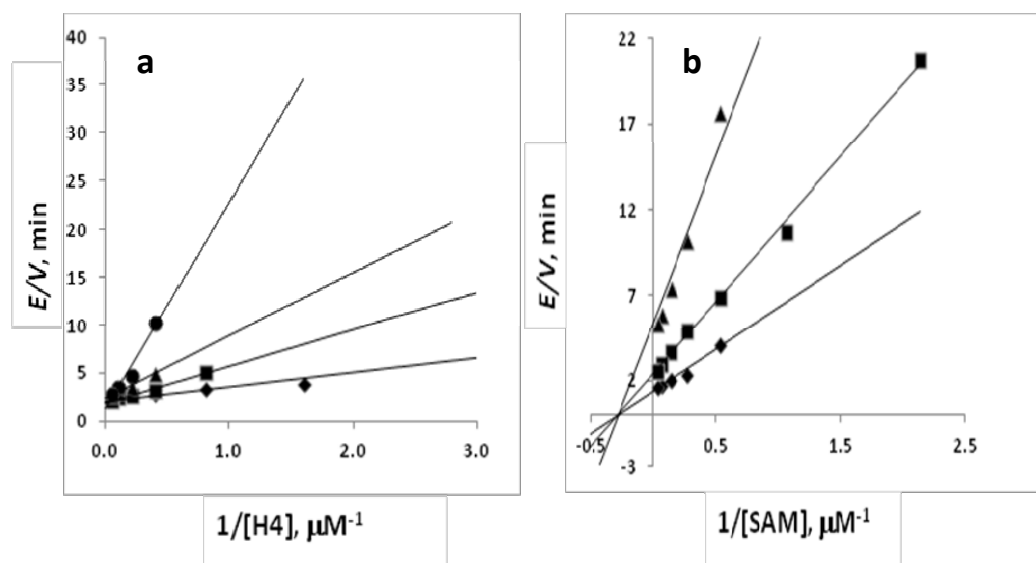


Figure SI-3. Kinetic analysis of 6 in the inhibition of PRMT1 plotted as double-reciprocal plots. a. Inhibition pattern of 6 at fixed [^{14}C]-AdoMet (5 μM) and varied H4(1-20) concentrations. The concentration of 6 was selected at 0 μM (\blacklozenge), 50 μM (\blacksquare), 100 μM (\blacktriangle) and 150 μM (\bullet) respectively. b. Inhibition pattern of 6 at fixed H4(1-20) (2 μM) and varied [^{14}C]-AdoMet concentrations. The concentration of 6 was fixed at 0 μM (\blacklozenge), 50 μM (\blacksquare) and 100 μM (\blacktriangle) respectively. 0.03 μM of His6x-rPRMT1 was added in all these assays.

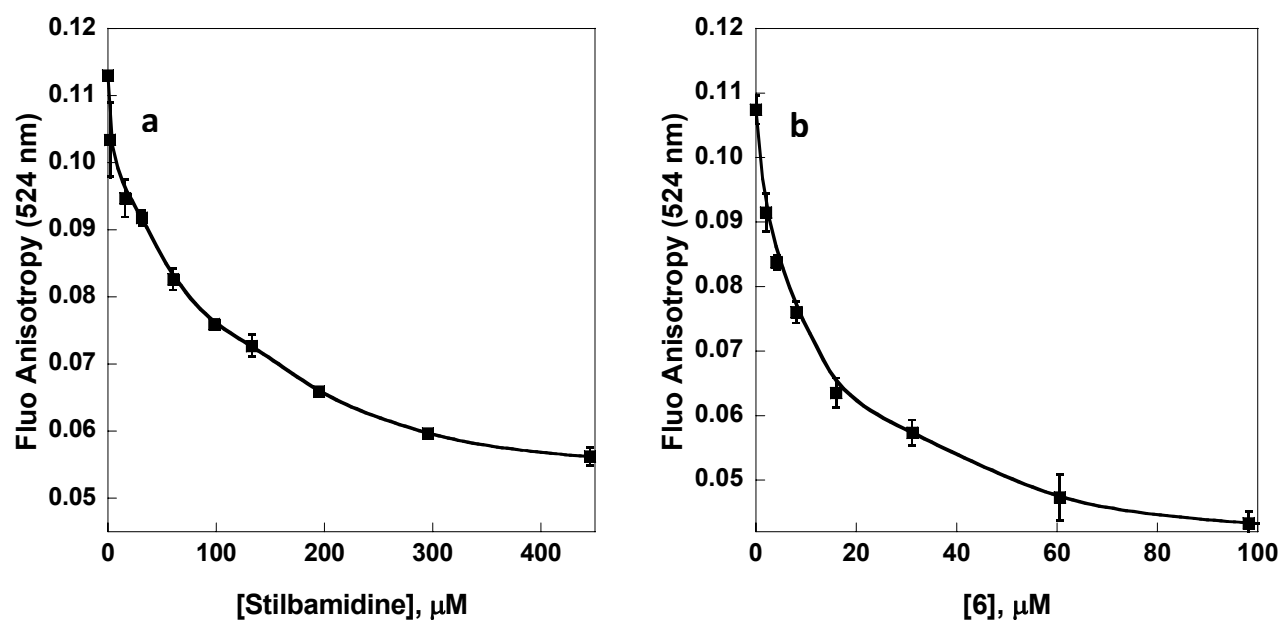


Figure SI-4. Stilbamidine and 6 compete with the substrate for binding to PRMT1. Fluorescence anisotropy (524 nm) of R4-FL-PRMT1 complex at different concentrations of stilbamidine (a) or 6 (b) was measured. The concentration of R4-FL and PRMT1 was fixed at 0.2 μM and 2.0 μM , respectively, for both titrations.

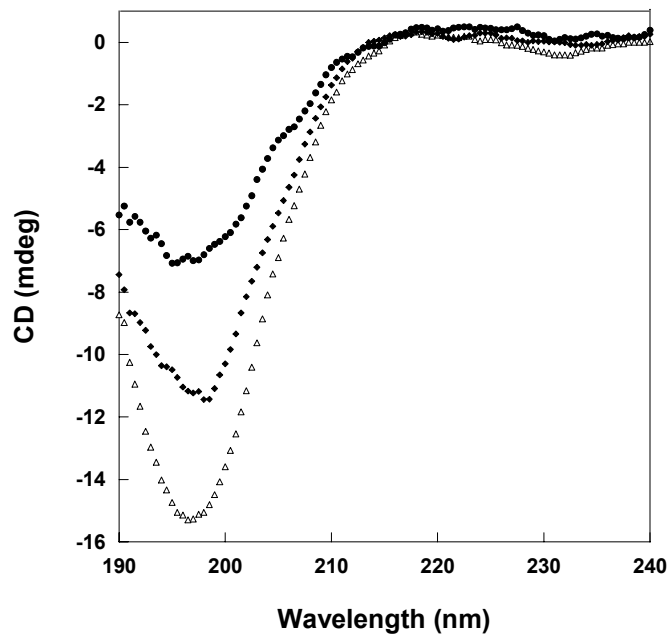


Figure SI-5. CD study of H4(1-20) association with 3. 100 μM of H4(1-20) was titrated with 0 μM (Δ), 100 μM (\blacklozenge), and 200 μM (\bullet) of 3 in 10 mM of Tris buffer (pH 7.4). CD spectrum change of H4(1-20) was monitored. The secondary structural data cannot be analyzed due to the formation of precipitate (H4(1-20) – compound 3 complex).

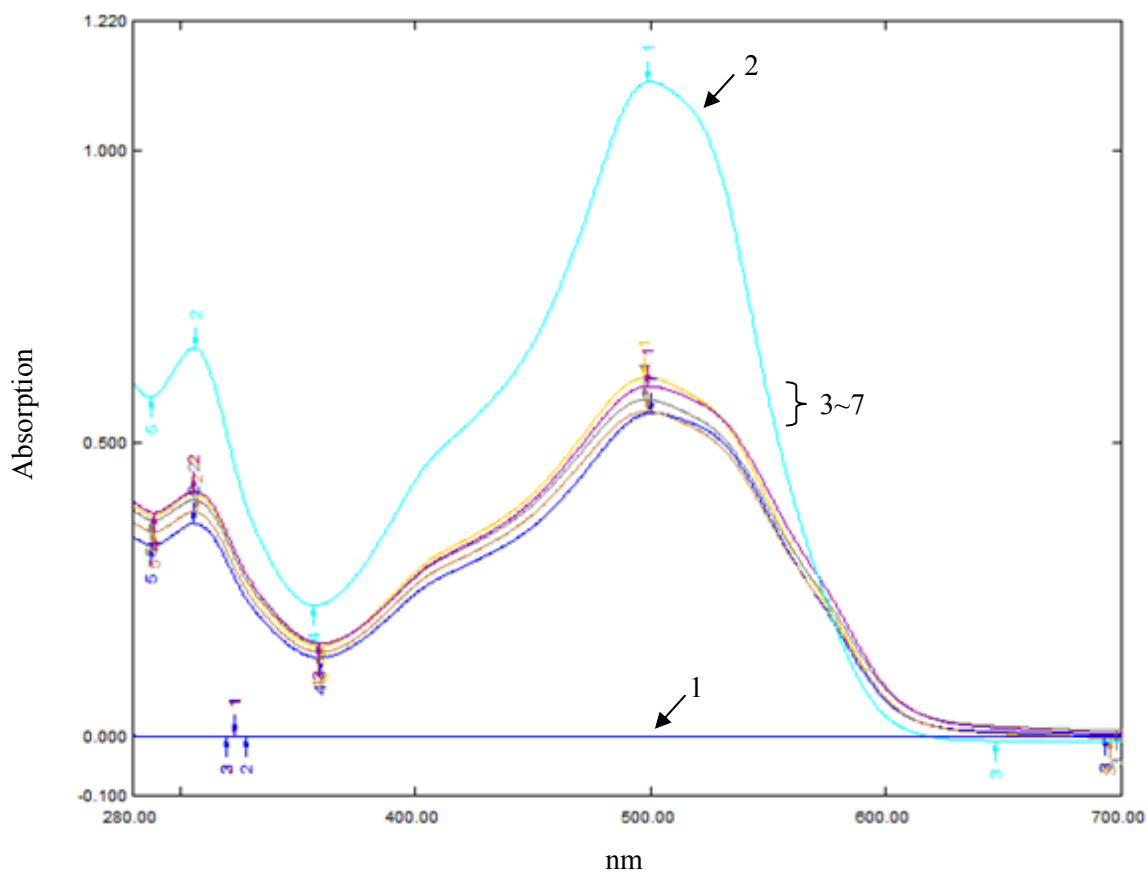


Figure SI-6. Salt effect on the UV-Vis spectrum of NS-1—H4-20 complex. 40 μM NS-1 and 5 μM H4-20 were mixed in the reaction buffer (50 mM HEPES (pH 8.0), 1 mM EDTA, 0.5 mM DTT) containing different concentrations of NaCl (0, 15, 75, 150, 300 mM). The UV-Vis spectra (700 nm ~ 280 nm) were taken on a Shimadzu UV-1700 spectrophotometer. 1. Reaction buffer; 2. 40 μM NS-1 in the reaction buffer; 3. 40 μM NS-1 + 5 μM H4-20 + 0 mM NaCl; 4. 40 μM NS-1 + 5 μM H4-20 + 15 mM NaCl; 5. 40 μM NS-1 + 5 μM H4-20 + 75 mM NaCl; 6. 40 μM NS-1 + 5 μM H4-20 + 150 mM NaCl; 7. 40 μM NS-1 + 5 μM H4-20 + 300 mM NaCl.

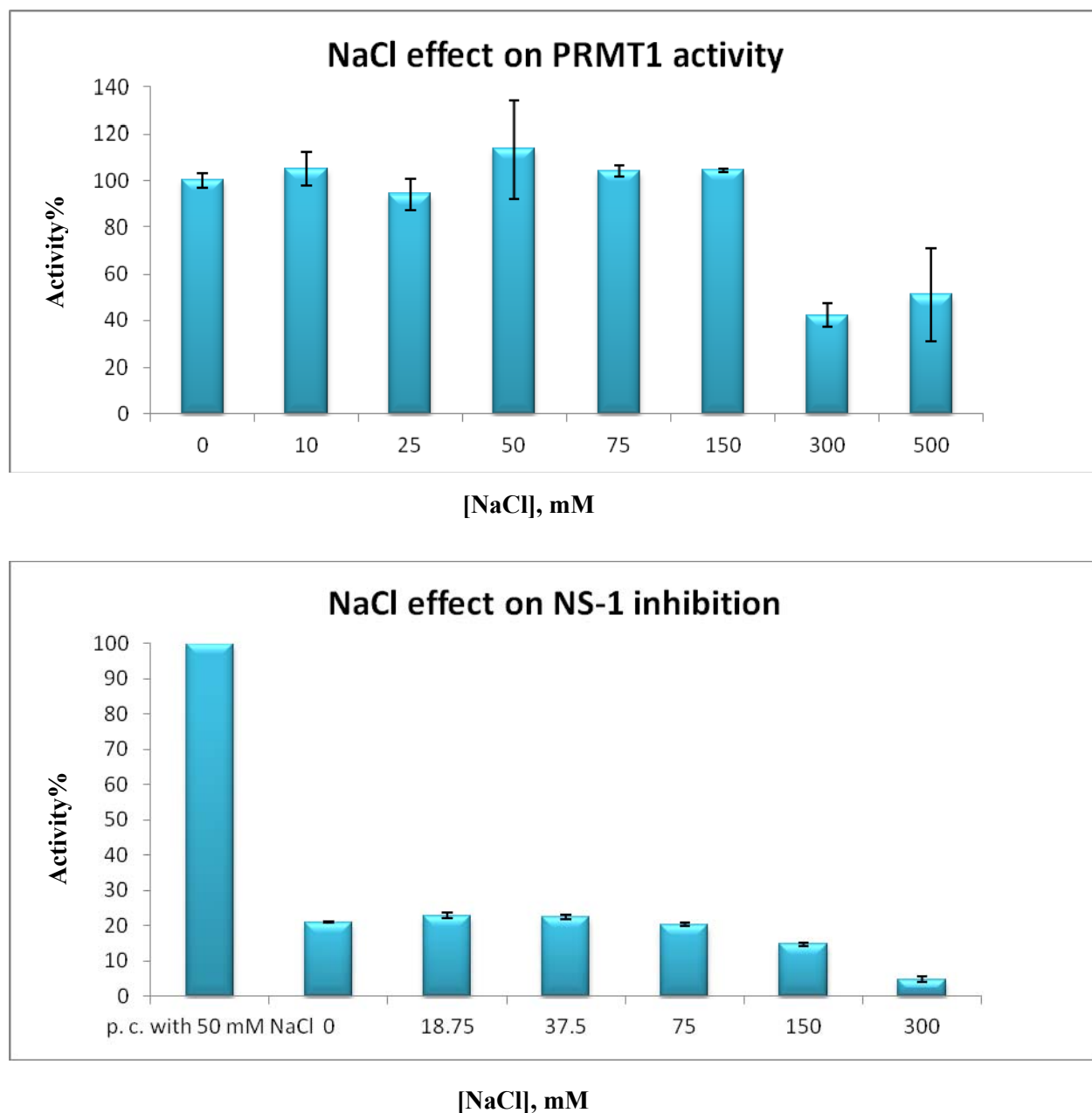
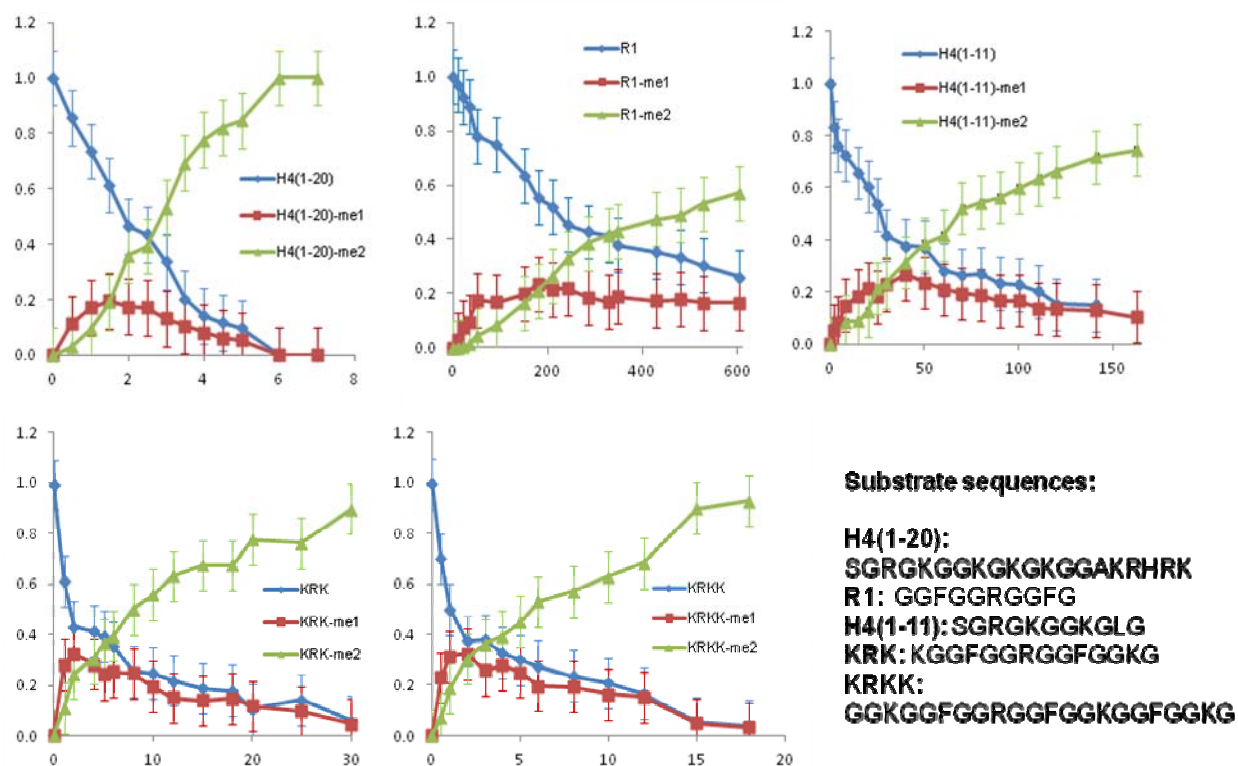


Figure SI-7. Salt effect on the inhibition of NS-1 on PRMT1 activity. 2 μM H4-20 and 5 μM ^{14}C -SAM were mixed with 20 μM NS-1 in the reaction buffer (50 mM HEPES (pH 8.0), 1 mM EDTA, 0.5 mM DTT) containing different concentrations of NaCl (0, 18.75, 37.5, 75, 150, 300 mM). 0.1 μM PRMT1 was added to initiate the methyltransfer reaction which lasted for 8

min at 30 °C. The reaction was quenched by loading the mixture onto P81 paper and the products were quantified by liquid scintillation.



substrate	$k_1/\text{min}^{-1} * \square\text{M}^{-2}$	$k_2/\text{min}^{-1} * \square\text{M}^{-2}$	P1/uM	peptide/uM	SAM/uM
H4(1-20)	0.076 ± 0.004	0.23 ± 0.03	0.4	2	15
KRKK	0.010 ± 0.00077	0.013 ± 0.0013	1	5	30
KRK	0.0031 ± 0.00026	0.0044 ± 0.00052	2	5	30
H4(1-11)	0.00031 ± 0.000011	0.00063 ± 0.000039	2	5	30
R1	0.000011 ± 0.00000031	0.000028 ± 0.000015	5	5	50

Figure SI-8. Relative abundance of peptide changes as a function of time during the methylation reaction by rPRMT1. Data was derived from relative intensity of peaks in MALDI-MS analysis.

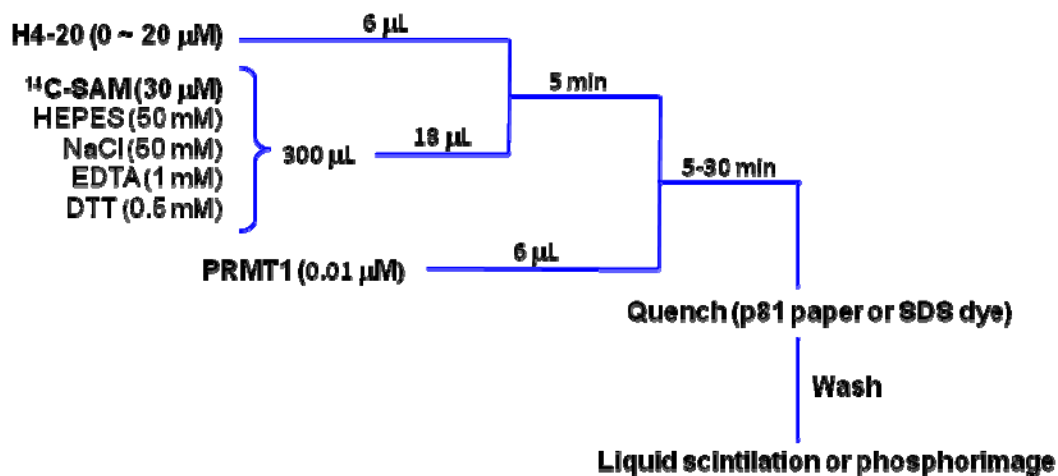
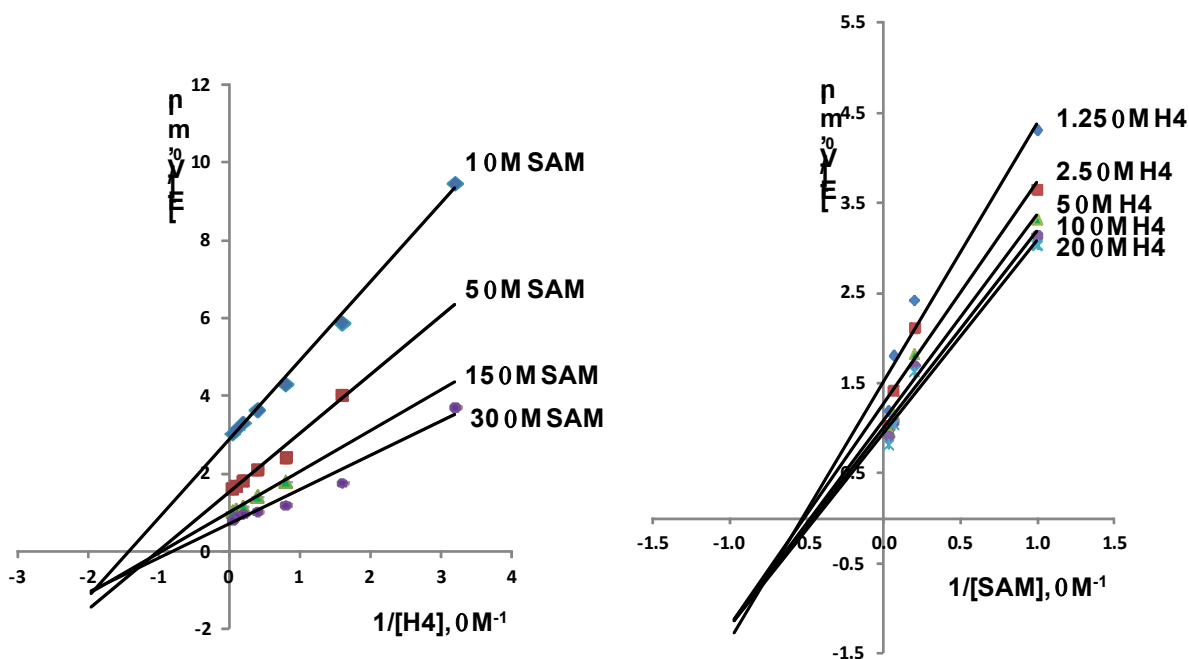


Figure SI-9. Scheme of the radioactive HMT assay.



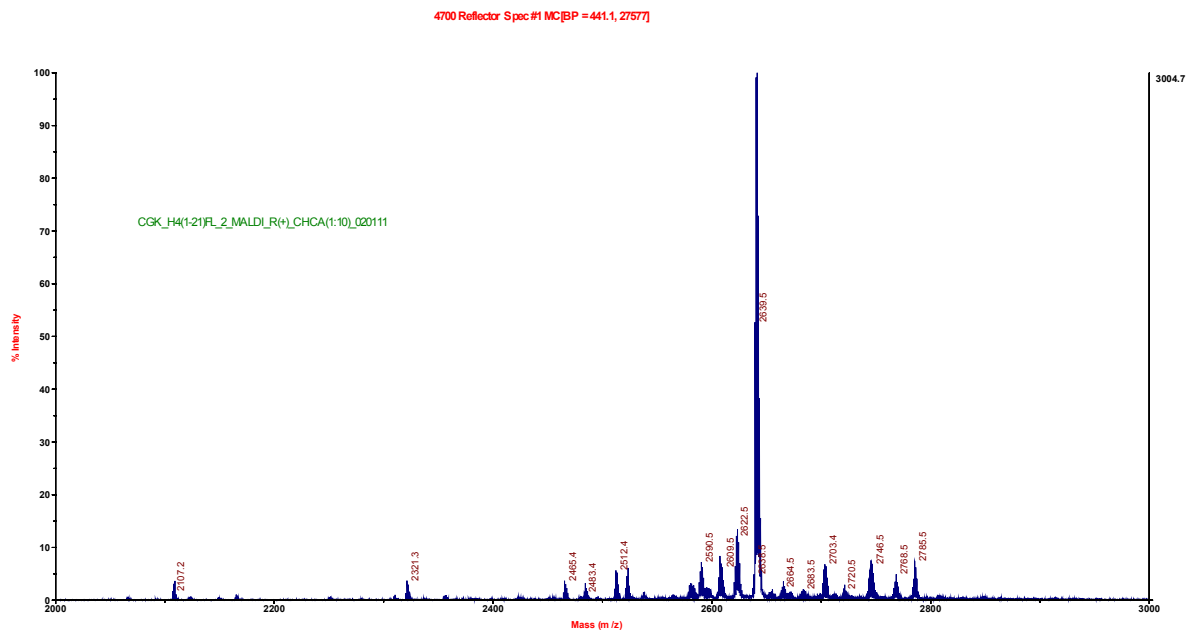
Double reciprocal plot - Different fixed concentrations of SAM at varied H4 concentrations

Double reciprocal plot - Different fixed concentrations of H4 at varied SAM concentrations

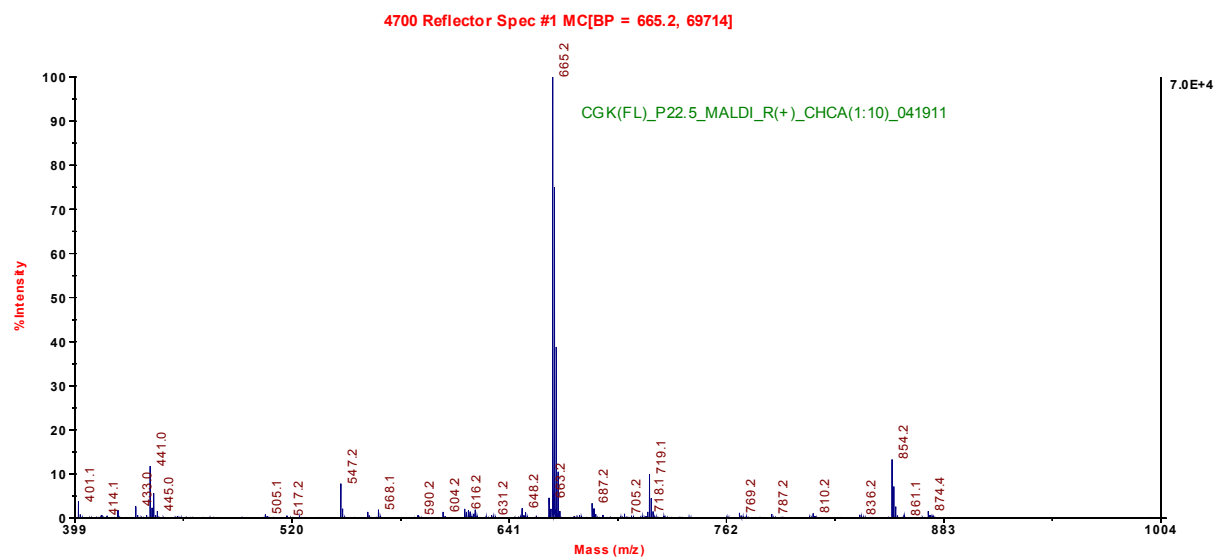
Figure SI-10. Sequential Bi-substrate Binding Model of PRMT1 with H4 and SAM.

Mass spectra for peptides

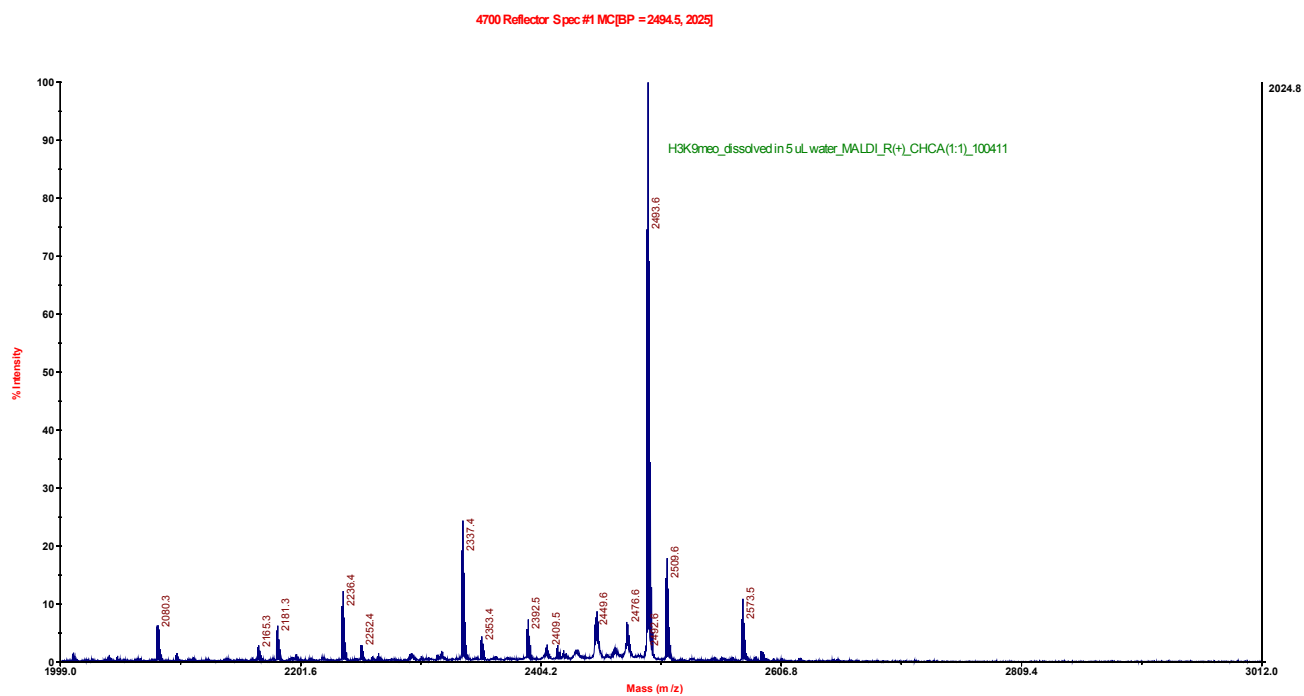
1. CGG-H4(1-21)FL



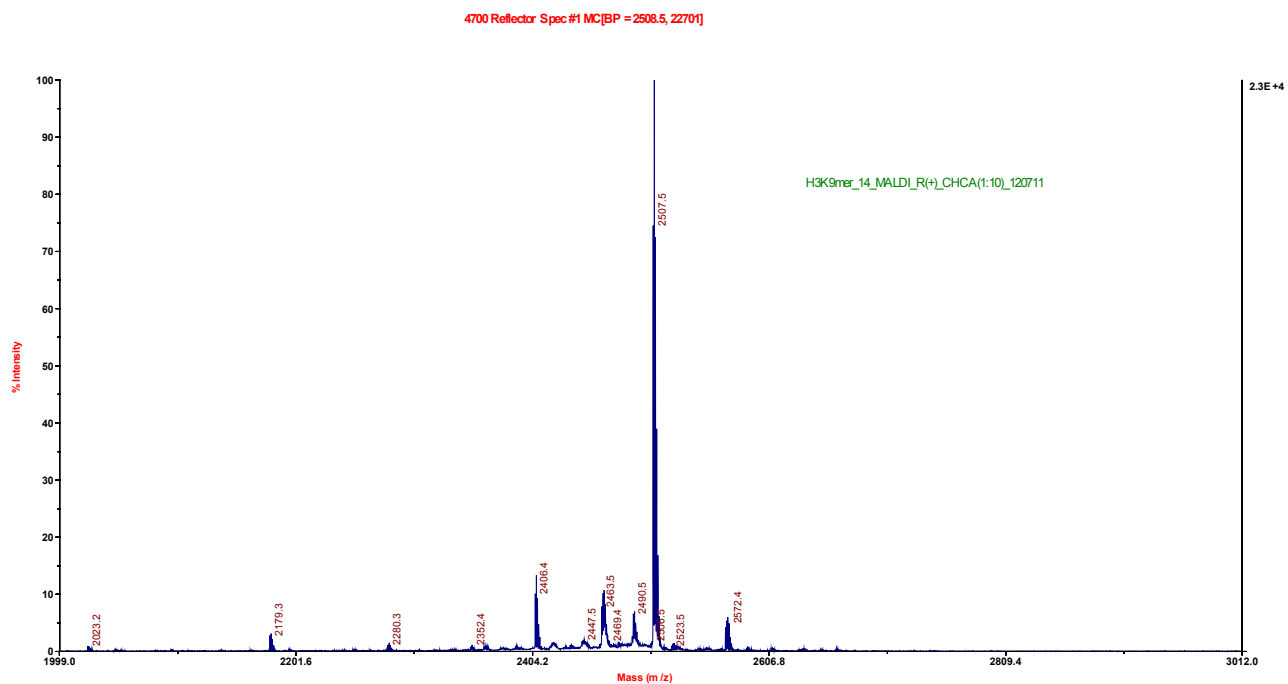
2. CGK-FL



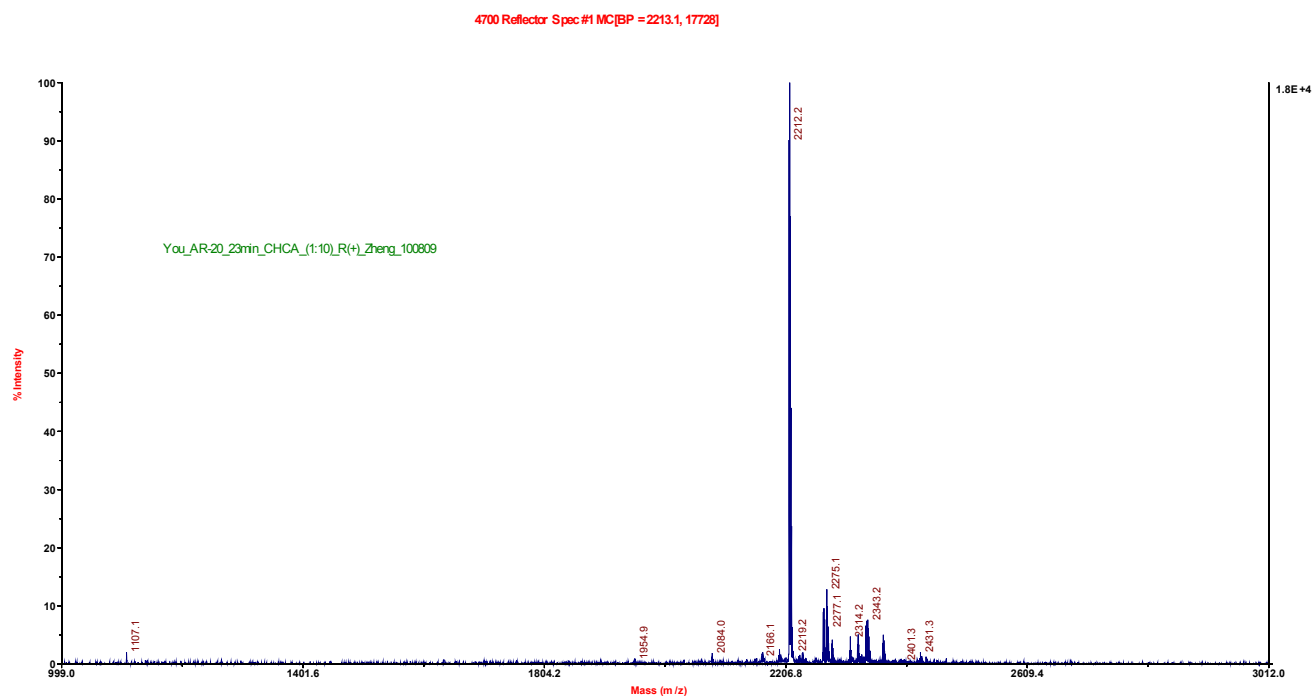
3. H3 (1-20) K9me0(other K→R)



4. H3 (1-20) K9me1(other K→R)



5. AR-20



REFERENCES

1. Holbert, M. A., and Marmorstein, R. (2005) Structure and activity of enzymes that remove histone modifications, *Curr Opin Struct Biol* 15, 673-680.
2. Boyes, J., Byfield, P., Nakatani, Y., and Ogryzko, V. (1998) Regulation of activity of the transcription factor GATA-1 by acetylation, *Nature* 396, 594-598.
3. Chahal, S. S., Matthews, H. R., and Bradbury, E. M. (1980) Acetylation of histone H4 and its role in chromatin structure and function, *Nature* 287, 76-79.
4. Jenuwein, T., and Allis, C. D. (2001) Translating the histone code, *Science* 293, 1074-1080.
5. Strahl, B. D., and Allis, C. D. (2000) The language of covalent histone modifications, *Nature* 403, 41-45.
6. Campbell & Reece. Organization of human genome 7e. fig. 19.4
7. Kouzarides, T. (2007) Chromatin modifications and their function, *Cell* 128, 693-705.
8. Biel, M., Wascholowski, V., and Giannis, A. (2005) Epigenetics--an epicenter of gene regulation: histones and histone-modifying enzymes, *Angew Chem Int Ed Engl* 44, 3186-3216.
9. Parry, R. V., and Ward, S. G. Protein arginine methylation: a new handle on T lymphocytes, *Trends Immunol* 31, 164-169.
10. Sims, R. J., 3rd, and Reinberg, D. (2006) Histone H3 Lys 4 methylation: caught in a bind?, *Genes Dev* 20, 2779-2786.
11. Akbarian, S., and Huang, H. S. (2009) Epigenetic regulation in human brain-focus on histone lysine methylation, *Biol Psychiatry* 65, 198-203.
12. Jha, S., Vande Pol, S., Banerjee, N. S., Dutta, A. B., Chow, L. T., and Dutta, A. Destabilization of TIP60 by human papillomavirus E6 results in attenuation of TIP60-dependent transcriptional regulation and apoptotic pathway, *Mol Cell* 38, 700-711.

13. El-Andaloussi N, V. T., Toueille M, Steinacher R, Focke F, Gehrig P, Covic M, Hassa PO, Schär P, Hübscher U, Hottiger MO. (2006) Arginine methylation regulates DNA polymerase beta, *Mol Cell* 22, 51-62.
14. Lau, P. N., and Cheung, P. Histone code pathway involving H3 S28 phosphorylation and K27 acetylation activates transcription and antagonizes polycomb silencing, *Proc Natl Acad Sci U S A*.
15. Santner, A., and Estelle, M. The ubiquitin-proteasome system regulates plant hormone signaling, *Plant J* 61, 1029-1040.
16. Boggio, R., Colombo, R., Hay, R. T., Draetta, G. F., and Chiocca, S. (2004) A mechanism for inhibiting the SUMO pathway, *Mol Cell* 16, 549-561.
17. Sun L, W. M., Lv Z, Yang N, Liu Y, Bao S, Gong W, Xu RM. (2011) Structural insights into protein arginine symmetric dimethylation by PRMT5, *Proc Natl Acad Sci U S A*. 108, 20538-20543.
18. Pal, S., and Sif, S. (2007) Interplay between chromatin remodelers and protein arginine methyltransferases, *Journal of cellular physiology* 213, 306-315.
19. Lee, D. Y., Teyssier, C., Strahl, B. D., and Stallcup, M. R. (2005) Role of protein methylation in regulation of transcription, *Endocrine reviews* 26, 147-170.
20. Krause, C. D., Yang, Z. H., Kim, Y. S., Lee, J. H., Cook, J. R., and Pestka, S. (2007) Protein arginine methyltransferases: evolution and assessment of their pharmacological and therapeutic potential, *Pharmacology & therapeutics* 113, 50-87.
21. Gary, J. D., and Clarke, S. (1998) RNA and protein interactions modulated by protein arginine methylation, *Progress in nucleic acid research and molecular biology* 61, 65-131.
22. Boisvert, F. M., Cote, J., Boulanger, M. C., and Richard, S. (2003) A proteomic analysis of arginine-methylated protein complexes, *Mol Cell Proteomics* 2, 1319-1330.
23. Bedford, M. T., and Richard, S. (2005) Arginine methylation an emerging regulator of protein function, *Mol Cell* 18, 263-272.

24. McBride, A. E., and Silver, P. A. (2001) State of the arg: protein methylation at arginine comes of age, *Cell* 106, 5-8.
25. Lee, J. H., Cook, J. R., Yang, Z. H., Mirochnitchenko, O., Gunderson, S. I., Felix, A. M., Herth, N., Hoffmann, R., and Pestka, S. (2005) PRMT7, a new protein arginine methyltransferase that synthesizes symmetric dimethylarginine, *The Journal of biological chemistry* 280, 3656-3664.
26. Zhang, Y., and Reinberg, D. (2001) Transcription regulation by histone methylation: interplay between different covalent modifications of the core histone tails, *Genes & development* 15, 2343-2360.
27. Clarke, S. (1993) Protein methylation, *Current opinion in cell biology* 5, 977-983.
28. Zurita-Lopez CI, S. T., Kelly R, Clarke SG. (2012) Human Protein Arginine Methyltransferase 7 (PRMT7) is a Type III Enzyme Forming ω -NG-Monomethylated Arginine Residues., *J Biol Chem*.
29. Bedford, M. T., and Clarke, S. G. (2009) Protein arginine methylation in mammals: who, what, and why, *Mol Cell* 33, 1-13.
30. Zhang X, C. X. (2003) Structure of the predominant protein arginine methyltransferase PRMT1 and analysis of its binding to substrate peptides., *Structure* 11, 509-520.
31. Lee DY, I. I., Purcell D, Zhang X, Cheng X, Stallcup MR. (2007) Surface-scanning mutational analysis of protein arginine methyltransferase 1: roles of specific amino acids in methyltransferase substrate specificity, oligomerization, and coactivator function., *Mol Endocrinol*. 21, 1381-1393.
32. Yue WW, H. M., Roe SM, Thompson-Vale V, Pearl LH. (2007) Insights into histone code syntax from structural and biochemical studies of CARM1 methyltransferase., *EMBO J* 26, 4402-4412.
33. Obianyo, O., Osborne, T. C., and Thompson, P. R. (2008) Kinetic mechanism of protein arginine methyltransferase 1, *Biochemistry* 47, 10420-10427.

34. Lakowski, T. M., and Frankel, A. (2008) A kinetic study of human protein arginine N-methyltransferase 6 reveals a distributive mechanism, *The Journal of biological chemistry* 283, 10015-10025.
35. Dorgan, K. M., Wooderchak, W. L., Wynn, D. P., Karschner, E. L., Alfaro, J. F., Cui, Y., Zhou, Z. S., and Hevel, J. M. (2006) An enzyme-coupled continuous spectrophotometric assay for S-adenosylmethionine-dependent methyltransferases, *Anal Biochem* 350, 249-255.
36. Wang, C., Leffler, S., Thompson, D. H., and Hrycyna, C. A. (2005) A general fluorescence-based coupled assay for S-adenosylmethionine-dependent methyltransferases, *Biochem Biophys Res Commun* 331, 351-356.
37. Biastoff, S., Teuber, M., Zhou, Z. S., and Drager, B. (2006) Colorimetric activity measurement of a recombinant putrescine N-methyltransferase from *Datura stramonium*, *Planta medica* 72, 1136-1141.
38. Hendricks, C. L., Ross, J. R., Pichersky, E., Noel, J. P., and Zhou, Z. S. (2004) An enzyme-coupled colorimetric assay for S-adenosylmethionine-dependent methyltransferases, *Anal Biochem* 326, 100-105.
39. Lee, D. Y., Ianculescu, I., Purcell, D., Zhang, X., Cheng, X., and Stallcup, M. R. (2007) Surface-scanning mutational analysis of protein arginine methyltransferase 1: roles of specific amino acids in methyltransferase substrate specificity, oligomerization, and coactivator function, *Molecular endocrinology (Baltimore, Md)* 21, 1381-1393.
40. Wang, H., Huang, Z. Q., Xia, L., Feng, Q., Erdjument-Bromage, H., Strahl, B. D., Briggs, S. D., Allis, C. D., Wong, J., Tempst, P., and Zhang, Y. (2001) Methylation of histone H4 at arginine 3 facilitating transcriptional activation by nuclear hormone receptor, *Science* 293, 853-857.
41. Strahl, B. D., Briggs, S. D., Brame, C. J., Caldwell, J. A., Koh, S. S., Ma, H., Cook, R. G., Shabanowitz, J., Hunt, D. F., Stallcup, M. R., and Allis, C. D. (2001) Methylation of histone H4 at arginine 3 occurs in vivo and is mediated by the nuclear receptor coactivator PRMT1, *Curr Biol* 11, 996-1000.
42. Wu, J., Zheng, Y. G. (2008) Fluorescent Reporters of the Histone Acetyltransferase, *Anal Biochem* 380, 106-110.

43. Spannhoff, A., Sippl, W., and Jung, M. (2009) Cancer treatment of the future: inhibitors of histone methyltransferases, *Int J Biochem Cell Biol* 41, 4-11.
44. Zheng, Y. G., Wu, J., Chen, Z., and Goodman, M. (2008) Chemical regulation of epigenetic modifications: Opportunities for new cancer therapy, *Medicinal research reviews* 28, 645-687.
45. Mai, A., and Altucci, L. (2009) Epi-drugs to fight cancer: from chemistry to cancer treatment, the road ahead, *Int J Biochem Cell Biol* 41, 199-213.
46. Cheng, D., Yadav, N., King, R. W., Swanson, M. S., Weinstein, E. J., and Bedford, M. T. (2004) Small molecule regulators of protein arginine methyltransferases, *The Journal of biological chemistry* 279, 23892-23899.
47. Spannhoff, A., Heinke, R., Bauer, I., Trojer, P., Metzger, E., Gust, R., Schule, R., Brosch, G., Sippl, W., and Jung, M. (2007) Target-based approach to inhibitors of histone arginine methyltransferases, *J Med Chem* 50, 2319-2325.
48. Spannhoff, A., Machmur, R., Heinke, R., Trojer, P., Bauer, I., Brosch, G., Schule, R., Hanefeld, W., Sippl, W., and Jung, M. (2007) A novel arginine methyltransferase inhibitor with cellular activity, *Bioorg Med Chem Lett* 17, 4150-4153.
49. Purandare, A. V., Chen, Z., Huynh, T., Pang, S., Geng, J., Vaccaro, W., Poss, M. A., Oconnell, J., Nowak, K., and Jayaraman, L. (2008) Pyrazole inhibitors of coactivator associated arginine methyltransferase 1 (CARM1), *Bioorg Med Chem Lett* 18, 4438-4441.
50. Heinke, R., Spannhoff, A., Meier, R., Trojer, P., Bauer, I., Jung, M., and Sippl, W. (2009) Virtual screening and biological characterization of novel histone arginine methyltransferase PRMT1 inhibitors, *ChemMedChem* 4, 69-77.
51. Mai, A., Cheng, D., Bedford, M. T., Valente, S., Nebbioso, A., Perrone, A., Brosch, G., Sbardella, G., De Bellis, F., Miceli, M., and Altucci, L. (2008) Epigenetic Multiple Ligands: Mixed Histone/Protein Methyltransferase, Acetyltransferase, and Class III Deacetylase (Sirtuin) Inhibitors, *J Med Chem* 51, 2279-2290.
52. Ragno, R., Simeoni, S., Castellano, S., Vicidomini, C., Mai, A., Caroli, A., Tramontano, A., Bonaccini, C., Trojer, P., Bauer, I., Brosch, G., and Sbardella, G. (2007) Small molecule inhibitors of histone arginine methyltransferases: homology modeling, molecular docking, binding mode analysis, and biological evaluations, *J Med Chem* 50, 1241-1253.

53. Mai, A., Valente, S., Cheng, D., Perrone, A., Ragno, R., Simeoni, S., Sbardella, G., Brosch, G., Nebbioso, A., Conte, M., Altucci, L., and Bedford, M. T. (2007) Synthesis and biological validation of novel synthetic histone/protein methyltransferase inhibitors, *ChemMedChem* 2, 987-991.
54. Osborne, T., Roska, R. L., Rajsiki, S. R., and Thompson, P. R. (2008) In Situ Generation of a Bisubstrate Analogue for Protein Arginine Methyltransferase 1, *J Am Chem Soc.*
55. Peterson, C. L., and Laniel, M. A. (2004) Histones and histone modifications, *Curr Biol* 14, R546-551.
56. Chen, D., Ma, H., Hong, H., Koh, S. S., Huang, S. M., Schurter, B. T., Aswad, D. W., and Stallcup, M. R. (1999) Regulation of transcription by a protein methyltransferase, *Science* 284, 2174-2177.
57. Meister, G., Eggert, C., Buhler, D., Brahms, H., Kambach, C., and Fischer, U. (2001) Methylation of Sm proteins by a complex containing PRMT5 and the putative U snRNP assembly factor pICln, *Curr Biol* 11, 1990-1994.
58. Wysocka, J., Allis, C. D., and Coonrod, S. (2006) Histone arginine methylation and its dynamic regulation, *Front Biosci* 11, 344-355.
59. Tang, J., Frankel, A., Cook, R. J., Kim, S., Paik, W. K., Williams, K. R., Clarke, S., and Herschman, H. R. (2000) PRMT1 is the predominant type I protein arginine methyltransferase in mammalian cells, *J Biol Chem* 275, 7723-7730.
60. Cheung, N., Chan, L. C., Thompson, A., Cleary, M. L., and So, C. W. (2007) Protein arginine-methyltransferase-dependent oncogenesis, *Nature cell biology* 9, 1208-1215.
61. Scorilas, A., Black, M. H., Talieri, M., and Diamandis, E. P. (2000) Genomic organization, physical mapping, and expression analysis of the human protein arginine methyltransferase 1 gene, *Biochem Biophys Res Commun* 278, 349-359.
62. Klonis, N., and Sawyer, W. H. (2000) Effect of solvent-water mixtures on the prototropic equilibria of fluorescein and on the spectral properties of the monoanion, *Photochem Photobiol* 72, 179-185.

63. Klonis, N., Clayton, A. H., Voss, E. W., Jr., and Sawyer, W. H. (1998) Spectral properties of fluorescein in solvent-water mixtures: applications as a probe of hydrogen bonding environments in biological systems, *Photochem Photobiol* 67, 500-510.
64. Nikolovska-Coleska, Z., Wang, R., Fang, X., Pan, H., Tomita, Y., Li, P., Roller, P. P., Krajewski, K., Saito, N. G., Stuckey, J. A., and Wang, S. (2004) Development and optimization of a binding assay for the XIAP BIR3 domain using fluorescence polarization, *Anal Biochem* 332, 261-273.
65. Schurter, B. T., Koh, S. S., Chen, D., Bunick, G. J., Harp, J. M., Hanson, B. L., Henschen-Edman, A., Mackay, D. R., Stallcup, M. R., and Aswad, D. W. (2001) Methylation of histone H3 by coactivator-associated arginine methyltransferase 1, *Biochemistry* 40, 5747-5756.
66. Bycroft, B. W., Chan, W. C., Chhabra, S. R., Teesdalespittle, P. H., and Hardy, P. M. (1993) A Novel Amino Protection Deprotection Procedure and Its Application in Solid-Phase Peptide-Synthesis, *J Chem Soc Chem Comm*, 776-777.
67. Segel, I. H. (1975) *Enzyme kinetics : behavior and analysis of rapid equilibrium and steady state enzyme systems*, Wiley, New York.
68. Goulet, I., Gauvin, G., Boisvenue, S., and Cote, J. (2007) Alternative splicing yields protein arginine methyltransferase 1 isoforms with distinct activity, substrate specificity, and subcellular localization, *The Journal of biological chemistry* 282, 33009-33021.
69. Mathioudaki, K., Papadokostopoulou, A., Scorilas, A., Xynopoulos, D., Agnanti, N., and Talieri, M. (2008) The PRMT1 gene expression pattern in colon cancer, *British journal of cancer* 99, 2094-2099.
70. Papadokostopoulou, A., Mathioudaki, K., Scorilas, A., Xynopoulos, D., Ardavanis, A., Kouroumalis, E., and Talieri, M. (2009) Colon cancer and protein arginine methyltransferase 1 gene expression, *Anticancer research* 29, 1361-1366.
71. Seligson, D. B., Horvath, S., Shi, T., Yu, H., Tze, S., Grunstein, M., and Kurdistani, S. K. (2005) Global histone modification patterns predict risk of prostate cancer recurrence, *Nature* 435, 1262-1266.
72. Hong, H., Kao, C., Jeng, M. H., Eble, J. N., Koch, M. O., Gardner, T. A., Zhang, S., Li, L., Pan, C. X., Hu, Z., MacLennan, G. T., and Cheng, L. (2004) Aberrant expression of CARM1,

a transcriptional coactivator of androgen receptor, in the development of prostate carcinoma and androgen-independent status, *Cancer* 101, 83-89.

73. Majumder, S., Liu, Y., Ford, O. H., 3rd, Mohler, J. L., and Whang, Y. E. (2006) Involvement of arginine methyltransferase CARM1 in androgen receptor function and prostate cancer cell viability, *Prostate* 66, 1292-1301.

74. Wang, L., Pal, S., and Sif, S. (2008) Protein arginine methyltransferase 5 suppresses the transcription of the RB family of tumor suppressors in leukemia and lymphoma cells, *Molecular and cellular biology* 28, 6262-6277.

75. Kim, J. M., Sohn, H. Y., Yoon, S. Y., Oh, J. H., Yang, J. O., Kim, J. H., Song, K. S., Rho, S. M., Yoo, H. S., Kim, Y. S., Kim, J. G., and Kim, N. S. (2005) Identification of gastric cancer-related genes using a cDNA microarray containing novel expressed sequence tags expressed in gastric cancer cells, *Clin Cancer Res* 11, 473-482.

76. Pal, S., Vishwanath, S. N., Erdjument-Bromage, H., Tempst, P., and Sif, S. (2004) Human SWI/SNF-associated PRMT5 methylates histone H3 arginine 8 and negatively regulates expression of ST7 and NM23 tumor suppressor genes, *Molecular and cellular biology* 24, 9630-9645.

77. Yildirim, A. O., Bulau, P., Zakrzewicz, D., Kitowska, K. E., Weissmann, N., Grimminger, F., Morty, R. E., and Eickelberg, O. (2006) Increased protein arginine methylation in chronic hypoxia: role of protein arginine methyltransferases, *American journal of respiratory cell and molecular biology* 35, 436-443.

78. Maas, R. (2005) Pharmacotherapies and their influence on asymmetric dimethylarginine (ADMA), *Vascular medicine (London, England)* 10 Suppl 1, S49-57.

79. McKinsey, T. A., Zhang, C. L., and Olson, E. N. (2002) Signaling chromatin to make muscle, *Current opinion in cell biology* 14, 763-772.

80. Zhang, X., and Cheng, X. (2003) Structure of the predominant protein arginine methyltransferase PRMT1 and analysis of its binding to substrate peptides, *Structure* 11, 509-520.

81. Pearlman, R. S. (1987) CONCORD: Rapid Generation of High Quality Approximate 3D Molecular Structures, *Chem. Des. Autom. News* 2, 1-7.

82. Moustakas, D. T., Lang, P. T., Pegg, S., Pettersen, E., Kuntz, I. D., Brooijmans, N., and Rizzo, R. C. (2006) Development and Validation of a Modular, Extensible Docking Program: DOCK 5, *J. Comput. Aided Mol. Des.* 20, 601-619.
83. Feng, Y., Xie, N., Wu, J., Yang, C., and Zheng, Y. G. (2009) Inhibitory study of protein arginine methyltransferase 1 using a fluorescent approach, *Biochem Biophys Res Commun* 379, 567-572.
84. Kuzmic, P. (1996) Program DYNAFIT for the analysis of enzyme kinetic data: application to HIV proteinase, *Anal Biochem* 237, 260-273.
85. Thompson, P. R., Kurooka, H., Nakatani, Y., and Cole, P. A. (2001) Transcriptional coactivator protein p300. Kinetic characterization of its histone acetyltransferase activity, *The Journal of biological chemistry* 276, 33721-33729.
86. Xie, N., Elangwe, E. N., Asher, S., and Zheng, Y. G. (2009) A dual-mode fluorescence strategy for screening HAT modulators, *Bioconjugate chemistry* 20, 360-366.
87. Li, M. Y., Huang, Y. J., Tai, P. C., and Wang, B. H. (2008) Discovery of the first SecA inhibitors using structure-based virtual screening, *Biochem. Biophys. Res. Commun.* 368, 839-845.
88. Li, M. Y., Ni, N. T., Chou, H. T., Lu, C. D., Tai, P. C., and Wang, B. H. (2008) Structure-based discovery and experimental verification of novel AI-2 quorum sensing inhibitors against *Vibrio harveyi*, *ChemMedChem* 3, 1242-1249.
89. Jakalian, A., Bush, B. L., Jack, D. B., and Bayly, C. I. (2000) Fast, Efficient Generation of High-Quality Atomic Charges. AM1-BCC Model: I. Method, *J. Comput. Chem.* 21, 132-146.
90. Jakalian, A., Jack, D. B., and Bayly, C. I. (2002) Fast, Efficient Generation of High-Quality Atomic Charges. AM1-BCC Model: II. Parameterization and Validation, *J. Comput. Chem.* 23, 1623-1641.
91. Tsai, K. C., Wang, S. H., Hsiao, N. W., Li, M. Y., and Wang, B. H. (2008) The effect of different electrostatic potentials on docking accuracy: A case study using DOCK5.4, *Bioorg. Med. Chem. Lett.* 18, 3509-3512.

92. (2007) QuACPAC, Release version 1.1 ed., pp Quality Atomic Charges, Proton Assignment and Canonicalization OpenEye Scientific Software, Inc, Santa Fe, NM.
93. (2007) FRED, Release version 2.2.3 ed., p Fast Rigid Exhaustive Docking, OpenEye Scientific Software, Inc., Santa Fe, NM.
94. (2005) SYBYL 7.1, Tripos Inc., St. Louis, MS.
95. Feher, M. (2006) Consensus scoring for protein-ligand interactions, *Drug discovery today* 11, 421-428.
96. Eldridge, M. D., Murray, C. W., Auton, T. R., Paolini, G. V., and Mee, R. P. (1997) Empirical scoring functions: I. The development of a fast empirical scoring function to estimate the binding affinity of ligands in receptor complexes, *J Comput Aided Mol Des* 11, 425-445.
97. Murray, C. W., Auton, T. R., and Eldridge, M. D. (1998) Empirical scoring functions. II. The testing of an empirical scoring function for the prediction of ligand-receptor binding affinities and the use of Bayesian regression to improve the quality of the model, *J Comput Aided Mol Des* 12, 503-519.
98. Verkhivker, G. M., Bouzida, D., Gehlhaar, D. K., Rejto, P. A., Arthurs, S., Colson, A. B., Freer, S. T., Larson, V., Luty, B. A., Marrone, T., and Rose, P. W. (2000) Deciphering common failures in molecular docking of ligand-protein complexes, *J Comput Aided Mol Des* 14, 731-751.
99. Stahl, M., and Rarey, M. (2001) Detailed analysis of scoring functions for virtual screening, *J Med Chem* 44, 1035-1042.
100. McGann, M. R., Almond, H. R., Nicholls, A., Grant, J. A., and Brown, F. K. (2003) Gaussian docking functions, *Biopolymers* 68, 76-90.
101. (2007) IDEA, Version 8.8 ed., Breadth Technology, Taipei, Taiwan.
102. Wu, J., Xie, N., Wu, Z., Zhang, Y., and Zheng, Y. G. (2009) Bisubstrate Inhibitors of the MYST HATs Esa1 and Tip60, *Bioorg Med Chem* 17, 1381-1386.

103. Thompson, P. R., Wang, D., Wang, L., Fulco, M., Pediconi, N., Zhang, D., An, W., Ge, Q., Roeder, R. G., Wong, J., Levvero, M., Sartorelli, V., Cotter, R. J., and Cole, P. A. (2004) Regulation of the p300 HAT domain via a novel activation loop, *Nature structural & molecular biology* 11, 308-315.
104. Kuzmic, P. (2006) A generalized numerical approach to rapid-equilibrium enzyme kinetics: application to 17beta-HSD, *Molecular and cellular endocrinology* 248, 172-181.
105. Bauer, U. M., Daujat, S., Nielsen, S. J., Nightingale, K., and Kouzarides, T. (2002) Methylation at arginine 17 of histone H3 is linked to gene activation, *EMBO reports* 3, 39-44.
106. Ma, H., Baumann, C. T., Li, H., Strahl, B. D., Rice, R., Jelinek, M. A., Aswad, D. W., Allis, C. D., Hager, G. L., and Stallcup, M. R. (2001) Hormone-dependent, CARM1-directed, arginine-specific methylation of histone H3 on a steroid-regulated promoter, *Curr Biol* 11, 1981-1985.
107. Xu X, H. S., Mayo MW, Bekiranov S. (2010) Application of machine learning methods to histone methylation ChIP-Seq data reveals H4R3me2 globally represses gene expression., *BMC Bioinformatics* 11, 396.
108. Fabbrizio, E., El Messaoudi, S., Polanowska, J., Paul, C., Cook, J. R., Lee, J. H., Negre, V., Rousset, M., Pestka, S., Le Cam, A., and Sardet, C. (2002) Negative regulation of transcription by the type II arginine methyltransferase PRMT5, *EMBO reports* 3, 641-645.
109. Yadav, N., Lee, J., Kim, J., Shen, J., Hu, M. C., Aldaz, C. M., and Bedford, M. T. (2003) Specific protein methylation defects and gene expression perturbations in coactivator-associated arginine methyltransferase 1-deficient mice, *Proceedings of the National Academy of Sciences of the United States of America* 100, 6464-6468.
110. Zhu, W., Mustelin, T., and David, M. (2002) Arginine methylation of STAT1 regulates its dephosphorylation by T cell protein tyrosine phosphatase, *The Journal of biological chemistry* 277, 35787-35790.
111. Bedford, M. T., Frankel, A., Yaffe, M. B., Clarke, S., Leder, P., and Richard, S. (2000) Arginine methylation inhibits the binding of proline-rich ligands to Src homology 3, but not WW, domains, *The Journal of biological chemistry* 275, 16030-16036.

112. Altschuler, L., Wook, J. O., Gurari, D., Chebath, J., and Revel, M. (1999) Involvement of receptor-bound protein methyltransferase PRMT1 in antiviral and antiproliferative effects of type I interferons, *J Interferon Cytokine Res* 19, 189-195.
113. Tang, J., Kao, P. N., and Herschman, H. R. (2000) Protein-arginine methyltransferase I, the predominant protein-arginine methyltransferase in cells, interacts with and is regulated by interleukin enhancer-binding factor 3, *The Journal of biological chemistry* 275, 19866-19876.
114. McBride, A. E., Weiss, V. H., Kim, H. K., Hogle, J. M., and Silver, P. A. (2000) Analysis of the yeast arginine methyltransferase Hmt1p/Rmt1p and its in vivo function. Cofactor binding and substrate interactions, *The Journal of biological chemistry* 275, 3128-3136.
115. Friesen, W. J., Paushkin, S., Wyce, A., Massenet, S., Pesiridis, G. S., Van Duyne, G., Rappsilber, J., Mann, M., and Dreyfuss, G. (2001) The methylosome, a 20S complex containing JBP1 and pICln, produces dimethylarginine-modified Sm proteins, *Molecular and cellular biology* 21, 8289-8300.
116. Torres-Padilla, M. E., Parfitt, D. E., Kouzarides, T., and Zernicka-Goetz, M. (2007) Histone arginine methylation regulates pluripotency in the early mouse embryo, *Nature* 445, 214-218.
117. Ancelin, K., Lange, U. C., Hajkova, P., Schneider, R., Bannister, A. J., Kouzarides, T., and Surani, M. A. (2006) Blimp1 associates with Prmt5 and directs histone arginine methylation in mouse germ cells, *Nature cell biology* 8, 623-630.
118. Feng Y, X. N., Wu J, Yang C, Zheng YG. (2009) Inhibitory study of protein arginine methyltransferase 1 using a fluorescent approach, *Biochem Biophys Res Commun* 379 567-572.
119. Zheng Y, M. F., Toptygin D, Brand L, Stivers JT, Cole PA. (2005) Fluorescence analysis of a dynamic loop in the PCAF/GCN5 histone acetyltransferase, *Biochemistry* 44, 10501-10509.
120. Johnson, K. A. (1992) Transient-State Kinetic Analysis of Enzyme Reaction Pathways *The Enzymes* 20, 1-61.
121. Feng, Y., Li, M., Wang, B., and Zheng, Y. G. (2010) Discovery and mechanistic study of a class of protein arginine methylation inhibitors, *J Med Chem* 53, 6028-6039.
122. Kouzarides, T. (2007) Chromatin modifications and their function, *Cell* 128, 693-705.

123. Li, B., Carey, M., and Workman, J. L. (2007) The role of chromatin during transcription, *Cell* 128, 707-719.
124. Berger, S. L. (2007) The complex language of chromatin regulation during transcription, *Nature* 447, 407-412.
125. Lachner, M., and Jenuwein, T. (2002) The many faces of histone lysine methylation, *Current opinion in cell biology* 14, 286-298.
126. Wang, G. G., Allis, C. D., and Chi, P. (2007) Chromatin remodeling and cancer, Part I: Covalent histone modifications, *Trends in molecular medicine* 13, 363-372.
127. Ruthenburg, A. J., Li, H., Patel, D. J., and Allis, C. D. (2007) Multivalent engagement of chromatin modifications by linked binding modules, *Nature reviews* 8, 983-994.
128. Shechter, D., Nicklay, J. J., Chitta, R. K., Shabanowitz, J., Hunt, D. F., and Allis, C. D. (2009) Analysis of histones in *Xenopus laevis*. I. A distinct index of enriched variants and modifications exists in each cell type and is remodeled during developmental transitions, *The Journal of biological chemistry* 284, 1064-1074.
129. Nicklay, J. J., Shechter, D., Chitta, R. K., Garcia, B. A., Shabanowitz, J., Allis, C. D., and Hunt, D. F. (2009) Analysis of histones in *Xenopus laevis*. II. mass spectrometry reveals an index of cell type-specific modifications on H3 and H4, *The Journal of biological chemistry* 284, 1075-1085.
130. Cuomo, A., Moretti, S., Minucci, S., and Bonaldi, T. (2010) SILAC-based proteomic analysis to dissect the "histone modification signature" of human breast cancer cells, *Amino acids*.
131. Lennartsson, A., and Ekwall, K. (2009) Histone modification patterns and epigenetic codes, *Biochimica et biophysica acta* 1790, 863-868.
132. Utley, R. T., Lacoste, N., Jobin-Robitaille, O., Allard, S., and Cote, J. (2005) Regulation of NuA4 histone acetyltransferase activity in transcription and DNA repair by phosphorylation of histone H4, *Molecular and cellular biology* 25, 8179-8190.
133. Cheung, W. L., Turner, F. B., Krishnamoorthy, T., Wolner, B., Ahn, S. H., Foley, M., Dorsey, J. A., Peterson, C. L., Berger, S. L., and Allis, C. D. (2005) Phosphorylation of histone

H4 serine 1 during DNA damage requires casein kinase II in *S. cerevisiae*, *Curr Biol* 15, 656-660.

134. Ogryzko, V. V., Schiltz, R. L., Russanova, V., Howard, B. H., and Nakatani, Y. (1996) The transcriptional coactivators p300 and CBP are histone acetyltransferases, *Cell* 87, 953-959.

135. Zhang, K., Williams, K. E., Huang, L., Yau, P., Siino, J. S., Bradbury, E. M., Jones, P. R., Minch, M. J., and Burlingame, A. L. (2002) Histone acetylation and deacetylation: identification of acetylation and methylation sites of HeLa histone H4 by mass spectrometry, *Mol Cell Proteomics* 1, 500-508.

136. Zhang, L., Eugeni, E. E., Parthun, M. R., and Freitas, M. A. (2003) Identification of novel histone post-translational modifications by peptide mass fingerprinting, *Chromosoma* 112, 77-86.

137. Schotta, G., Lachner, M., Sarma, K., Ebert, A., Sengupta, R., Reuter, G., Reinberg, D., and Jenuwein, T. (2004) A silencing pathway to induce H3-K9 and H4-K20 trimethylation at constitutive heterochromatin, *Genes & development* 18, 1251-1262.

138. Beck, H. C., Nielsen, E. C., Matthiesen, R., Jensen, L. H., Sehested, M., Finn, P., Grauslund, M., Hansen, A. M., and Jensen, O. N. (2006) Quantitative proteomic analysis of post-translational modifications of human histones, *Mol Cell Proteomics* 5, 1314-1325.

139. Phanstiel, D., Brumbaugh, J., Berggren, W. T., Conard, K., Feng, X., Levenstein, M. E., McAlister, G. C., Thomson, J. A., and Coon, J. J. (2008) Mass spectrometry identifies and quantifies 74 unique histone H4 isoforms in differentiating human embryonic stem cells, *Proceedings of the National Academy of Sciences of the United States of America* 105, 4093-4098.

140. Pesavento, J. J., Bullock, C. R., LeDuc, R. D., Mizzen, C. A., and Kelleher, N. L. (2008) Combinatorial modification of human histone H4 quantitated by two-dimensional liquid chromatography coupled with top down mass spectrometry, *The Journal of biological chemistry* 283, 14927-14937.

141. Schiltz, R. L., Mizzen, C. A., Vassilev, A., Cook, R. G., Allis, C. D., and Nakatani, Y. (1999) Overlapping but distinct patterns of histone acetylation by the human coactivators p300 and PCAF within nucleosomal substrates, *The Journal of biological chemistry* 274, 1189-1192.

142. Doyon, Y., Selleck, W., Lane, W. S., Tan, S., and Cote, J. (2004) Structural and functional conservation of the NuA4 histone acetyltransferase complex from yeast to humans, *Molecular and cellular biology* 24, 1884-1896.
143. Kimura, A., and Horikoshi, M. (1998) Tip60 acetylates six lysines of a specific class in core histones in vitro, *Genes Cells* 3, 789-800.
144. Yamamoto, T., and Horikoshi, M. (1997) Novel substrate specificity of the histone acetyltransferase activity of HIV-1-Tat interactive protein Tip60, *The Journal of biological chemistry* 272, 30595-30598.
145. Smith, E. R., Cayrou, C., Huang, R., Lane, W. S., Cote, J., and Lucchesi, J. C. (2005) A human protein complex homologous to the Drosophila MSL complex is responsible for the majority of histone H4 acetylation at lysine 16, *Molecular and cellular biology* 25, 9175-9188.
146. Cai, Y., Jin, J., Swanson, S. K., Cole, M. D., Choi, S. H., Florens, L., Washburn, M. P., Conaway, J. W., and Conaway, R. C. (2010) Subunit composition and substrate specificity of a MOF-containing histone acetyltransferase distinct from the male-specific lethal (MSL) complex, *The Journal of biological chemistry* 285, 4268-4272.
147. Kan, P. Y., Caterino, T. L., and Hayes, J. J. (2009) The H4 tail domain participates in intra- and internucleosome interactions with protein and DNA during folding and oligomerization of nucleosome arrays, *Molecular and cellular biology* 29, 538-546.
148. Shogren-Knaak, M., and Peterson, C. L. (2006) Switching on chromatin: mechanistic role of histone H4-K16 acetylation, *Cell Cycle* 5, 1361-1365.
149. Chicoine, L. G., Schulman, I. G., Richman, R., Cook, R. G., and Allis, C. D. (1986) Nonrandom utilization of acetylation sites in histones isolated from Tetrahymena. Evidence for functionally distinct H4 acetylation sites, *The Journal of biological chemistry* 261, 1071-1076.
150. Allis, C. D., Chicoine, L. G., Richman, R., and Schulman, I. G. (1985) Deposition-related histone acetylation in micronuclei of conjugating Tetrahymena, *Proceedings of the National Academy of Sciences of the United States of America* 82, 8048-8052.
151. Daujat, S., Bauer, U. M., Shah, V., Turner, B., Berger, S., and Kouzarides, T. (2002) Crosstalk between CARM1 methylation and CBP acetylation on histone H3, *Curr Biol* 12, 2090-2097.

152. Song, O. K., Wang, X., Waterborg, J. H., and Sternglanz, R. (2003) An Nalpha-acetyltransferase responsible for acetylation of the N-terminal residues of histones H4 and H2A, *The Journal of biological chemistry* 278, 38109-38112.
153. Osborne, T. C., Obianyo, O., Zhang, X., Cheng, X., and Thompson, P. R. (2007) Protein arginine methyltransferase 1: positively charged residues in substrate peptides distal to the site of methylation are important for substrate binding and catalysis, *Biochemistry* 46, 13370-13381.
154. Whitmore, L., and Wallace, B. A. (2004) DICHROWEB, an online server for protein secondary structure analyses from circular dichroism spectroscopic data, *Nucleic acids research* 32, W668-673.
155. Luger, K., Mader, A. W., Richmond, R. K., Sargent, D. F., and Richmond, T. J. (1997) Crystal structure of the nucleosome core particle at 2.8 Å resolution, *Nature* 389, 251-260.
156. Kabsch, W., and Sander, C. (1983) Dictionary of protein secondary structure: pattern recognition of hydrogen-bonded and geometrical features, *Biopolymers* 22, 2577-2637.
157. Wang, J., Wang, W., Kollman, P. A., and Case, D. A. (2006) Automatic atom type and bond type perception in molecular mechanical calculations, *J Mol Graph Model* 25, 247-260.
158. Vriend, G. (1990) WHAT IF: a molecular modeling and drug design program, *J Mol Graph* 8, 52-56, 29.
159. Case, D. A., Darden, T. A., Cheatham, III, T. E., Simmerling, C. L., Wang, J., Duke, R. E., Luo, R., Crowley, M., Walker, R. C., Zhang, W., Merz, K. M., Wang, B., Hayik, S., Roitberg, A., Seabra, G., Kolossváry, I., Wong, K. F., Paesani, F., Vanicek, J., Wu, X., Brozell, S. R., Steinbrecher, T., Gohlke, H., Yang, L., Tan, C., Mongan, J., Hornak, V., and Cui, G., Mathews, D. H., Seetin, M. G., Sagui, C., Babin, V. and Kollman, P.A. (2008) *AMBER* 10, University of California, San Francisco.
160. Hornak, V., Abel, R., Okur, A., Strockbine, B., Roitberg, A., and Simmerling, C. (2006) Comparison of multiple Amber force fields and development of improved protein backbone parameters, *Proteins* 65, 712-725.
161. Mongan, J., Simmerling, C., McCammon, J. A., Case, D. A., and Onufriev, A. (2007) Generalized Born model with a simple, robust molecular volume correction, *J Chem Theory Comput* 3, 156-169.

162. Heyer, L. J., Kruglyak, S., and Yooseph, S. (1999) Exploring expression data: identification and analysis of coexpressed genes, *Genome research* 9, 1106-1115.
163. Vyskot, B., Siroky, J., Hladilova, R., Belyaev, N. D., and Turner, B. M. (1999) Euchromatic domains in plant chromosomes as revealed by H4 histone acetylation and early DNA replication, *Genome / National Research Council Canada = Genome / Conseil national de recherches Canada* 42, 343-350.
164. Dion, M. F., Altschuler, S. J., Wu, L. F., and Rando, O. J. (2005) Genomic characterization reveals a simple histone H4 acetylation code, *Proceedings of the National Academy of Sciences of the United States of America* 102, 5501-5506.
165. Turner, B. M. (1989) Acetylation and deacetylation of histone H4 continue through metaphase with depletion of more-acetylated isoforms and altered site usage, *Experimental cell research* 182, 206-214.
166. Turner, B. M., and O'Neill, L. P. (1995) Histone acetylation in chromatin and chromosomes, *Seminars in cell biology* 6, 229-236.
167. Ceol, C. J., and Horvitz, H. R. (2004) A new class of *C. elegans* synMuv genes implicates a Tip60/NuA4-like HAT complex as a negative regulator of Ras signaling, *Dev Cell* 6, 563-576.
168. Kurdistani, S. K., Tavazoie, S., and Grunstein, M. (2004) Mapping global histone acetylation patterns to gene expression, *Cell* 117, 721-733.